Journal of Materials Chemistry B

ROYAL SOCIETY OF CHEMISTRY

REVIEW

View Article Online
View Journal | View Issue

Cite this: J. Mater. Chem. B, 2024, 12, 7692

Nanocellulose-based hydrogels as versatile materials with interesting functional properties for tissue engineering applications

Arnaud Kamdem Tamo [abcd]

Tissue engineering has emerged as a remarkable field aiming to restore or replace damaged tissues through the use of biomimetic constructs. Among the diverse materials investigated for this purpose, nanocellulose-based hydrogels have garnered attention due to their intriguing biocompatibility, tunable mechanical properties, and sustainability. Over the past few years, numerous research works have been published focusing on the successful use of nanocellulose-based hydrogels as artificial extracellular matrices for regenerating various types of tissues. The review emphasizes the importance of tissue engineering, highlighting hydrogels as biomimetic scaffolds, and specifically focuses on the role of nanocellulose in composites that mimic the structures, properties, and functions of the native extracellular matrix for regenerating damaged tissues. It also summarizes the types of nanocellulose, as well as their structural, mechanical, and biological properties, and their contributions to enhancing the properties and characteristics of functional hydrogels for tissue engineering of skin, bone, cartilage, heart, nerves and blood vessels. Additionally, recent advancements in the application of nanocellulose-based hydrogels for tissue engineering have been evaluated and documented. The review also addresses the challenges encountered in their fabrication while exploring the potential future prospects of these hydrogel matrices for biomedical applications.

Received 25th February 2024,
Accepted 21st May 2024

DOI: 10.1039/d4tb00397g

rsc.li/materials-b

1 Introduction

In the medical field, tissue engineering plays a pivotal role by integrating principles from biology, engineering, and materials science to develop functional biological substitutes that can repair or replace damaged or diseased tissues.[1–3] This multidisciplinary approach addresses critical healthcare challenges, offering transformative solutions for disease management, organ transplantation, and regenerative therapies.[4] Addressing the persistent shortage of viable donor organs, tissue engineering represents a paradigm shift. By integrating the body regenerative capacities with advanced biocompatible materials, it enables the controlled fabrication of functional tissues and organs in laboratory settings, thus mitigating the risk of immune rejection and offering hope to patients.[5,6]

In recent years, the field of tissue engineering has witnessed a paradigm shift towards the exploration of advanced biomaterials that can emulate the complex and dynamic microenvironment of native tissues.[7,8] Biomaterials constitute the foundation of advancements in tissue engineering, offering unique properties that are indispensable for the successful regeneration of damaged or diseased tissues.[9] These biomaterials are commonly chosen for their biocompatibility, ensuring a harmonious interaction with living cells and tissues without inducing adverse reactions.[1,8] Biomaterials also possess tunable physical and mechanical properties, allowing for the customization of scaffolds to mimic the specific characteristics of the target tissue. Their ability to provide structural support, promote cell adhesion, and guide cellular behavior makes them essential for fabricating three-dimensional frameworks that facilitate tissue engineering.[8,10] Furthermore, biomaterials can serve as carriers for biomolecules and cells, enhancing their therapeutic potential. In addition to their biocompatibility, biomaterials are also biodegradable, ensuring a controlled release of encapsulated molecules, aligning with the natural healing process, and eliminating the need for scaffold removal.[11–13] While presenting interesting properties and characteristics for their use in tissue engineering, biomaterials are generally combined with other materials and biomolecules to enhance their properties for specific biomedical applications.[14,15]

[a] Institute of Microsystems Engineering IMTEK, University of Freiburg, 79110 Freiburg, Germany. E-mail: arnaudkamdem38@yahoo.com
[b] Freiburg Center for Interactive Materials and Bioinspired Technologies FIT, University of Freiburg, 79110 Freiburg, Germany
[c] Freiburg Materials Research Center FMF, University of Freiburg, 79104 Freiburg, Germany
[d] Ingénierie des Matériaux Polymères (IMP), Université Claude Bernard Lyon 1, INSA de Lyon, Université Jean Monnet, CNRS, UMR 5223, 69622 Villeurbanne CEDEX, France

This combination approach allows for the fabrication of more complex and functional systems tailored to particular needs, such as the engineering of specific tissues or the customization of medical devices.[16,17] The synergy between biomaterials and other components often enhances biocompatibility, mechanical strength, and the ability to induce desired cellular responses.[18,19]

Among the various types of biomaterials commonly used to design functional constructs for repairing damaged tissues and organs, nanocellulose-based hydrogels have emerged as a promising class of materials, demonstrating remarkable potential for a myriad of applications in tissue engineering.[20,21] Nanocellulose, derived from cellulose fibers at the nanoscale level, possesses unique properties that make it an ideal candidate for designing tailored functional constructs in tissue engineering.[22,23] Its nanoscale dimensions contribute to a high surface area, allowing for enhanced cellular interactions and promoting cell adhesion and proliferation. Nanocellulose is biocompatible and exhibits remarkable mechanical strength.[7,24,25] Moreover, its tunable properties enable the fabrication of hydrogels with customizable stiffness and porosity, providing a platform for mimicking specific tissue microenvironments.[26,27] The fibrous nature of nanocellulose also facilitates the formation of intricate 3D structures, closely resembling the architecture of native tissues.[28,29] These properties, coupled with its biodegradability, make nanocellulose a versatile biomaterial for creating functional constructs tailored to the unique requirements of tissue engineering.[10,21]

In the spectrum of recent advancements in tissue engineering, hydrogels play a crucial role.[7,8,10] With their unique ability to retain water in a three-dimensional network structure, hydrogels mimic the natural extracellular matrix, creating a nurturing environment for cell growth, proliferation, and differentiation.[7,30] Hydrogel versatility in accommodating various cell types and bioactive molecules amplifies their significance, allowing precise engineering for intricate cellular interactions. This biomimetic approach extends to their mechanical properties, tailored to match specific tissues, making hydrogels invaluable for guiding tissue engineering processes.[31,32] Additionally, hydrogels address challenges in tissue engineering, playing a fundamental role in controlled drug delivery and scaffold design. They encapsulate therapeutic agents, ensuring targeted release and providing architectural frameworks for tissue engineering.[12,33] Furthermore, hydrogels can be infused with bioactive signals to guide cell behavior, 3D directing them towards differentiation and the formation of functional tissues. This process is essential in tissue engineering.

In the field of tissue engineering, integrating nanocellulose into matrices to design composite hydrogels contributes to enhancing the properties of the resulting composites.[34–36] Nanocellulose, derived from plant or bacteria sources, possesses exceptional strength, biocompatibility, and versatility, making it an ideal biomimetic reinforcement material. When incorporated into hydrogels, nanocellulose enhances the mechanical stability and structural integrity of the resulting biomaterial hydrogels.[8,37,38] Moreover, nanocellulose biocompatibility fosters a conducive environment for cellular interactions in the hydrogel matrix.[8,24] Nanocellulose, with its hydroxyl groups (–OH) and other functional groups, can provide an ideal scaffold for cell adhesion, proliferation, and differentiation. These functional groups facilitate hydrogen bonding and electrostatic interactions with cell surface molecules, promoting cellular attachment and signaling cascades essential for tissue regeneration.[7,10,30,37] Beyond its contributions to tissue engineering, nanocellulose ability to facilitate controlled drug release makes it invaluable in targeted therapies and regenerative medicine.[39–41] By incorporating bioactive molecules into nanocellulose-based hydrogel carriers, scientists could precisely regulate drug release, promising biomimetic responses in a targeted manner.[13,42]

Extensive research in the literature has highlighted the significant potential of nanocellulose-based hydrogels for repairing diverse types of damaged tissues. Studies demonstrated the versatility of nanocellulose in tissue engineering applications, showcasing its ability to mimic the native extracellular matrix, promote cell adhesion and proliferation, and exhibit excellent biocompatibility. Researchers have successfully utilized nanocellulose hydrogels to address various tissue repair needs, including wound healing, bone, nerve and cardiac engineering as well as cartilage repair.[16,17,43,44] The tunable properties of these hydrogels allow for the fabrication of tailored hydrogel constructs with customizable stiffness and porosity, providing an adaptable platform for different tissue microenvironments.[22] The review delves into the potential of nanocellulose-reinforced hydrogels for tissue engineering. It initially underscores the pivotal role of hydrogels in this field. Various aspects of nanocellulose are covered, including its types, properties, sources, biocompatibility, and biodegradability. Moreover, it discusses engineering techniques and crosslinking strategies aimed at integrating nanocellulose with other materials to create composite hydrogels. The review further emphasizes the biomimetic properties of nanocellulose-based hydrogels, such as their ability to deliver bioactive molecules, promote cell adhesion and proliferation, and mimic signals from the extracellular matrix. It explores the diverse applications of these hydrogels in bone, cartilage, nerve, vascular, and skin tissue engineering. Additionally, it outlines commonly used characterization methods for assessing the mechanical, structural, and biological attributes of these polymer materials. Recent advancements in utilizing nanocellulose-based hydrogels for tissue engineering are also evaluated and described. Finally, the review addresses the challenges encountered during their fabrication process and explores potential future prospects for these functional hydrogel matrices in biomedical applications.

2 Nanocellulose: properties and types

Nanocellulose, derived from cellulose, exhibits remarkable properties and exists in various forms. It is characterized by its nanoscale dimensions, high aspect ratio, and exceptional mechanical strength. Nanocellulose can be categorized into three main types: cellulose nanocrystals (CNCs), cellulose nanofibrils (CNFs), and bacterial nanocellulose (BNC). CNCs are rigid, rod-like nanoparticles with dimensions on the order

of nanometers. CNFs, on the other hand, are long, flexible fibrils with diameters ranging from tens to hundreds of nanometers. BNC is produced by certain bacteria and forms a unique, highly pure form of nanocellulose. Each type offers distinct advantages and applications across various industries.

2.1 Exploring nanocellulose: insights into nanocrystals and nanofibrils

Nanocellulose, a versatile and sustainable biomaterial, encompasses a spectrum of types, each with its unique properties and applications. The primary categories of nanocellulose include CNCs, CNFs, and BNC (as illustrated in Fig. 1 and 2a–c). Nanocellulose, can be sourced from both plants and bacteria, each offering distinct properties and extraction techniques.[45–47] Plant-based nanocellulose, primarily obtained from natural sources such as wood pulp, cotton, hemp, and agricultural residues, serves as a notable example of sustainable engineering practices.[48,49] Wood pulp, derived from various tree species, remains a predominant source, serving as the foundation for producing both CNCs and CNFs. The extraction process involves breaking down the complex cellulose structure into nano-sized entities, resulting in CNCs and CNFs renowned for their exceptional mechanical strength and biocompatibility.[50–53] In contrast, BNC represents a cutting-edge approach to nanocellulose production. Cultivated through microbial fermentation, BNC is synthesized by acetic acid bacteria, notably *Gluconacetobacter xylinus*, using glucose-containing substrates.[54] This method yields an ultra-pure and mechanically robust nanocellulose variant, offering distinct advantages such as high purity, mechanical strength, and biocompatibility. BNC stands out as a prime choice for biomedical applications, including tissue engineering and wound healing, owing to its unique properties derived from its bacterial origins.[55,56]

CNCs are often produced through acid hydrolysis, a chemical process where cellulose-based materials are treated with strong acids, causing the amorphous regions of cellulose to be removed, leaving behind crystalline nanoparticles (Fig. 1A).[60,61] CNFs, on the other hand, can be obtained through mechanical disintegration, wherein cellulose-based substrates are subjected to high shear forces using techniques like homogenization or microfluidization. These mechanical forces break down the fibers into nanoscale fibrils, creating a suspension of CNFs.[27,55] In contrast, the production of BNC commonly involves specific bacteria like Komagataeibacter xylinus and follows a complex series of biochemical processes (Fig. 1B). In the BNC production pathway, glucose acquired from the surroundings undergoes isomerization to glucose-1-phosphate, subsequently reacting with uridine-5-triphosphate (UTP) to generate uridine diphosphate glucose (UDP-glucose). Catalyzed by cellulose synthase A and activated by cyclic-di-GMP, linear 1,4 glucan chains are synthesized. These chains are then discharged through pores in the bacterial cell wall.[46,62] The entire process is regulated by the bacterial cellulose synthesis ABCD operon, where bcsA encodes the catalytic subunit, and bcsB produces a regulatory subunit that binds to c-di-GMP, a crucial step in initiating cellulose production. The exact functions of bcsC and bcsD remain somewhat ambiguous, although it is suggested that bcsC might play a role in the formation of pores in the cell membrane. Following fermentation, the resulting pellicle comprises cellulose, secondary metabolites, microbial biomass, and residual nutrients.[46,63] This pellicle can be subjected to purification, ultimately yielding a highly pure crystalline cellulose matrix. Despite its molecular formula being similar to plant-derived cellulose, BNC exhibits distinct physical and chemical properties that render it exceptionally valuable in diverse applications. The production process meticulously follows biochemical pathways, ensuring the synthesis of cellulose in bacterial cultures. Komagataeibacter xylinus produces bacterial cellulose extracellularly in four allomorphic forms, I–IV, with celluloses I and II being the most extensively studied.[46,63]

The hierarchical structure of cellulose fibers displays an intricate and orderly arrangement across various levels, ranging from the macroscopic organization of the cell wall to the molecular configuration of cellulose chains as illustrated in the Fig. 2 and 3a. At the macroscopic level, cellulose fibers exhibit a well-defined hierarchical structure within the cell wall. This structure comprises layers of cellulose microfibrils embedded in a matrix of hemicelluloses and lignin (Fig. 2A).[64] These microfibrils, in turn, consist of bundles of cellulose chains organized in a crystalline lattice. Delving further into the microscopic scale, cellulose microfibrils reveal a highly structured assembly of cellulose molecules. This assembly results in crystalline regions interspersed with less organized, amorphous regions (Fig. 1A and 3b).[65] The stability of the crystalline cellulose structure is primarily upheld by hydrogen bonding interactions between adjacent cellulose chains, establishing a robust and secure framework. Cellulose, a complex polysaccharide predominantly found in the cell walls of plants, algae, and select bacteria, boasts a meticulously organized microstructure that underlies its exceptional mechanical strength and adaptability.[48,66] Composed of linear chains of glucose molecules linked by β-1,4-glycosidic bonds, cellulose forms intricate crystalline structures due to the regular arrangement of its constituent units. This systematic assembly operates across various scales, with each contributing to the unique properties of cellulose.[35,67] At the nanoscale, individual cellulose chains align into extended, flat ribbons, held together by hydrogen bonds, resulting in the formation of robust, inflexible structures known as cellulose microfibrils. These microfibrils, with diameters measuring several nanometers, align themselves into bundles within plant cells, forming a mesh-like network. The hydrogen bonds between these chains provide cohesion and stability, significantly bolstering cellulose tensile strength.[68–70] Expanding to a larger scale, cellulose microfibrils come together to create macroscopic units, constituting cellulose fibers. These fibers are bound together by van der Waals forces and additional hydrogen bonds, culminating in the formation of a dense and stable material.[71–73] This intricately organized structure, with its interplay of crystalline and amorphous regions, defines the exceptional mechanical integrity of cellulose and serves as the foundation for its diverse applications in various industrial and biological contexts.[74,75] Due to the unique arrangement of cellulose microfibrils, cellulose fibers exhibit impressive mechanical properties, including high tensile strength and stiffness. In the context of plant cell walls, cellulose

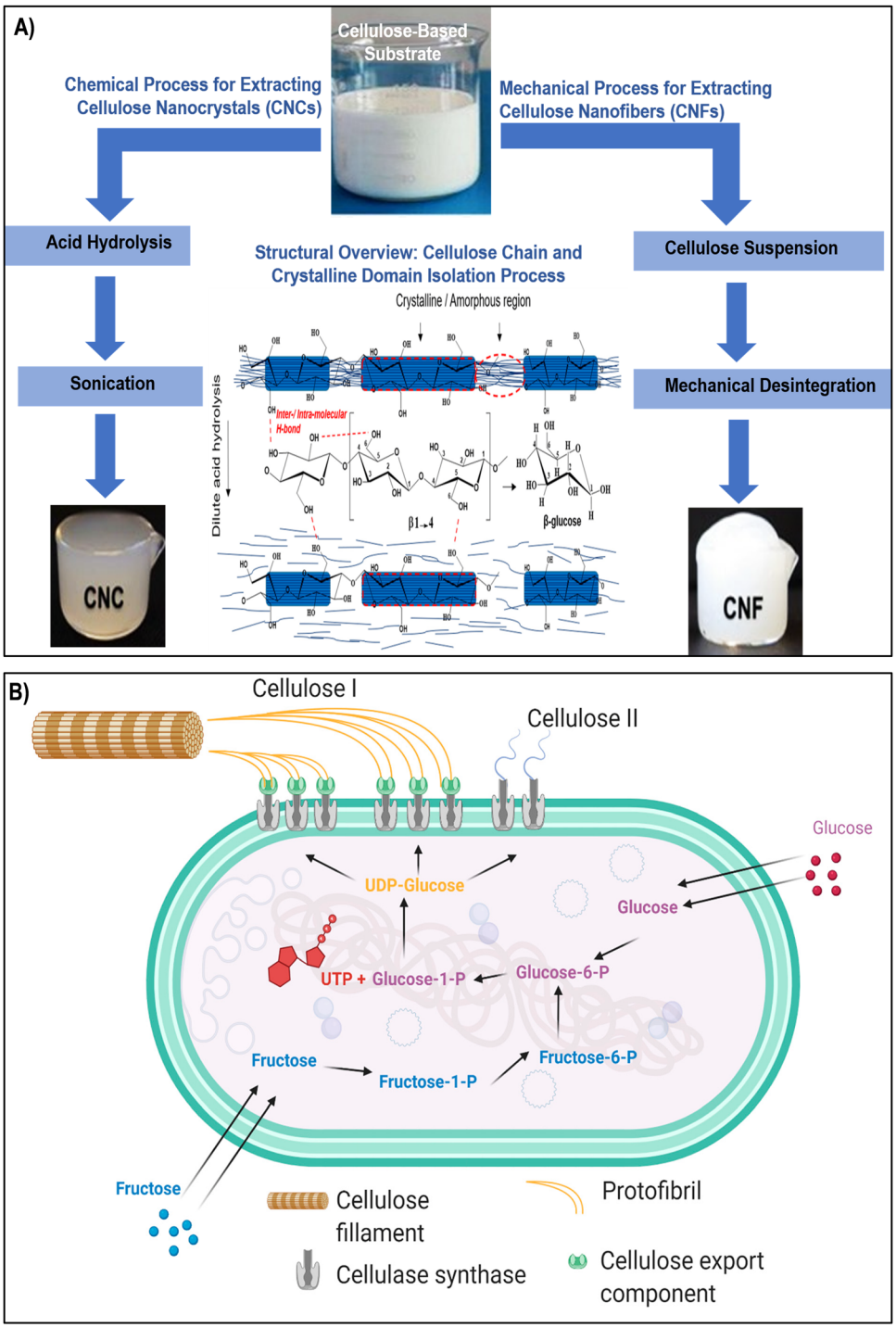

Fig. 1 (A) Two established methods for the isolation of CNCs and CNFs involve acid hydrolysis and mechanical disintegration, accompanied by a hypothetical schematic representing the dilute acid pretreatment process aimed at extracting crystalline regions from cellulose amorphous domains. The middle section illustrates the configuration of the cellulose repeating unit, highlighting the β-(1,4) glycosidic linkage influenced by intra/intermolecular hydrogen bonding. Reproduced with permission from ref. 57 Copyright © 2019 Elsevier. (B) Schematic diagram depicting the biosynthesis pathways of bacterial cellulose I and II from glucose and fructose. Reproduced with permission from ref. 46 Copyright © 2021 MDPI.

microfibrils are embedded within a matrix of hemicellulose, pectin, and lignin (Fig. 2A). This composite structure provides plants with structural integrity, enabling them to withstand mechanical stress and maintain their shape. The precise arrangement of cellulose microfibrils within this matrix contributes to the rigidity of plant cell walls, allowing plants to grow tall and maintain their form against gravitational forces.[8,24,75,76] Plant fibers, depicted in Fig. 2B, comprise elongated cylindrical cells with an outer primary cell wall (S1), an inner secondary cell wall (S2), and a central hollow channel (lumen). S2, rich in microfibrils,

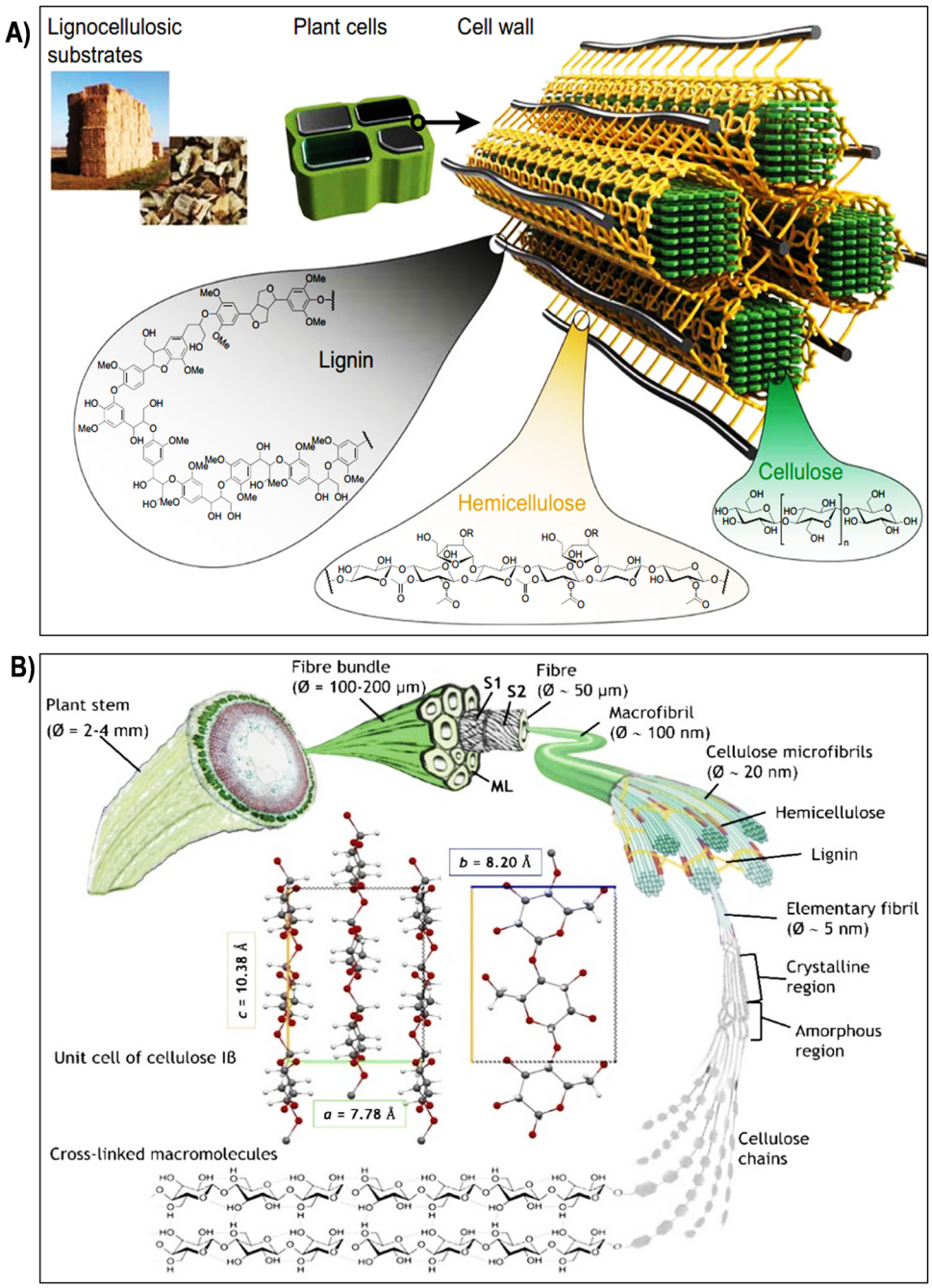

Fig. 2 (A) Composition and structure of lignocellulosic plant cell walls. Lignocellulosic plant cell walls primarily consist of cellulose, hemicellulose, and lignin. Reproduced with permission from ref. 58 Copyright © 2020 Springer. (B) Schematic illustration of the hierarchical structure of cellulose, starting from its macroscopic origin in the plant stem (depicted here with flax). Cellulose microfibrils, which form the secondary cell wall of fibers, are surrounded by hemicelluloses, lignin, and pectins, creating an interlocking matrix gel. The unit cell of cellulose Iβ, predominant in flax and cotton, is depicted with its *a*, *b*, and *c* lattice constants. Reproduced with permission from ref. 59 Copyright © 2022 Royal Society of Chemistry.

primarily consists of crystalline cellulose, representing about 95% of cotton fiber weight and 65–80% of flax fiber weight.[59] Other components include waxes, protein, pectate, and minerals in cotton, and hemicellulose, pectins, proteins, and lignin (2–2.5%) in flax. The interaction between cellulose and hemicellulose, along with hemicellulose covalent bonds, influences fiber macro-mechanical behavior. Cellulose molecules form microfibrils through hydrogen bonding, adopting crystalline or semi-crystalline structures with lattice parameters.[59–79] Cellulose I occurs naturally in two crystalline forms: Iα and Iβ, with Iβ predominant in flax and cotton, characterized by lattice constants a = 7.80 Å, b = 8.20 Å, and c = 10.38 Å.[59,80] Amorphous regions lacking hydrogen bonding are also present. Various treatments target cellulose hydroxyl groups in both ordered and disordered regions, affecting swelling and crystallinity (Fig. 2B).

The microstructure of cellulose has significant implications for various industries. In papermaking, the arrangement of cellulose fibers influences the texture, strength, and absorbency of the paper.[85,86] Additionally, advancements in nanotechnology have led to the isolation of cellulose nanocrystals and nanofibrils, exploiting the unique microstructure of cellulose for the development of nanocomposites and biomedical materials. These nanoscale cellulose entities exhibit exceptional mechanical properties and have gained attention for their potential applications in a wide range of fields.[66,87]

2.1.1 Cellulose nanocrystals (CNCs). CNCs, often referred to as cellulose nanowhiskers, represent a class of nanomaterials characterized by exceptional structural and mechanical properties. Their nanoscale dimensions, typically in the range of 5 to 20 nm in diameter and 100 to 500 nm in length, contribute to their high aspect ratio.[88,89] In addition, their morphology results in a large surface area, ranging from 30 to 300 $m^2 g^{-1}$, providing extensive interfaces for interactions with other materials. Moreover, CNCs possess excellent thermal stability, with a degradation temperature often exceeding 300 °C, making them suitable for high-temperature applications.[90,91] Their optical properties, such as reflectance and birefringence, add to their uniqueness, enabling applications in optical devices and sensors.[92] CNC biocompatibility and biodegradability further enhance their appeal for biomedical applications, making them promising candidates for drug delivery systems, tissue engineering, and various nanocomposites, contributing to advancements in materials science and engineering.[93,94] Under the microscope, CNCs appear as tiny, rod-shaped particles with dimensions in the nanometer range. These particles exhibit a high degree of crystallinity, appearing as well-defined crystalline structures.[35,75,95] Their uniform size and shape contribute to their remarkable mechanical properties. The images reveal the organized arrangement of individual nanocrystals, highlighting their characteristic needle-like appearance and surface morphology (as shown in Fig. 3d).[35] The highly ordered structure of CNCs is a result of the controlled hydrolysis process used to extract them from cellulose sources.[96]

The preparation of CNCs involves several advanced methods, each tailored to yield nanocrystals with specific properties for diverse applications. One common approach is acid hydrolysis (Fig. 1A and 3b), where cellulose fibers are treated with strong acids, such as sulfuric acid or hydrochloric acid, under controlled conditions. This process selectively removes the less crystalline or amorphous regions of cellulose, leaving behind highly crystalline CNCs with characteristic rod-like shapes.[97] Another method involves enzymatic hydrolysis, wherein enzymes like cellulase break down cellulose fibers into nanocrystals. This technique offers a more environmentally friendly alternative compared to acid hydrolysis and allows precise control over CNC dimensions.[98] In addition, mechanical disintegration techniques, such as microfluidization and homogenization, utilize mechanical forces to physically break down cellulose fibers into nanoscale dimensions. These methods assiocated with chemical treatments are efficient in producing CNCs with tunable sizes and morphologies.[99] Additionally, chemical oxidation techniques, including TEMPO (2,2,6,6-tetramethylpiperidine-1-oxyl)-mediated oxidation, involve the use of specific chemical catalysts to oxidize cellulose, resulting in CNCs with negatively charged surfaces, enhancing their stability in aqueous solutions.[100,101] Emerging methods include deep eutectic solvent (DES) treatment, where cellulose fibers are dissolved in a DES and then precipitated to obtain CNCs. This method is environmentally sustainable and produces high-quality CNCs suitable for various applications.[102,103] Ultrasonication, which utilizes ultrasound waves to disintegrate cellulose fibers, is another versatile method. It allows for the production of CNCs on both laboratory and industrial scales, with the size and properties of the CNCs controlled by the duration and intensity of ultrasound treatment.[104,105] Additionally, methods like steam explosion and combined mechanical-chemical treatments have been explored to enhance the efficiency of CNC extraction, ensuring a more sustainable and economical process.[106] These diverse preparation methods empower scientists to obtain CNCs with tailored characteristics, enabling their utilization in advanced materials, nanocomposites, drug delivery systems, and biomedical applications, thus driving innovations in various fields of science and technology (Fig. 3g).

2.1.2 Cellulose nanofibrils (CNFs). CNFs are a remarkable class of nanomaterials characterized by a set of distinctive features. These nanofibrils consist of intertwined nanofibers with diameters typically ranging from 5 to 30 nm with lengths that can approach several microns.[107] One of the exceptional attributes of CNFs is their transparency, a unique feature that allows for their use in creating transparent films for various applications.[25,37,74] Microscopical examination of CNFs (Fig. 3e) showcases a different morphology compared to CNCs. CNFs appear as entangled, fibrous networks with a high aspect ratio, resembling long, interconnected strands. These fibrils exhibit a mix of crystalline and amorphous regions, giving them a unique appearance under the microscope. CNF image reveals their ability to form intricate networks, indicating their potential for applications requiring high surface area and mechanical strength. The image also captures the fine structure of individual fibrils, highlighting their nanoscale dimensions and the presence of both ordered and disordered regions.[82] When incorporated into hydrogels and other materials, CNFs significantly enhance their mechanical properties, including stiffness and tensile strength, making them valuable as reinforcement agents.[108,109] In tissue engineering, CNFs serve as fundamental building blocks for scaffolds, providing a nanoscale architecture that can closely mimic the extracellular matrix, thereby promoting cell adhesion, proliferation, and differentiation.[7,8,10] This biocompatibility make CNFs ideal for various biomedical applications, ensuring their safety and effectiveness in in tissue engineering endeavors.[52,53,109] The remarkable combination of mechanical strength, flexibility, and transparency, along with their capacity to mimic natural tissue environments, positions CNFs as a versatile and promising platform for creating advanced biomaterials and scaffolds, contributing to significant advancements in the fields of materials science and tissue engineering (Fig. 3g).[7,8,24,53,109]

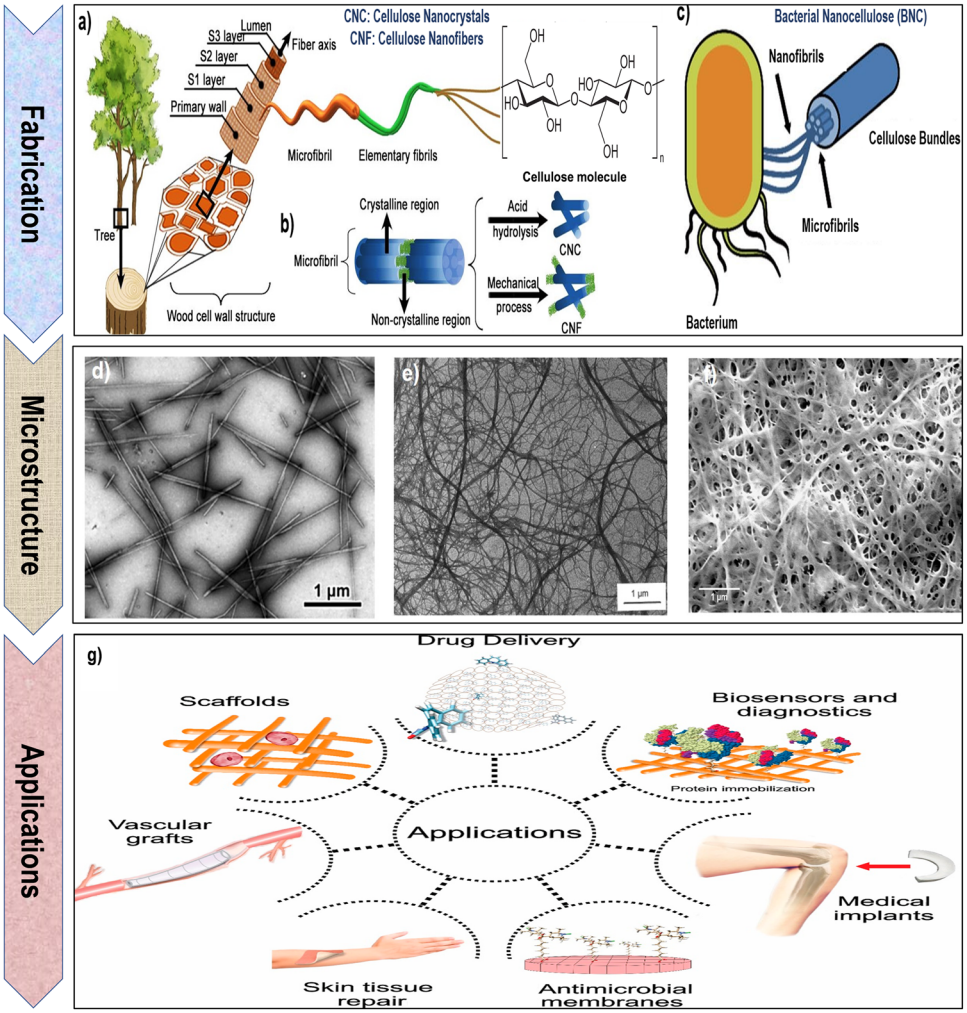

Fig. 3 (a) and (b) Schematic representation of the process for extracting cellulose nanocrystals (CNCs) and cellulose nanofibrils (CNFs) from the cell walls of wood and plants. Reproduced with permission from ref. 81 Copyright © 2023 MDPI, as well as (c) bacterial nanocellulose (BNC) from bacteria. Reproduced with permission from ref. 66 Copyright © 2023 Springer. (d) Transmission electron microscopy (TEM) image of CNCs. Reproduced with permission from ref. 35 Copyright © 2012 American Chemical Society. (e) Scanning electron microscopy (SEM) image of CNFs. Reproduced with permission from ref. 82 Copyright © 1997 John Wiley & Sons, Inc. (f) Field emission scanning electron microscopy (FESEM) image of BNC. Reproduced with permission from ref. 83 Copyright © 2020 Springer Nature. (g) Schematic illustration of diverse biomedical applications for nanocellulose. Reproduced with permission from ref. 84 Copyright © 2020 MDPI.

The production of CNFs from plant biomasses or other cellulose sources mainly involves various physical and mechanical methods aimed at breaking down cellulose fibers into nanoscale fibrils. One common technique is mechanical disintegration, where cellulose fibers are subjected to high shear forces using methods such as microfluidization, homogenization, or grinding. These mechanical forces separate the fibers into smaller entities, eventually yielding CNFs.[110–112] Microfluidization, in particular, involves forcing cellulose fibers through a narrow channel at high velocities, resulting in effective fibrillation due to shear and cavitation forces.[111] Another method is high-pressure homogenization, where cellulose fibers are forced through a narrow gap at high pressures, causing them to shear and fibrillate into nanoscale dimensions.[112] Ultrasonication, utilizing ultrasound waves, induces mechanical agitation and cavitation, leading to the disintegration of cellulose fibers into CNFs.[104] These methods are advantageous as they do not involve chemical treatments, preserving the natural properties of CNFs. In addition to mechanical approaches, physical methods like cryocrushing have been explored. In this method, cellulose fibers are frozen in liquid nitrogen and then shattered, resulting in fine fibrillation due to the brittle nature of the frozen material. These techniques generate CNFs with high aspect ratios, offering excellent reinforcement potential in various applications.[113] Furthermore, combination methods, such as enzymatic pretreatment and mechanical disintegration, have been employed to enhance the efficiency of CNFs production.[8,25,114] Enzymatic treatments, partially break down cellulose fibers, making them more amenable to subsequent mechanical disintegration. These physical and mechanical methods enable the production of CNFs with specific characteristics, including fibril length,

width, and surface properties, tailored for diverse applications such as nanocomposites, films, coatings, and biomedical materials.[115,116] By optimizing these methods, scientists can obtain CNFs with desired properties, contributing significantly to advancements in nanotechnology and sustainable materials development.

2.1.3 Bacterial nanocellulose (BNC). BNC stands out as a highly promising and versatile nanomaterial, produced by various ubiquitous fermentation bacteria (Fig. 3c). While BNC has found diverse applications in commercial sectors, its exceptional potential in the field of medical applications remains a focal point of interest.[117] Several bacterial genera, including *Acetobacter*, *Achromobacter*, *Bacillus*, *Sarcina*, *Aerobacter*, *Agrobacterium*, *Escherichia*, *Azotobacter*, *Rhizobium*, *Enterobacter*, *Klebsiella*, and *Salmonella*, have been identified as cellulose producers in the synthesis of BNC.[118,119] BNC synthesis unfolds through a complex series of stages, starting with the activation of monosaccharides through sugar nucleotides development, followed by polymerization leading to the assembly of repeating sugar units. Subsequently, the addition of acyl groups occurs if present, culminating in the excretion of BNC from the cell cytoplasm to the external environment through the cell membrane.[120,121] This process, undertaken *via* microorganisms, employs two primary methods: the static culture approach, resulting in the formation of a dense, leathery white BNC pellicle at the air–liquid interface; and the stirred culture technique, wherein cellulose is produced in a dispersed manner within the culture medium, forming peculiar pellets or suspended microfibers.[120,121]

BNC possesses an impressive array of features that elevate its value in industrial and biomedical applications. Its outstanding purity, often reaching 99.9%, ensures it is virtually free from impurities, making it an ideal choice for biomedical applications where material purity is paramount.[122] BNC exhibits a degree of polymerization within the range of 4000 to 8000, coupled with a crystallinity spanning from 75% to 80%. The elementary crystallites exhibit a length of 100–150 nm, with a lateral size of 8–10 nm.[123–126] BNC plays a crucial role in biomedical engineering due to its unique properties. Its biocompatibility, high porosity, remarkable mechanical strength and water-holding capacity, and capacity to be tailored into diverse forms make it an ideal material for various biomedical applications.[16,127,128] From wound dressings to tissue scaffolds, bacterial cellulose serves as a versatile and effective component, contributing to advancements in regenerative medicine and tissue engineering. Additionally, its natural origin and biodegradability align with the growing emphasis on sustainable and eco-friendly practices in biomedical research and applications.[54,118,129–132] Moreover, BNC is highly biocompatible and non-toxic, allowing safe direct contact with biological tissues without causing adverse reactions.[133,134] Its substantial and high surface area facilitates efficient interactions with various molecules, making it ideal for drug delivery systems.[135] The nanofibrous architecture of BNC, characterized by substantial fiber diameters and lengths, offers an extensive surface area-to-volume ratio. With numerous hydroxyl groups and inherent hydrophilicity, BNC exhibits enhanced reactivity, positioning it as a highly suitable material for surface modifications and functionalization.[136] Microscopical image of BNC (as highlighted in the Fig. 3f) exhibits a unique, nanofibrous network composed of ultrafine cellulose fibers. These fibers are highly uniform in diameter and appear densely packed, creating a compact and stable material. BNC displays a characteristic mesh-like structure with a high degree of porosity, providing a large surface area for interactions with surrounding environments.[83,119] The image showcases the smooth and homogeneous surface of BNC fibers, underscoring their high purity and quality. BNC micrograph often reveals an intricate arrangement of fibers, forming a three-dimensional scaffold with a nanoscale texture.[83,119]

In summary, nanocellulose, a versatile material with unique properties, holds significant promise for biomedical applications. Its inherent features, such as biocompatibility, high surface area, and tunable mechanical strength, make it an excellent candidate for various biomedical uses. The nanoscale dimensions of nanocellulose allow precise manipulation, facilitating tailored applications in drug delivery, tissue engineering, and wound healing. Moreover, its renewable and sustainable nature aligns with the growing emphasis on eco-friendly biomedical solutions. The combination of these properties positions nanocellulose as a valuable resource for advancing innovations in the biomedical field.[55,118,129] Fig. 3g emphasizes several biomedical applications of nanocellulose hydrogels.

2.2 Tailoring nanocellulose properties through functionalization

Functionalizing nanocellulose is pivotal for optimizing its properties and expanding its applicability.[136,137] Nanocellulose, featuring high surface area, biocompatibility, and mechanical strength, undergoes diverse surface modifications, including oxidation, coupling, coating, *etc.* These methods tailor its surface chemistry, introducing functionalities like carboxyl, hydroxyl, or amino groups.[26] This customization enhances compatibility with other materials, crucial for uniform dispersion in nanocomposites or favorable interactions. In addition, functionalization enables precise control over wettability, adhesion, and reactivity, making nanocellulose versatile for varied applications.[138] In biomedicine, this material serves as a foundation for drug delivery, wound dressings, and tissue engineering. Tailoring nanocellulose for targeted drug release or antimicrobial properties enhances its suitability.[83,139] In sustainability, functionalized nanocellulose plays a vital role in green technologies, aiding water treatment and reinforcing biodegradable composites.[108,140] Table 1 provides a comprehensive overview of the different functionalization methods, along with their respective advantages and disadvantages, aiding in the selection of the most suitable method for fabricating functionalized nanocellulose-based hydrogels for tissue engineering applications.

In the Fig. 4, the mechanisms behind key chemical modifications of nanocellulose are highlithed.

2.2.1. Esterification. Esterification is a chemical modification method that entails reacting nanocellulose hydroxyl (OH) groups with carboxylic acids or acid chlorides. The outcome of

Table 1 Nanocellulose functionalization strategies for hydrogel fabrication: principles, advantages, and disadvantages

Functionalization methods	Principles	Advantages	Disadvantages	Ref.
Esterification	Introduction of ester groups to nanocellulose surface through reaction with carboxylic acid derivatives.	• Enhanced hydrophobicity • Improved mechanical properties • Tunable surface chemistry	• Requires harsh reaction conditions • Formation of byproducts • Difficulties in controlling degree of substitution	141–143
Etherification	Introduction of ether groups to nanocellulose surface *via* reaction with alkyl or aryl halides.	• Increased stability against moisture • Enhanced mechanical properties • Improved dispersibility	• Limited reaction selectivity • Formation of heterogeneous products • Moderate to low functionalization efficiency	144 and 145
Silanization	Coating of nanocellulose with organosilanes to modify surface properties.	• Enhanced hydrophobicity or hydrophilicity • Improved compatibility with other materials • Enhanced chemical stability	• Requires specific handling and storage conditions for silanes • Potential toxicity of unreacted silanes • May introduce heterogeneous surface coverage	146–148
Sulfonation	Introduction of sulfonate groups onto nanocellulose surface through reaction with sulfonating agents.	• Enhanced water solubility • Improved interaction with polar solvents • Increased surface charge	• Harsh reaction conditions • Potential degradation of cellulose structure • Formation of side products	149–152
Carboxymethylation	Attachment of carboxymethyl groups to nanocellulose surface using chloroacetic acid or its derivatives.	• Introduction of carboxyl groups for further functionalization • Increased water solubility • Improved dispersibility	• Requires alkaline conditions • Formation of byproducts • Potential decrease in mechanical properties	153–156
Phosphorylation	Introduction of phosphate groups onto nanocellulose surface through reaction with phosphorus-containing compounds.	• Enhanced bioactivity for tissue regeneration • Improved flame retardancy • Increased surface reactivity	• Complex synthesis routes may require multiple steps • Potential cytotoxicity of reactants • Potential decrease in mechanical properties	157–159
Polycondensation	Formation of covalent bonds between nanocellulose and polymeric chains through condensation reactions.	• Enhanced mechanical properties of resulting hydrogel • Improved stability against environmental factors • Tunable network structure	• Complex reaction kinetics • Difficulty in controlling polymer chain length • Formation of heterogeneous networks	160 and 161
Cationization	Introduction of positively charged groups onto nanocellulose surface *via* reaction with cationic reagents.	• Enhanced interaction with negatively charged molecules (*e.g.*, proteins, cells) • Improved dispersion in polar solvents • Increased stability in aqueous environments	• Potential cytotoxicity of cationic reagents • Non-specific binding to negatively charged species • Limited control over degree of functionalization	162–164
Coating	Application of a thin layer of functional material onto nanocellulose surface.	• Versatile: can be used to introduce various functionalities • Controlled deposition of coating material • Preservation of inherent properties of nanocellulose	• Limited durability of coating • Potential delamination • Difficulty in achieving uniform coverage	165–167
Adsorption	Adsorption of functional molecules onto nanocellulose surface *via* physical interactions.	• Simple and cost-effective method • Minimal alteration of nanocellulose structure • Versatile: wide range of molecules can be adsorbed	• Weak bonding between adsorbate and nanocellulose • Difficulty in controlling adsorption efficiency • Potential desorption under certain conditions	168–170
Initiation	Introduction of reactive sites onto nanocellulose surface to initiate	• Precise control over location and density of functional groups	• Requires specific initiation agents	171 and 172

Table 1 (*continued*)

Functionalization methods	Principles	Advantages	Disadvantages	Ref.
	subsequent polymerization or modification reactions.	• Compatibility with various polymerization methods • Enables grafting of diverse monomers	• Limited scalability for large-scale applications • Potential decrease in cellulose crystallinity	
Oxidation	Introduction of oxygen-containing functional groups (*e.g.*, hydroxyl, carboxyl) onto nanocellulose surface using oxidizing agents.	• Increased hydrophilicity • Enhanced reactivity for further functionalization • Improved dispersibility	• Harsh reaction conditions • Potential degradation of cellulose structure • Formation of undesired byproducts	100, 127 and 173

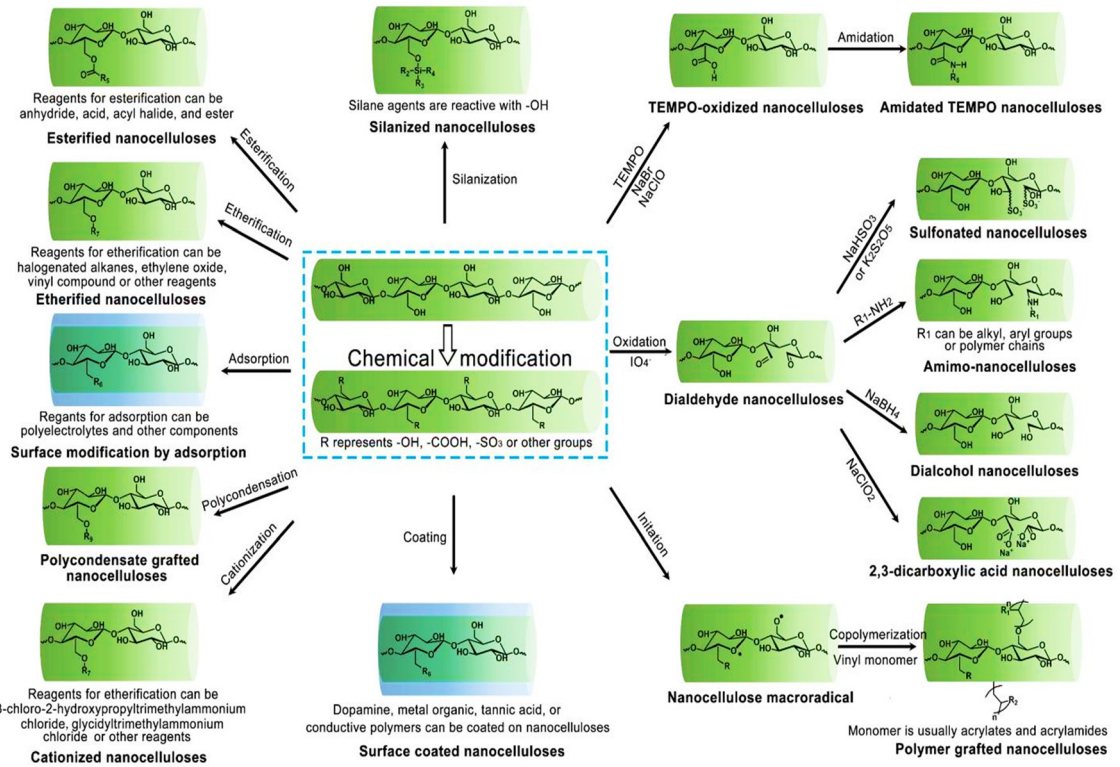

Fig. 4 Overview of customizing nanocellulose functionality. Reproduced with permission from ref. 81 Copyright © 2023 MDPI.

this reaction is the creation of ester linkages, where an oxygen atom bridges nanocellulose and the carboxyl groups.[141] In esterification, the reaction can happen across the entire cellulose polymer chains, creating typical cellulose esters, or it can take place on the outer surface of cellulose fibers, preserving the crystalline structure inside.[143] This alteration introduces hydrophobicity, reducing the material affinity for water and increasing its compatibility with nonpolar substances.[174] One notable advantage of esterified nanocellulose is its potential in controlled drug release applications. By adjusting the degree of substitution, the quantity of ester groups attached to nanocellulose can be controlled, thus regulating the release of drugs and other bioactive agents. This precision in drug release is particularly advantageous in pharmaceutical and medical applications, ensuring the efficient release of therapeutic compounds.[154,175] Enhanced hydrophobicity of esterified nanocellulose also makes it a valuable component in composite materials, where compatibility with hydrophobic matrices is essential for achieving uniform dispersion and optimal reinforcement.[142,143] Emam and Shaheen[176] achieved new hybrid hydrogels with pH and thermo-responsive properties by incorporating succinylated cellulose nanocrystals (Su-CNC) into the hydrogel network at various degrees of substitution. The Su-CNC was blended with poly(*N*-isopropylacrylamide) (PNIPAm) *via* free radical polymerization.[176] These hydrogels were then evaluated for their ability to release Famotidine in different pH environments. The results demonstrated that all Su-CNC/PNIPAm hydrogels exhibited significant temperature responsiveness, with decreased swelling and hydrophilicity at 35 °C and above. This led to the more hydrophobicity character

and thus the hydrogel shrinkage occurred.[176] Additionally, at pH 6, the hydrogels showed high equilibrium swelling ratios particularly Su-CNC/PNIPAm 2, which displayed notable pH responsiveness, suggesting its potential for pH-controlled drug release applications (Fig. 5A).[176] In tissue engineering, esterified cellulose can be utilized to improve properties of the resulting hydrogels. In recent research, Fang *et al.*[177] developed a new method for fabricating a composite hydrogel with polyvinyl alcohol and xylan, using sodium tri-metaphosphate (STMP) as a cross-linker (Fig. 5B). This method emphasized enhancing the compressive properties of the hydrogel through the inclusion of esterified cellulose nanofibrils (CNFs), which are eco-friendly. Although the addition of CNFs resulted in a reduction in the compressive strength of the hydrogels, the strength values remained relatively high at 2.34–4.57 MPa under 70% strain, making them competitive among similar hydrogels (Fig. 5C).[177] Significantly, CNFs improved the compressive resilience of the hydrogels, achieving up to 99.67% height recovery after 1000 compression cycles at 30% strain. This highlighted the notable impact of esterified CNFs on

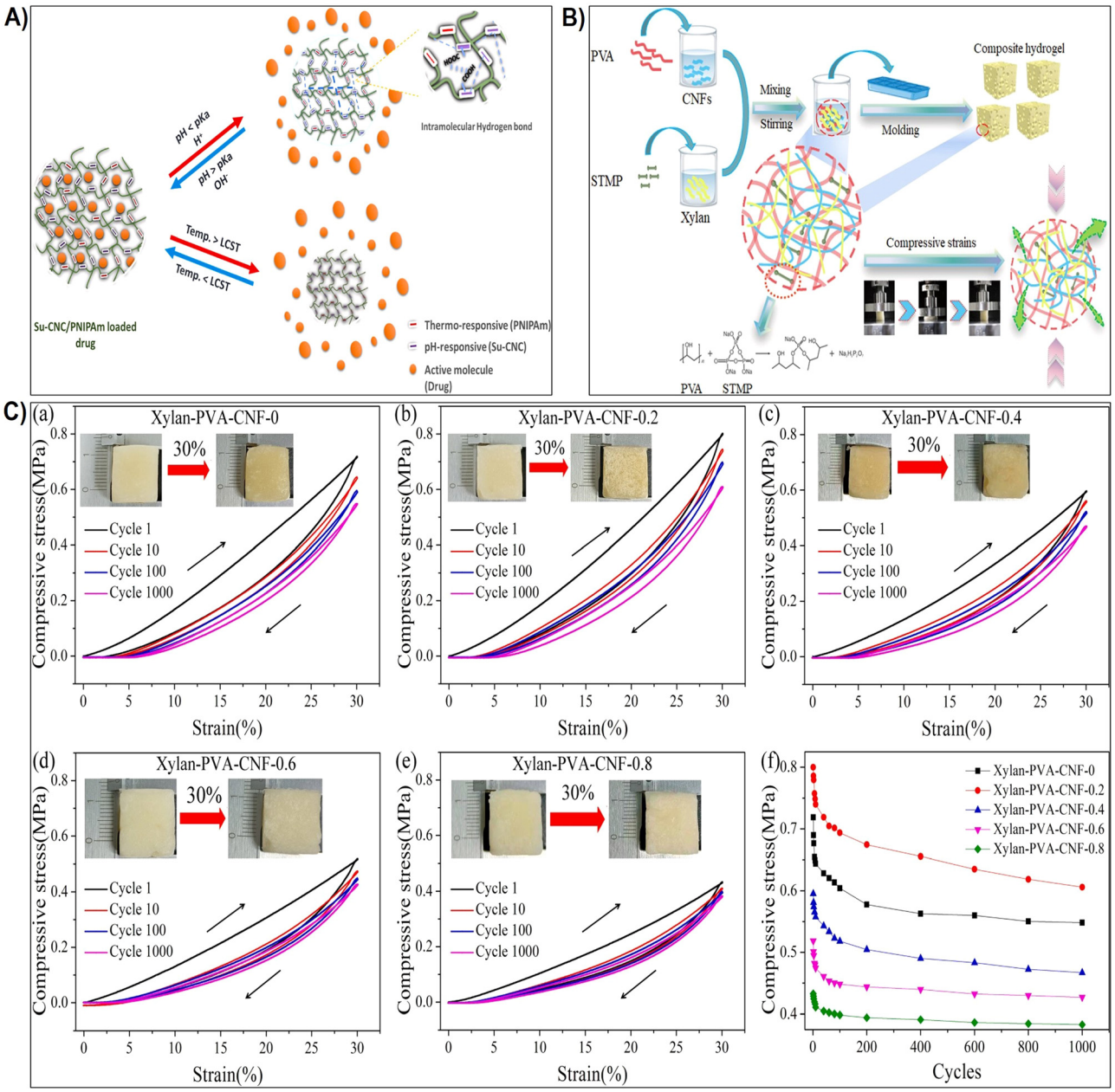

Fig. 5 (A) Schematic representation illustrating the influence of pH and thermo-responsiveness on the drug release. Reproduced with permission from ref. 176 Copyright © 2022 Elsevier. (B) Schematic depiction of the hydrogel preparation process and the proposed behavior of the hydrogel under compression. Reproduced with permission from ref. 177 Copyright © 2023 Elsevier. (C) (a)–(e) Strength-strain curves of xylan/PVA/CNF hydrogels at maximum strains of 30% and after 1000 cycles of loading–unloading; (f) maximum strength plotted against the number of compressive test cycles. Reproduced with permission from ref. 177 Copyright © 2023 Elsevier.

enhancing the recovery ability of the hydrogels, positioning these hydrogels as promising candidates for biomedical applications, particularly in soft-tissue engineering (Fig. 5C).[177]

2.2.2. Etherification. Etherification is a chemical modification process wherein ether linkages are introduced onto nanocellulose surfaces. This is achieved by reacting the hydroxyl groups of nanocellulose with alkyl halides or alkylene oxides. During this reaction, the hydroxyl groups (–OH) on the nanocellulose chains are replaced by ether linkages, which consist of an oxygen atom connected to two carbon atoms.[144,145] This modification enhances the stability and compatibility of nanocellulose, making it a vital component for reinforcing polymers in composite materials. By forming these ether linkages, nanocellulose gains improved resistance to environmental factors and becomes more compatible with a broader range of materials, ensuring its effectiveness as a reinforcing agent in various industrial applications.[139,145] For instance, in a study conducted by Xie *et al.*,[178] to enhance the packaging capabilities of cellulose-based films, composite films of cellulose/polyvinyl alcohol (Cel/PVA) were produced. This involved crosslinking the hydroxyl groups (–OH) within cellulose and PVA, as well as dehydrating/etherifying adjacent PVA chains. The film structure, morphology, mechanical and barrier properties, water resistance, food preservation, and degradation in soil were extensively analyzed.[178] The cellulose-based film (Cel/PVA-10-H), containing 10% PVA and thermally treated at 165 °C, exhibited superior performance. This was primarily due to the crosslinked structure formed by the hydroxyl groups of cellulose and PVA, enhancing tensile strength (77.17 MPa) and elongation at break (9.96%). The film also displayed excellent water resistance and less sensitivity to high humidity, with good preservation and biodegradability.[178]

2.2.3. Silanization. It is a vital chemical modification technique entailing the bonding of silane molecules equipped with reactive groups to nanocellulose surfaces. During this process, silane molecules chemically bind to the nanocellulose, forming a strong and stable interface.[179] This modification significantly enhances the hydrophobicity of nanocellulose, making it less prone to water absorption while improving its compatibility with both organic and inorganic substances. The enhanced hydrophobicity resulting from silanization is crucial for various applications.[147,180] Silanization process can be used to enhance the functionality of nanocellulose as a nanofiller in polymers by modifying its interfacial properties. In the study conducted by Frank *et al.*,[179] three hydrophobic silanization reagents were employed to modify cellulose nanofibrils (CNFs), forming silane-modified CNFs (Si-CNFs). Analytical techniques were utilized to assess the effects.[179] Results showed that silanization produced a nanometer-scale siloxane layer on CNFs, enhancing stability in chloroform-based casting solutions and dispersion in polyhydroxyalkanoates composites. However, increased surface modification inversely affected biodegradability, with extensively silanized samples showing no mineralization, indicating a dense siloxane coating hindering microbial access.[179] In addition, silanized cellulose-based hydrogels have shown promise in tissue engineering for repairing damaged tissues. For example, Hu *et al.*[148] introduced a new composite hydrogel, blending water-soluble chitosan (CS)/hyaluronic acid (HA) with silanized-hydroxypropyl methylcellulose (Si-HPMC) (CS/HA/Si-HPMC) (Fig. 6A). These injectable hydrogels were tested for cartilage tissue engineering without chemical crosslinking agents. Mechanical tests revealed that higher Si-HPMC content led to increased swelling and rheological properties, reduced compressive strength, and faster degradation.[148] Certain formulations, particularly those with 3.0% Si-HPMC and 2.5/4.0% CS/HA, displayed suitable physical and bioactive properties for cartilage tissue engineering (Fig. 6A). *In vitro* experiments with chondrocyte-encapsulated hydrogels showed that an optimal Si-HPMC amount enhanced cell proliferation and extracellular matrix deposition. The hydrogel with 3% Si-HPMC exhibited a regeneration rate of approximately 79.5% at 21 days, suggesting promising potential for *in vivo* bone regeneration and serving as injectable scaffolds for tissue compatibility (Fig. 6A). The findings demonstrated the hydrogel efficacy in joint cartilage repair through tissue engineering.[148] Similarly, Boyer *et al.*[181] developed and characterized an injectable, self-hardening, mechanically reinforced hydrogel (Si-HPCH) made of silanised hydroxypropymethyl cellulose (Si-HPMC) mixed with silanised chitosan for articular cartilage regeneration. The cytocompatibility of Si-HPCH was tested *in vitro* using human adipose stromal cells.[181] *In vivo* experiments involved implanting Si-HPCH mixed with hASC into the subcutis of nude mice to observe cell viability. Additionally, Si-HPCH, with or without canine ASC (cASC), was tested for repairing osteochondral defects in canine femoral condyles. Results showed that Si-HPCH supported hASC viability and activity *in vitro* and *in vivo*, and promoted osteochondral regeneration in canine models, suggesting its potential as a treatment option.[181] In another study, natural cellulosic scaffolds from *Borassus flabellifer* immature endosperm underwent enhancement through chemical oxidation and surface functionalization processes.[182] The oxidized cellulose scaffolds (OCS) were treated with a detergent exchange decellularization process, followed by sodium periodate mediated oxidation, and organosilane-based surface modification using amino (NH_2)-terminated 3-aminopropyltriethoxysilane (APTES) and methyl (CH_3)-terminated octadecyltrichlorosilane (OTS) (Fig. 6B). These modifications improved physiochemical, morphological, and mechanical properties, including swelling capacity, total porosity, surface area, degradation kinetics, and mechanical behavior.[182] Biocompatibility analysis demonstrated enhanced cellular adhesion, proliferation, and osteoblast differentiation, along with increased mineralization (from Fig. 6C to Fig. 6H). Subcutaneous implantation in rats showed active angiogenesis, enhanced degradation, and excellent biocompatibility, suggesting potential for bone tissue repair in non-loading bearing applications.[182]

2.2.4. Sulfonation and sulfatation. Sulfonation is a chemical modification process that involves introducing sulfonic acid groups onto nanocellulose surfaces. This chemical modification is typically achieved through reaction with a sulfonating agent, such as sulfuric acid (H_2SO_4) or chlorosulfonic acid ($ClSO_3H$). The reaction introduces sulfonic acid ($–SO_3H$) groups onto the cellulose chains. This modification

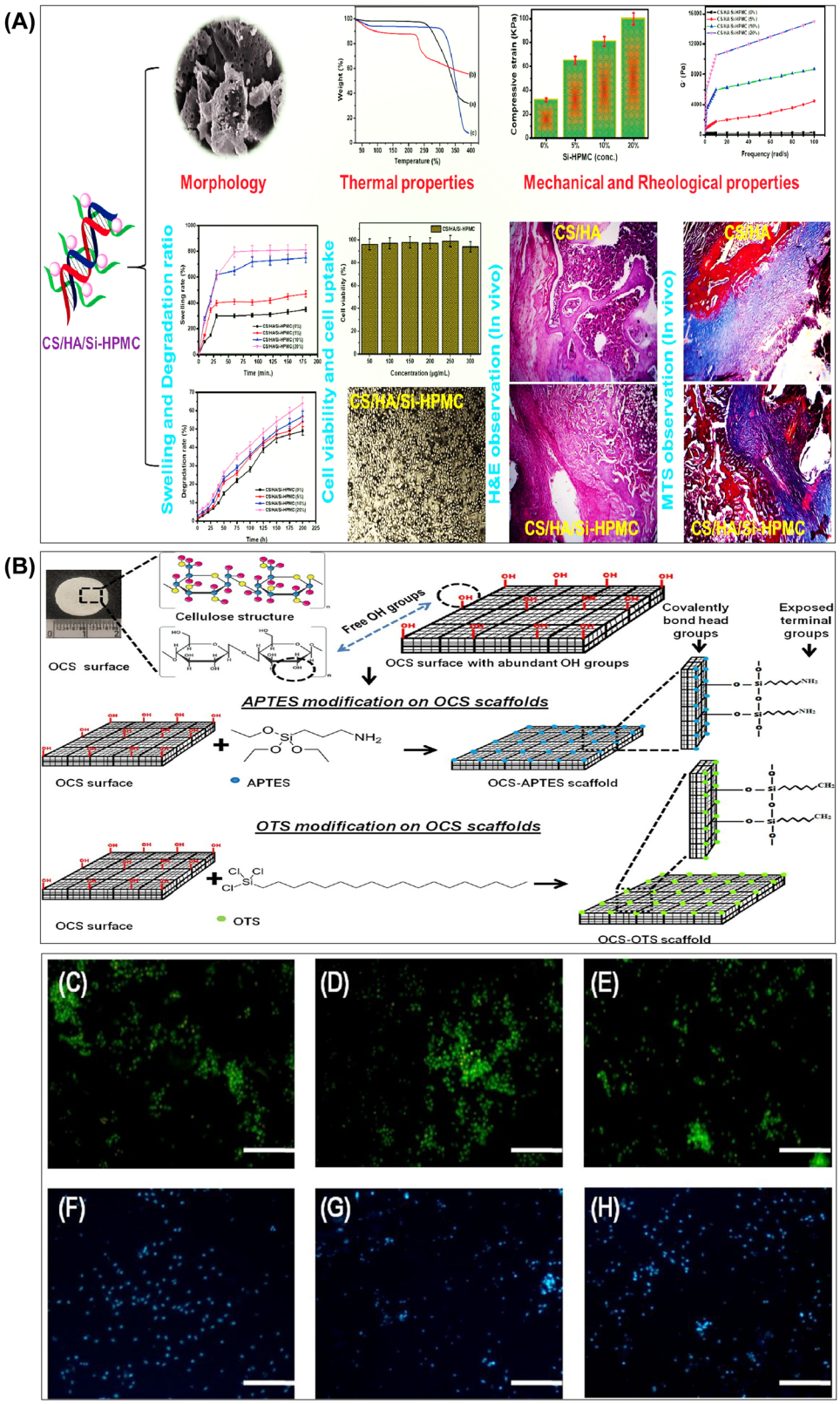

Fig. 6 (A) Summary of results obtained from the investigation of the structural and biological properties of chitosan/hyaluronic acid hydrogel reinforced with silanized-hydroxypropyl methylcellulose as an injectable interpenetrating network for cartilage tissue engineering. Reproduced with permission from ref. 148 Copyright © 2021 Taylor & Francis. (B) Schematic representation of surface functionalization of OCS scaffolds using APTES and OTS *via* chemical grafting to form self-assembled monolayers. Representative images of (C) OCS scaffold, (D) OCS-APTES scaffold, and (E) OCS-OTS scaffold. Cell colonization assessed by Hoechst staining in (F) OCS scaffold, (G) OCS-APTES scaffold, and (H) OCS-OTS scaffold (scale bar: C–H, 100 μm). Reproduced with permission from ref. 182 Copyright © 2022 American Chemical Society.

significantly enhances the material water solubility and chemical reactivity.[149] Sulfonated nanocellulose plays a pivotal role in enhancing the properties of hydrogels, making them particularly valuable for wound healing applications because of their exceptional swelling behavior.[183,184]

However, it is worth noting that there are notable differences between sulfonation and sulfatation of nanocellulose.[185,186] Sulfonation typically involves the reaction of nanocellulose with a sulfonating agent under specific conditions to introduce sulfate groups onto the surface. This process may require harsh reaction conditions and can lead to the degradation of cellulose chains if not carefully controlled.[186] This process results in a high density of sulfate groups distributed along the cellulose chains, imparting a strong negative charge to the nanocellulose surface. This modification enhances the hydrophilicity of nanocellulose and introduces ion-exchange properties, making it useful in various applications.[186,187] On the other hand, sulfatation involves the reaction of nanocellulose with sulfate-containing reagents or precursors, such as sulfur trioxide or sulfuric acid esters. Sulfatation reactions are often milder and can be conducted under more controlled conditions, reducing the risk of cellulose degradation.[188,189] Additionally, sulfatation may offer more flexibility in terms of the degree of substitution and the distribution of sulfate groups on the nanocellulose surface. Unlike sulfonation, sulfatation primarily targets the hydroxyl groups at the C6 position of the glucose units in cellulose, leading to the formation of sulfate esters (–OSO_3H) at this position.[188,190] This selective modification results in a lower density of sulfate groups compared to sulfonation but still imparts a negative charge to the nanocellulose surface. Sulfatation also enhances the hydrophilicity of nanocellulose and introduces ion-exchange properties, similar to sulfonation.[186,188,190]

When exposed to water or physiological fluids, these hydrogels absorb and retain a significant amount of liquid, forming a gel-like structure.[187] This characteristic is particularly advantageous in wound healing applications, where maintaining a moist environment around the wound is crucial for optimal healing. The hydrogel ability to absorb and retain moisture helps create a conducive environment for tissue engineering, accelerates wound healing, and minimizes the risk of infection.[149,191] For instance, Fan *et al.*[184] synthesized carboxymethyl cellulose sulfates by reacting carboxymethyl cellulose with $N(SO_3Na)_3$, formed from sodium bisulfite and sodium nitrite in water. Reaction conditions influenced the degree of substitution (DS), assessed *via* barium sulfate nephelometry.[184] Anticoagulant activity of carboxymethyl cellulose sulfates with varied DS, concentration, and molecular weights was studied through activated partial thromboplastin time, thrombin time, and prothrombin time. Their impact on wound healing was assessed by wound closure rate and histological analysis. Results demonstrated enhanced anticoagulant activity and accelerated wound healing with carboxymethyl cellulose sulfates treatment.[184] In addition, sulfonated cellulose-based hydrogels were widely used for tissue engineering applications.[150,192,193] Dixit *et al.*[193] fabricated an injectable interpenetrating hydrogel system to mimic the extracellular matrix (ECM) and promote the differentiation of stem cells into chondrocytes (Fig. 7A). The hydrogel replicated the gradual stiffening and growth factor presentation of natural ECM, employing silk fibroin for stiffening and sulfated-carboxymethyl cellulose (s-CMC) for growth factor presentation.[193] Combined with tyraminated-carboxymethyl cellulose (t-CMC) and cross-linked with HRP/H_2O_2, the hydrogel provided a soft environment initially, promoting chondrogenic differentiation, which gradually stiffened over time for joint support (Fig. 7A). The presence of s-CMC facilitated the prolonged presentation of growth factors like TGF-β, inducing chondrogenic differentiation of stem cells and deposition of cartilage ECM components. This hydrogel system served as a reservoir of biological cues for cartilage regeneration while offering mechanical support (Fig. 7A).[193] Furthermore, Bhutada *et al.*[150] developed electrospun poly(hydroxybutyrate)/gelatin fibers with anionic sulfated carboxymethylcellulose to immobilize growth factors, mimicking natural electrostatic interactions in the extracellular matrix. This fibrous scaffold effectively bound cationic molecules, remaining cytocompatible and stable in morphology and function.[150] Transforming growth factor-β1 remained immobilized for at least 4 weeks with minimal release (3%). Fibroblast growth factor-2 and connective tissue growth factor, when immobilized, induced proliferation and fibrogenic differentiation of mesenchymal stem cells from infrapatellar fat pad, comparable to or better than free growth factors. These findings highlighted the potential of sCMC conjugated PG fibers in tissue engineering applications.[150] In addition, Huang *et al.*[192] assessed cellulose sulfate suitability as a scaffold for cartilage tissue engineering. The cellulose sulfate mimicked chondroitin sulfate C (CSC), a natural glycosaminoglycan, in sulfation levels and distribution (Fig. 7B). This partially sulfated cellulose (pSC) was integrated into gelatin construct using electrospinning.[192] Scaffold characteristics, including fiber morphology, stability in water, growth factor interaction, and support for mesenchymal stem cell (MSC) chondrogenesis *in vitro*, were analyzed. All scaffolds maintained stability with micron-sized fibers.[192] Increasing pSC concentration correlated with higher levels of transforming growth factor-beta 3 on scaffolds. The scaffold with the highest pSC concentration facilitated enhanced MSC chondrogenesis, demonstrated by increased collagen type II production and expression of cartilage-specific genes (Fig. 7B). These findings underscored pSC sulfate potential as a scaffold for cartilage tissue engineering.[192] In drug delivery, sulfonation imparts nanocellulose with unique features such as increased drug loading capacity and controlled release behavior. The hydrophilic nature of sulphonated nanocellulose allows for efficient encapsulation of water-soluble drugs, while its negatively charged surface facilitates the binding of positively charged drugs. This modification enables precise control over drug release kinetics, contributing to the development of drug delivery systems with improved therapeutic efficacy and reduced side effects.[194] Su *et al.*[195] fabricated polyelectrolyte complexes (PEC) microcapsules, comprising sodium cellulose sulfate-chitosan hydrochloride (sample 1), along with variants patched using sodium tripolyphosphate (sample 2), sodium pyrophosphate (sample 3), and sodium hexametaphosphate (sample 4), all fabricated under mild conditions. The microcapsules exhibited excellent drug loading capacity and encapsulation efficiency

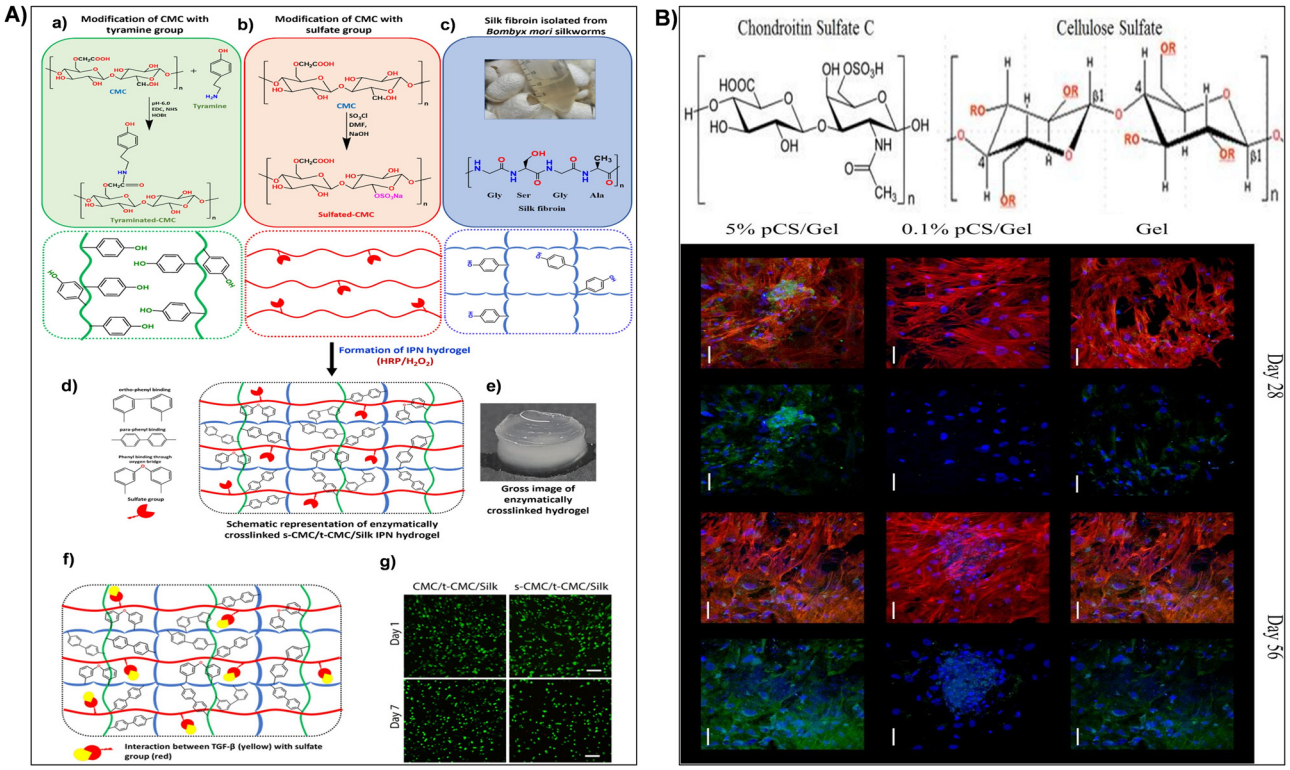

Fig. 7 (A) (a)–(e) Illustration of interpenetrating network (IPN) hydrogel formation using tyraminated-CMC (t-CMC), sulfated-CMC (s-CMC), and silk fibroin *via* enzymatic crosslinking (HRP/H_2O_2). (a) Chemical modification of CMC to t-CMC (upper box) and schematic representation of t-CMC polymeric chains (lower box). (b) Chemical modification of CMC to s-CMC (upper box) and schematic representation of s-CMC polymeric chains (lower box). (c) Isolation of silk fibroin from Bombyx mori silkworms (upper box) and schematic representation showing tyrosine residues on silk fibroin (lower box). (d) Enzymatically crosslinked polymeric network of s-CMC/t-CMC/silk IPN hydrogel. (e) Macroscopic image of enzymatically crosslinked s-CMC/t-CMC/silk IPN hydrogel. Reproduced with permission from ref. 193 Copyright © 2024 Royal Society of Chemistry. (B) (a) Structure of chondroitin sulfate C (CSC) or chondroitin-6-sulfate (a) and cellulose sulfate (b) where R = $-SO_3Na$ or $-H$ depending on degree of sulfation. (b) Confocal microscopy images of cells on Gel, 0.1% pSC/Gel, and 5% pSC/Gel in CCM at day 28 and 56. Red indicates F-actin, blue indicates the nucleus, and green indicates collagen type II. Merged image showing all three stains is on the left and the same image showing nucleus (blue) and collagen type II (green) staining is on the right for each group at each time point. Magnification = 40×. Scale bar = 50 μm. Reproduced with permission from ref. 192 Copyright © 2017 Mary Ann Liebert, Inc.

(max. 66.9 ± 4.6% and 74.2 ± 5.1%).[195] *In vitro* release studies indicated that samples 2 and 3 had a higher cumulative drug release rate of 5-aminosalicylic acid and released completely within 12 hours. The drug release mechanisms were identified as mainly diffusion-controlled for samples 1 and 3, while samples 2 and 4 followed a non-Fickian transport mechanism. These findings suggested that PEC microcapsules, consolidated by polyphosphates, held promise as drug delivery vehicles with sustained release profiles.[195]

2.2.5. Carboxymethylation. Carboxymethylation of nanocellulose involves chemically attaching carboxymethyl groups (–CH_2–COOH) to the structure of nanocellulose. This is typically achieved by reacting nanocellulose with sodium chloroacetate in the presence of an alkali, such as sodium hydroxide.[156,196] During the reaction, hydroxyl groups on the nanocellulose surface are substituted with carboxymethyl groups, imparting a negative charge to the nanocellulose and enhancing its water solubility.[197] Furthermore, carboxymethylation significantly enhances the biocompatibility of nanocellulose, making it compatible with biological systems and tissues. In tissue engineering, carboxymethylated nanocellulose offers several advantages. The introduction of carboxymethyl groups enhances the biocompatibility and water dispersibility of nanocellulose, making it more suitable for biological applications.[198] Carboxymethylated nanocellulose can be incorporated into composite hydrogels for tissue engineering, providing a biomimetic environment that supports cell growth and tissue engineering.[199–202] In a study, Janarthanan *et al.*[201] synthesized carboxymethyl cellulose (CMC)–glycol chitosan (GC) hydrogel using 3D printing for tissue engineering (Fig. 8A). Hydrogels of different compositions (C70G30, C50G50, and C30G70) were fabricated under physiological conditions. Scanning electron microscopy showed their crosslinked porous structure. These gels exhibited good swelling, porosity, and *in vitro* degradation profiles.[201] Initial cytotoxicity tests using mouse osteoblastic cells confirmed the biocompatibility of the hydrogels, especially the C50G50 grade, which also demonstrated excellent printability and stability post-printing. Optimized 3D printing parameters produced stable lattice structures (Fig. 8B). Stability tests in various conditions confirmed the robustness of the hydrogels, attributed to imine bonds and ionic interactions.[201] Lactoferrin-incorporated C50G50 hydrogels

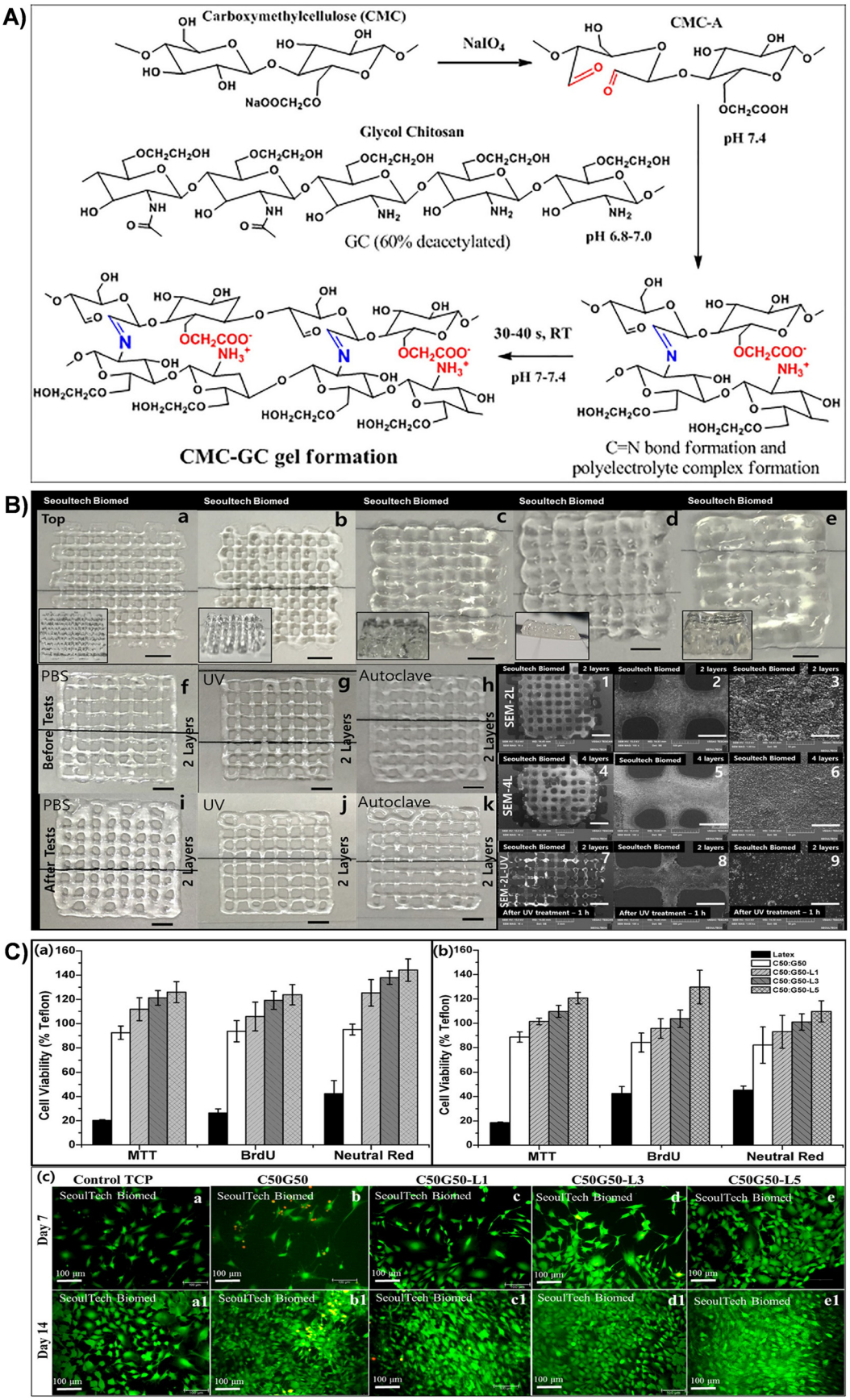

Fig. 8 (A) Schematic representation of gel formation *via* the Schiff base reaction between the aldehyde group of CMC-A and the amine group of GC, resulting in imine bond formation and polyelectrolyte complex formation. (B) 3D printed C50G50 gel lattice structures with stability tests: top views of samples with (a)–(e) 2, 4, 6, 8, and 16 layers (scale bar: 2 mm). Side views provided as inserts. Stability tests: digital images of 2-layer structures before (f)–(h) and after (i)–(k) exposure to PBS, UV irradiation, and autoclaving. SEM images of 2-(1–3) and 4-layer structures (4–6) at various magnifications [scale bar: (1,4) – 2 mm; (2,5) – 500 μm; (3,6) – 50 μm]. SEM images of 2-layer structure samples after UV treatment (1 h) (7–9) (scale bar: (7) – 2 mm; (8) – 500 μm; (9) – 50 μm). (C) Viability assays of MC3T3 and BM MSC cells using MTT, BrdU, and Neutral red assays for different lactoferrin-incorporated CMC-GC gels. Live/dead assay images of lactoferrin-incorporated CMC-GC gels seeded with MC3T3 cells at days 7 and 14. Reproduced with permission from ref. 201 Copyright © 2020 Elsevier.

exhibited sustained release over 21 days and demonstrated high biocompatibility (>80%) *in vitro*, confirmed by cytotoxicity assays (MC3T3 cells, bone marrow mesenchymal stem cells) and live/dead assay (MC3T3 cells). Increased osteoblast cell viability correlated with higher lactoferrin concentrations, suggesting potential as ink for 3D printing in tissue engineering (Fig. 8C).[201] In another study, polyvinyl alcohol (PVA) underwent crosslinking with glutaraldehyde (GA), with varying mole ratios of GA/PVA and different amounts of plant-derived carboxymethyl cellulose (CMC). Porous scaffolds were formed through freeze-drying.[202] The objective was to examine the influence of CMC integration and crosslinking density on scaffold pore structure, swelling behavior, mechanical traits, and potential for engineered cartilage. The PVA/CMC scaffold exhibited lower glass transition temperature (T_g) and Young's modulus compared to the PVA control. CMC addition altered pore architecture and enhanced scaffold swelling. Toxicity and cell attachment tests were conducted, suggesting tailored PVA/CMC scaffolding could support cartilage formation.[202] In addition, the carboxymethylated nanocellulose demonstrates improved dispersibility, making it highly suitable for applications in drug delivery systems, where uniform dispersion of nanocellulose particles is essential for controlled drug release. Carboxymethylated nanocellulose can serve as a versatile carrier for pharmaceutical agents.[39,203,204] The carboxymethyl groups provide functional sites for drug loading through electrostatic interactions or chemical conjugation. The nanocellulose matrix can encapsulate and protect drugs, enabling controlled release over time. The biocompatibility and tunable properties of carboxymethylated cellulose make it an attractive candidate for drug delivery systems with reduced toxicity and improved therapeutic efficacy.[39,153,205–207] For instance, Ali *et al.*[208] formulated novel near-infrared (NIR) light-responsive hydrogels using reactive oxygen species-cleavable thioketal cross-linkers and norbornene modified carboxymethyl cellulose. These hydrogels, swiftly formed under physiological conditions, developed porous structures upon generating N_2 gas. Indocyanine green (ICG) and doxorubicin (DOX) were co-encapsulated within these hydrogels.[208] Under NIR-irradiation, the hydrogels exhibited controlled DOX release (>96%), facilitated by thioketal bond cleavage through ROS generated from ICG. Conversely, minimal DOX release (<25%) occurred without NIR-light. Notably, the hydrogels demonstrated high cytocompatibility with HEK-293 cells, while NIR-irradiated DOX + ICG-loaded hydrogels effectively suppressed HeLa cancer cell proliferation, enhancing the therapeutic outcome.[208] Furthermore, layered double hydroxides (LDHs) infused with non-steroidal anti-inflammatory drugs (NSAIDs) such as ibuprofen, ketoprofen, and ketorolac were combined with carboxymethylcellulose (CMC) to improve their rheological properties, sustain release, and enhance mucoadhesion. High drug-loaded LDH-NSAID particles were successfully synthesized, showing aggregation and positive charges facilitating interaction with CMC.[155] The resulting dispersions behaved as viscous fluids, with ketoprofen leading to a more gel-like consistency. Compared to formulations with pure drugs, CMC/LDH-NSAID dispersions exhibited prolonged drug release, primarily influenced by anion exchange. These formulations demonstrated significant mucoadhesive properties, requiring further optimization for enhanced release and rheological characteristics.[155]

2.2.6 Phosphorylation. This a chemical modification process involving the introduction of phosphate groups onto nanocellulose surfaces. This modification enhances the material affinity for calcium ions, a crucial component in bone mineralization. Phosphorylated nanocellulose plays a pivotal role in the field of bone tissue engineering.[157] By promoting bioactivity and mineralization, it provides an ideal environment for effective bone engineering. The introduced phosphate groups facilitate interactions with calcium ions, mimicking the natural mineralization process in bones.[209] This bioactive characteristic not only encourages the adhesion and proliferation of bone cells but also supports the formation of a mineralized matrix, essential for the integration of implants and the engineering of bone tissues. In the context of bone mineralization, phosphorylated nanocellulose-based hydrogels can serve as scaffolds for calcium phosphate deposition. Calcium phosphate is a key component of bone mineral, providing structural support and rigidity. When introduced into a biological environment, phosphorylated nanocellulose can attract calcium ions, facilitating their binding and subsequent mineralization. This process mimics the natural mineralization that occurs in bone tissue and can contribute to the development of biomimetic materials for bone engineering and tissue engineering applications.[158,209] Phosphorylated nanocellulose stands as a promising biomaterial, offering enhanced capabilities in fostering bone engineering and contributing significantly to advancements in the field of regenerative medicine.[210,211] Various research works involving phosphorylated cellulose based scaffolds for bone tissue engineering have been highlighted in the literature.[158,212] Wang *et al.*[212] introduced phosphorylated cellulose nanofibrils (pCNF), into a dextran/methacrylated gelatin-based aqueous two-phase emulsion (ATPE) system (p_ATPE) for extrusion-based bioprinting of preosteoblastic cells. The inclusion of pCNF improved emulsion stability, altered rheological behaviors, enhanced damping capacity, and mineralization ability of crosslinked hydrogels.[212] To showcase p_ATPE ink printability in extrusion-based 3D printing, complex structures were fabricated, demonstrating filament fidelity and printing accuracy (Fig. 9A).

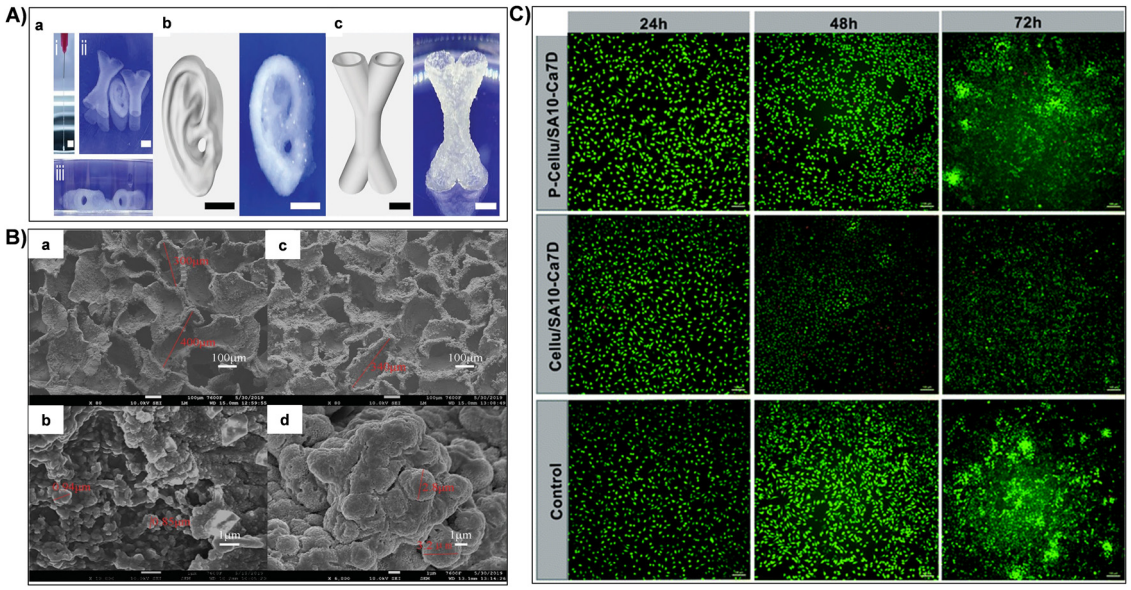

Fig. 9 (A) (i) Continuous extrusion of composite inks demonstrating structural integrity post-extrusion. Representative images from (ii) frontal and (iii) lateral views of printed structures immersed in PBS after 7 days. (b) and (c) Representative images of printed centimeter-scale hydrogels featuring complex structures (human ear and X-shaped hollow tubes). Reproduced with permission from ref. 212 Copyright © 2024 John Wiley & Sons, Inc. (B) SEM images showcasing the surface of Cellu/SA10-Ca7D (a) and (b) and P-Cellu/SA10-Ca7D (c) and (d): (a) and (c) low magnification; (b) and (d) high magnification. Reproduced with permission from ref. 158 Copyright © 2021 Royal Society of Chemistry. (C) Live/dead staining of L929 cells at 24 h, 48 h, and 72 h for Cellu/SA10-Ca7D and P-Cellu/SA10-Ca7D. Scale bar: 100 μm. Reproduced with permission from ref. 158 Copyright © 2021 Royal Society of Chemistry.

Resulting macroporous hydrogels with pCNF exhibited increased cell activity, viability, alkaline phosphatase activity, and osteoblastic gene expression, facilitating the formation of biomineralized nodules *in vitro*. This integration significantly enhanced the physiochemical and biological performance of macropore-forming bioinks, rendering them suitable for engineering *in vitro* bone models.[212] Moreover, in the study conducted by Zha *et al.*,[158] cellulose (Cellu)/sodium alginate (SA) composite (Cellu/SA) sponges were prepared using the freeze-drying technique. Incorporating SA into the cellulose matrix effectively enhanced the macroporous properties of the composite scaffolds. Phosphate groups were then grafted onto the composite sponge surface *via* esterification reaction to stimulate apatite crystal formation.[158] In order to induce hydoxyapatite formation, original sponges and phosphorylated sponges were immersed in simulated body fluid solution at 37 °C for 7 days. The obtained samples were labeled as Cellu/SA (00, 10, 20, 30)-Ca7D and P-Cellu/SA (00, 10, 20, 30)-Ca7D. SEM micrographs revealed robust deposition of apatite nanoparticles, forming rod-like crystals and promoting greater mineralization on phosphorylated cellulose (P-Cellu)/SA sponge (Fig. 9B).[158] The calcium/phosphate molar ratio of the surface-applied hydroxyapatite was determined as 1.45. Biocompatibility of the sponges was demonstrated through CCK8 assay and live/dead fluorescence staining of L929 cells, with over 80% cell activity observed (Fig. 9C). Consequently, the study concludes that these mineralized phosphorylated cellulose/SA composite sponges hold promise for bone repair.[158]

2.2.7 Polycondensation. This chemical modification plays a crucial role in strengthening nanocellulose materials for load-bearing applications. In this process, covalent bonds are formed between nanocellulose chains, resulting in a more interconnected and robust structure.[160,213] The primary goal of polycondensation is to enhance the mechanical strength of nanocellulose, making it suitable for applications where structural integrity and durability are paramount.[214] For instance, a hybrid of polycondensate-coated cellulose nanofiber (CNF) was developed by polymerizing coupling agent monomers onto the CNF surface, enhancing its compatibility with polylactic acid (PLA). The coated CNFs significantly improved the dispersion of CNFs within PLA and boosted mechanical, thermal, and processing properties of resulting composites.[214] A 2.5 wt% addition of polycondensate-coated CNFs increased tensile strength, Young's modulus, and tensile toughness by approximately 27%, 51%, and 68% respectively, while also enhancing elasticity and melt strength.[214] By creating covalent bonds between nanocellulose chains, polycondensation effectively reinforces the material, improving its load-bearing capacity. This enhanced mechanical strength is especially vital in applications such as load-bearing implants and scaffolds, where the material needs to withstand significant forces and maintain its structural integrity over time.[215] Examples of these applications include bone implants, where polycondensed nanocellulose ensures that the materials can support the weight and mechanical stresses in the living organism, promoting successful tissue engineering and long-lasting performance.[161,214] Nanocellulose could be modified through polycondensation reactions to boost its surface activity, thus enhancing its capability to inhibit bacterial growth and expanding its potential for biomedical applications. In the present study, aminoalkyl-grafted bacterial cellulose (BC) membranes were

prepared through alkoxysilane polycondensation with 3-aminopropyltriethoxysilane (APTES).[215] Morphological and chemical composition analyses confirmed successful grafting of aminoalkylsilane groups onto BC membranes *via* covalent bonding. Surface morphology and roughness altered post-chemical grafting. Additionally, APTES grafting rendered the membranes less hydrophilic compared to native BC.[215] These modified membranes exhibited potent antibacterial activity against *Staphylococcus aureus* and *Escherichia coli*, while remaining non-toxic to normal human dermal fibroblasts. These findings suggested the potential of aminoalkyl-grafted BC membranes for biomedical applications.[215]

2.2.8 Cationization. The process involves introducing positive charges onto nanocellulose surfaces. This is typically achieved through chemical modification, where amino or quaternary ammonium groups are attached to the cellulose structure.[216,217] The process often utilizes reactions with epoxides, amines, or other cationic agents. This modification is crucial for enhancing interactions with negatively charged molecules, particularly in biomedical applications.[216] Cationized nanocellulose plays a crucial role in gene delivery systems by acting as a carrier for genetic material. Through the introduction of positive charges, cationized nanocellulose can effectively bind to DNA, forming stable complexes. This interaction is essential for facilitating the transportation of DNA into cells during gene delivery processes. The positively charged nanocellulose complexes are attracted to the negatively charged cell membranes, which enables efficient cell transfection.[218] By improving the binding affinity between the carrier (cationized nanocellulose) and the genetic material, this modification ensures successful gene delivery, an essential process in various biomedical applications such as gene therapy and genetic research.[218,219] For instance, cellulose nanocrystal (CNC), recognized for its abundance and biocompatibility, was explored for various applications due to its properties such as ultrafine structure, transparency, purity, crystallinity, and strength. Kim *et al.*[220] developed CNC/zinc/DNA (CZD) nanocomplexes without chemical conjugations, utilizing a ligand-to-metal charge transfer transition (LMCT) between divalent metal ions and CNC phosphate groups with DNA. First, divalent metal ions were introduced to DNA to enable the LMCT transition for DNA incorporation into CNC.[220] Optimization of CZD formation conditions was achieved, and gene transfection efficacy was confirmed in myocardial and skin cells. CZD effectively delivered DNA into cells, leading to high gene expression, proposing a chemical-conjugation-free gene delivery system utilizing CNC.[220] Furthermore, cationized nanocellulose-based hydrogels have been utilized in tissue engineering for diverse applications. Their capacity to emulate the extracellular matrix, coupled with their positive charge, enhances cell adhesion, proliferation, and differentiation.[162,163] This cationic attribute boosts the bioactivity of nanocellulose, facilitating crucial cellular processes vital for tissue engineering. Additionally, the water-retention ability and mechanical strength of cationized nanocellulose render it suitable for hydrogel formulations. These hydrogels can act as three-dimensional matrices for encapsulating cells, offering a supportive milieu for cell proliferation.[162,163] In the study conducted by Pajorova *et al.*,[165] a commercially available mesh underwent surface and physicochemical enhancement through coating with wood-derived cellulose nanofibrils (CNFs). Three types of coatings were examined: positively charged cationic cellulose nanofibrils (cCNFs), negatively charged anionic cellulose nanofibrils (aCNFs), and a blend of both (c + aCNFs), aiming to serve as carriers for skin cells.[165] Fig. 10A illustrates the schematic depiction of the process employed to fabricate various coating topographies on cellulose meshes using cCNF and aCNF solutions. SEM analysis (Fig. 10B) showed CNF-coated mesh topographies varied based on CNF volume and charge. Solutions of 150 μL (a150, c150) covered mesh fibers and pores, while 600 μL (c600, a600) formed thin films. cCNFs mostly formed flat coatings, while aCNFs created 3D microtopographies. AFM determined surface roughness: a600 had Ra median of 9.04 nm, c600 had 10.20 nm, and c + a had 55.76 nm (Fig. 10B). Normal human dermal fibroblasts (NHDFs) and human adipose-derived stem cells (ADSCs) were seeded onto these carriers to assess adhesion, spreading, morphology, and proliferation. Notably, aCNF coating significantly boosted proliferation for both cell types, while cCNF enhanced ADSC adhesion exclusively.[165] The 3D structure of cCNF coating promoted NHDF survival. The c + aCNF composite exhibited advantages from both CNF types, showing potential for future skin tissue engineering applications (Fig. 10C).[165] In addition, Damouny *et al.*[164] fabricated injectable hydrogels for tissue engineering using a mixture of hyaluronic acid (HA), gelatin, and cationic cellulose nanocrystals (cCNCs). These components formed a 3D network through electrostatic interactions and hydrogen bonding. The hydrogels had low viscosity for easy injection, maintained stability under low stresses, and recovered their structure quickly.[164] Higher cCNC content reduced swelling and slowed degradation compared to pure HA and HA-gelatin samples. Biological tests showed high cell viability, with fibroblast proliferation reaching about 200% compared to the control group after 11 days. These findings suggested promising applications in biomedical fields like dermal fillers and tissue regeneration scaffolds.[164]

2.2.9 Coating. Coating is a strategic modification process where thin films are meticulously applied onto nanocellulose surfaces, imparting crucial enhancements for drug delivery applications. In this process, nanocellulose particles are enveloped in a protective layer, boosting their stability and enabling precise control over drug release. These coated nanocellulose particles play a pivotal role in pharmaceutical applications.[221,222] Coating on nanocellulose is typically achieved through various techniques, such as physical adsorption, chemical grafting, or layer-by-layer assembly.[40,214,222–224] In physical adsorption, polymers or other materials adhere to the nanocellulose surface through non-covalent interactions. Chemical grafting involves forming covalent bonds between the coating material and nanocellulose, providing a more stable attachment. Layer-by-layer assembly alternates the deposition of oppositely charged materials, creating a multilayered coating.[138,166] The coating serves as a shield, safeguarding the integrity of the nanocellulose core. This protective layer not only prevents premature drug release but also ensures the stability of the encapsulated therapeutic agents. In a recent study, a

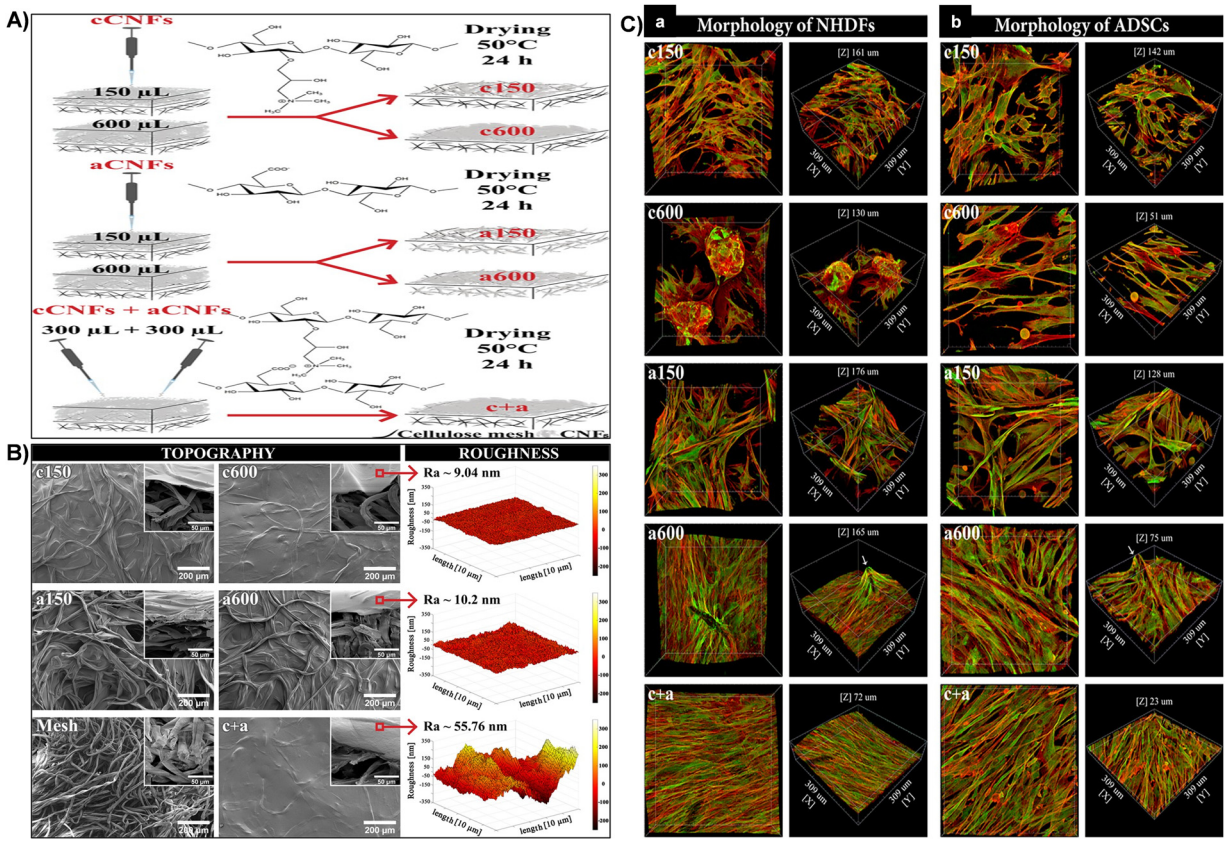

Fig. 10 (A) Schematic representation of the process for fabricating diverse coating topographies on cellulose meshes using cCNF and aCNF solutions. (B) Surface topography and roughness. SEM images of c150, c600, a150, a600, and c + aCNF-coated and uncoated meshes (front and side views, inset). AFM measured roughness of c600, a600, and c + aCNF-coated meshes (right). (C) Cellular morphology of NHDFs (A) and ADSCs (B) influenced by CNF-coated mesh topography after 7 days of cultivation. 3D projection microscopy images showing cells on CNF-coated meshes. F-actin of cell cytoskeleton stained in red, vinculin in green. Confocal microscope, 40× objective magnification. Reproduced with permission from ref. 165 Copyright © 2021 American Chemical Society.

straightforward yet efficient technique for coating cellulose onto chitosan (CS) hydrogel beads and utilizing them as drug carriers was proposed. The beads underwent a one-pot, one-step process where cellulose, dissolved in 1-ethyl-3-methylimidazolium acetate, an ionic liquid (IL), was applied as a coating.[225] Water molecules within the CS beads diffused outward upon encountering the cellulose-IL mixture, serving as an anti-solvent. This facilitated the coating of the bead surface with regenerated cellulose. Verapamil hydrochloride (VRP), a model drug, was impregnated into the cellulose-coated CS hydrogel beads to test their potential as a drug carrier.[225] Submersion of the VRP-impregnated beads in simulated gastric fluid (pH 1.2) resulted in the release of VRP in an almost linear pattern, indicating controlled drug release. These easily manufactured cellulose-coated CS beads demonstrated promise as carriers for drug release control.[225] Coating nanocellulose was also successfully used to fabricate composite hydrogels for tissue engineering applications. Kumar *et al.*[226] detailed the creation of additively manufactured 45S5 Bioglass scaffolds reinforced with functionalized multi-walled carbon nanotubes (CNTs) coated with cellulose nanowhiskers (CNWs). Carboxymethyl cellulose (CMC) served as an ink carrier with suitable shear thinning behavior. The reinforcement and coating led to a 32% increase in compressive strength and an 88% increase in toughness.[226] Microcomputed tomography revealed suitable scaffold porosity and interconnectivity. The CNWs coating enhanced surface roughness, potentially aiding bone cell attachment. *In vitro* studies in simulated body fluid (SBF) confirmed scaffold bioactivity, suggesting efficient fabrication of hybrid scaffolds for bone tissue engineering.[226] Additionally, in another investigation, aligned electrospun cellulose/CNCs nanocomposite nanofibers (ECCNNs) loaded with bone morphogenic protein-2 (BMP-2) were employed for the first time.[227] The study focused on examining the osteogenic differentiation of human mesenchymal stem cells (BMSCs) *in vitro* and collagen assembly direction as well as cortical bone regeneration *in vivo* using a rabbit calvaria bone defect model, supported by micro computed tomography and histology analyses.[227] The results demonstrated the beneficial biological compatibility of aligned ECCNNs scaffolds loaded with BMP-2. BMSCs exhibited growth orientation along the aligned nanofiber morphology, leading to increased alizarin red stain, alkaline phosphatase activity, and calcium content *in vitro*.[227]

2.2.10 Adsorption. Adsorption refers to the process by which molecules, ions, or other substances adhere to or accumulate on the surface of nanocellulose. Nanocellulose, with its

high surface area and fibrous structure, provides an extensive and accessible surface for interactions with other compounds. During adsorption, molecules are attracted to the surface of nanocellulose due to various forces, such as van der Waals forces, hydrogen bonding, electrostatic interactions, and chemical bonding.[169,170,228] Nanocellulose, with its expansive surface area and unique structural properties, exhibits exceptional adsorption capabilities. The high surface area allows nanocellulose to efficiently adsorb bioactive molecules, a phenomenon crucial for various applications.[229,230] In the context of enzyme immobilization, nanocellulose acts as a versatile platform. Enzymes, when adsorbed onto nanocellulose surfaces, retain their catalytic activity. This immobilization technique enhances enzyme stability and reusability, making it invaluable in industrial processes and biocatalysis applications.[231–233] In a recent study, 2,2,6,6-tetramethylpiperidine-1-oxyl-oxidized cellulose nanofibers (TOCNs) with a width of approximately 4 nm and a large specific surface area were investigated. TOCN, a negatively charged bionanomaterial with carboxy groups on its surface, demonstrated promising physical properties. Particularly, it was explored as an adsorbent for biomolecules in biotechnological applications.[168] The research focused on the adsorption behavior of pyrroloquinoline quinone-dependent glucose dehydrogenase (PQQ-GDH) on TOCN and evaluated the activity, structure, and long-term stability of the enzyme. Transmission electron microscopy revealed aligned enzyme adsorption on TOCNs, while circular dichroism determined the enzyme structure. Interestingly, the adsorbed enzyme displayed enhanced activity and stability, suggesting TOCN potential as a biomolecule immobilization material for developing stable and active enzyme-based biomaterials.[168] Additionally, the adsorptive capacity of nanocellulose also plays a pivotal role in biosensing technologies. By adsorbing specific biomolecules onto nanocellulose surfaces, biosensors can detect target analytes with high sensitivity and specificity. This application is instrumental in medical diagnostics, environmental monitoring, and food safety analysis.[234,235] A research study presented the development of a colorimetric biosensor utilizing nanocellulose (NC) supports drop-deposited onto a cellulose paper substrate for detecting glucose in point-of-care applications. Microcrystalline cellulose (MCC) was oxidized with 2,2,6,6-tetramethylpiperidine-*N*-oxyl radical, sodium hypochlorite, and potassium bromide to produce carboxylated NC.[236] Carboxyl-NC was applied onto cellulose substrate and employed as support for glucose oxidase (GOx), horseradish peroxidase (HRP), and ABTS reactions, aiming for a color-based glucose detection system.[236] The sensor, integrated with GOx on the carboxyl-NC/cellulose substrate, exhibited a linear response to glucose concentrations ranging from 1.5 to 13.0 mM. This renewable-material-based test-strip demonstrated enhanced color homogeneity and linear response compared to conventional systems.[236] Moreover, the adsorption of bioactive molecules onto nanocellulose serves as a foundation for drug delivery systems. Pharmaceuticals and therapeutic agents can be efficiently adsorbed onto nanocellulose carriers, ensuring controlled release and delivery.[234,237–239] Sodium alginate-bacterial cellulose (SA-BC) had been developed as a nanocomposite hydrogel with multi-layered porous surfaces using an *in situ* biosynthesis modification method. Glycerol-pretreated Moso bamboo enzymatic hydrolysate served as the carbon source for glucose substitution, forming SA-bamboo-BC.[239] Different dosages of SA (0.25%, 0.5%, 0.75%, and 1%) were combined with BC through hydrogen bonding. Among them, SA-bamboo-BC-0.75 exhibited enhanced thermal properties compared to native BC. pH-dependent dynamic swelling/deswelling showed increased swelling ratio at pH 7.4 (613%) and lower at pH 1.2 (366%), attributed to $-COO^-$ electrostatic repulsion.[239] Bovine serum albumin (BSA) adsorbed on lignin from MBEH showed poor drug release, while lysozyme displayed higher drug release (92.79% over 60 h at pH 7.4) due to static attraction with $-COO^-$ of SA-bamboo-BC-0.75. SA-bamboo-BC demonstrated sufficient swelling, drug-release, and biocompatibility for substrate use.[239] In tissue engineering, enhancing hydrogel surfaces through adsorption of cellulolytic materials is crucial for improving cell–matrix interactions. A study involved fabricating thermoplastic polyurethane (TPU) nanofibers *via* electrospinning, followed by surface modification with cellulose nanofibrils (CNF) using ultrasonic assistance, resulting in TPU/CNF nanofibers.[240] Subsequently, TPU/CNF-polydopamine (PDA) composite nanofibers with core/shell structure were formed through PDA coating. The addition of CNF facilitated uniform PDA coating, enhancing water absorption and hydrophilicity, while also improving mechanical properties and cell attachment, indicating potential for tissue engineering scaffolds.[240]

2.2.11 Initiation. Initiation is a chemical modification method used to tailor the properties of nanocellulose. It begins by introducing radical initiators, which are compounds that generate highly reactive radicals upon activation. These initiators are typically grafted onto the nanocellulose surfaces. Once the radicals are formed, they serve as reactive sites for subsequent polymerization reactions.[171,172] One of the key outcomes of initiation and subsequent graft polymerization is the significant enhancement of mechanical properties of nanocellulose. These properties include tensile strength, flexibility, and toughness. The grafted polymers form a network structure on the nanocellulose surface, reinforcing its mechanical integrity.[241] For instance, a strategy employing interpenetrating polymer networks was proposed to create double network hydrogels from cellulose and polyacrylamide, boasting robust mechanical strength and pH-responsive traits. The synergistic bonding between the networks dissipated mechanical energy, as confirmed by stress–strain and rheology tests.[242] The resulting cellulose–polyacrylamide interpenetrating network (C-PAM IPN) hydrogels exhibited compressive strength and modulus up to 5.62 and 22.47 MPa, respectively, significantly surpassing cellulose-only hydrogels. Additionally, these resilient C-PAM IPN hydrogels displayed pH sensitivity across various solutions, offering a versatile strategy for enhancing cellulose-based hydrogel properties.[242] In addition, cellulose-based hydrogels, prepared through free radical polymerization, can be effectively utilized for biomedical purposes. In a study, stimuli-responsive

polymer (poly(dimethylaminoethyl methacrylate)) was successfully grafted onto cellulose through free radical polymerization of a vinyl/divinyl monomer in cellulose solution.[243] Subsequent irradiation with ionizing radiation (at doses of 10, 30, or 100 kGy) increased grafting and crosslinking efficiency. Dynamic viscoelastic behavior analysis showed solid-like behavior with a complex modulus range of 14–39 kPa, suitable for biomedical applications. Incorporating Ag particles and adsorbing Fe^{3+} ions enhanced the hydrogel functionalities, potentially useful in wound treatment.[243] Furthermore, favorable hydrogels with strong wet tissue adhesion and biocompatibility have garnered attention as replacements for traditional sutures in wound closing. Inspired by mussel adhesive protein, a series of dopamine modified carboxymethyl cellulose (CMC-DA) hydrogels were synthesized *in situ* using enzymatic crosslinking with horseradish peroxidase (HRP) and H_2O_2. This enzymatic catalytic method efficiently initiated radical polymerization.[244] The resulting biomimetic CMC-DA hydrogel exhibited a 6-fold increase in wet tissue adhesion strength (28.5 kPa) compared to commercial fibrin glue. Gelation time, swelling ratio, and rheological properties were controllable by adjusting HRP, H_2O_2, and CMC-DA concentrations. These hydrogels demonstrated good biodegradation and biocompatibility *in vitro*, indicating promising potential as tissue adhesive materials.[244]

2.2.12 Oxidation. Oxidation of nanocellulose involves the introduction of carbonyl and carboxyl groups, enhancing its reactivity and versatility. This chemical modification is particularly crucial for biomedical applications.[245,246] The oxidation of nanocellulose involves modifying its structure by introducing oxygen-containing functional groups, typically through chemical treatments like periodate oxidation or TEMPO-mediated oxidation. In periodate oxidation, sodium periodate is employed to cleave the C2–C3 bond in the anhydroglucose units of cellulose, creating aldehyde groups.[124,247–249] TEMPO-mediated oxidation involves the use of 2,2,6,6-tetramethylpiperidine-1-oxyl (TEMPO) and sodium bromide to selectively oxidize the primary hydroxyl groups to carboxylate (Fig. 11A).[37,250–252] These groups significantly increase its chemical reactivity.[245,246] In the field of biomedical engineering, oxidized nanocellulose finds valuable applications, especially in wound dressings, tissue engineering, and drug delivery systems.[249,253,254] In wound dressings, the enhanced reactivity allows for better integration with wound surfaces, promoting faster healing. The introduction of oxygen-containing functional groups enhances the hydrophilicity of nanocellulose, making it ideal for tissue engineering. The modified surface facilitates cell adhesion and proliferation, essential aspects for tissue engineering.[254] For instance, in a recent work, Wu *et al.*[255] aimed to enhance the biocompatibility of bacterial cellulose pellicle (BCP) for biomedical purposes like wound dressing. The authors addressed the lack of antibacterial properties in BCP, crucial for its medical application. They modified BCP using TEMPO-mediated oxidation and formed TEMPO-oxidized BCP (TOBCP) with anionic C6 carboxylate groups.[255] Silver nanoparticles (AgNP) were synthesized on TOBC nanofiber surfaces without a reducing agent. Various analyses confirmed the morphology and structure of the pellicles with AgNP. The TOBCP/AgNP released Ag^+ continuously and exhibited high biocompatibility (>95% cell viability) and significant antibacterial activities (100% against *E. coli* and 99.2% against *S. aureus*). This study suggests TOBCP/AgNP as a promising wound dressing material.[255] Additionally, in drug delivery systems, oxidized nanocellulose provides compatibility with various pharmaceutical compounds. The presence of carbonyl and carboxyl groups enables controlled drug loading and release, ensuring precise therapeutic delivery.[256] In a recent investigation study, Xie *et al.*[257] focused on developing controlled drug delivery systems utilizing bio-renewable materials. They successfully created a system based on mesoporous oxidized cellulose beads (OCBs) through an eco-friendly method. Carboxyl groups introduced by the TEMPO/NaClO/$NaClO_2$ system enabled pH-responsive properties in the cellulose beads, allowing drug retention at pH = 1.2 and release at pH = 7.0. Adjusting the oxidation degree controlled release rates, with higher oxidation led to faster release due to increased re-swelling and hydrophilicity.[257] Zero-order release kinetics suggested constant drug release rates, potentially minimizing side effects and administration frequency. The study also examined the impact of different drugs and solvents on release behavior and drug state within the beads, demonstrating the potential of pH-responsive oxidized cellulose beads for controlled drug release due to their biocompatibility, cost-effectiveness, and adjustable release rates.[257] Additionally, suitable and cost-effective nanocarriers capable of capturing and delivering antibiotics to restrict microbial spread is a pressing need. To address this, in a recent study, a two-step strategy involved citric acid-induced hydrolysis of cellulose pulp (NFC) followed by TEMPO-mediated oxidation, resulting in carboxylated nanofibrillated cellulose (TNFC-5) with high carboxyl content.[258] TNFC-5 efficiently captured antibiotics regardless of hydrophilicity, exhibiting high drug loading (>40%) and entrapment efficiency (>80%). TNFC-5 demonstrated sustained release and antibacterial activity against *Escherichia coli* and *Staphylococcus aureus* for up to one week, offering a green, cheap, and eco-friendly alternative for antibiotic delivery. This study proposed TNFC-5 material as a promising candidate for treating bacterial infections by penetrating biofilms and eradicating bacterial colonies.[258] Moreover, oxidized cellulose-based hydrogels have been widely investigated for tissue engineering applications.[173,259,260] For instance, Lan *et al.*[173] explored the potential of generating functional replacements for avascular inner knee menisci through cell-based 3D bioprinting (Fig. 11B). Human meniscus fibrochondrocytes (hMFC) from surgical castoffs and cellulose nanofiber-alginate hydrogels were investigated.[173] Different fomulations of inks were prepared in this study. As an example, sample 6040 comprised a blend of 60% TCNF and 40% ALG, while 7030 consisted of 70% TCNF and 30% ALG, and 8020 contained 80% TCNF with 20% ALG. Rheological properties of TEMPO-oxidized cellulose nanofiber/alginate (TCNF/ALG) precursors were measured for optimal bioprinting formulations (Fig. 11C). Human mesenchymal stem cells (hMFCs) mixed with suitable TCNF/ALG precursors were bioprinted into disc constructs, then underwent chondrogenesis. The constructs exhibited significant biocompatibility, with high cell viability observed within the

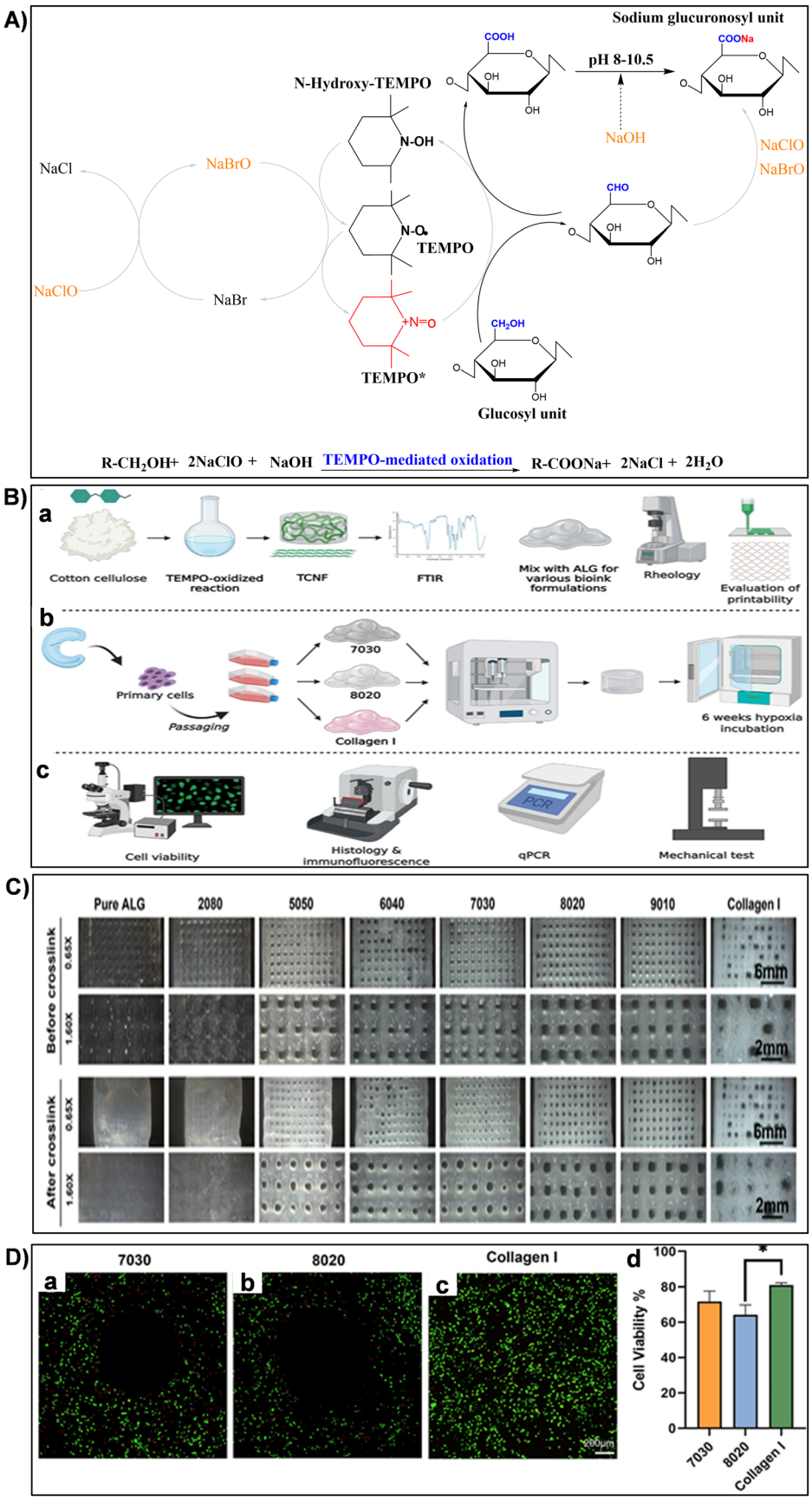

Fig. 11 (A) Illustration of TEMPO-mediated oxidation mechanism converting cellulose primary hydroxy groups to sodium C6-carboxylate groups using TEMPO/NaBr/NaClO in water at pH 10. Reproduced with permission from ref. 251 Copyright © 2018 Elsevier. (B) Experimental design schematic: (a) biomaterial formation and characterization, (b) engineered tissue formation, and (c) evaluation of engineered tissues. Reproduced with permission from ref. 173 Copyright © 2021 Frontiers. (C) Printed mesh structures utilizing various TCNF/ALG precursor formulations. Reproduced with permission from ref. 173 Copyright © 2021 Frontiers. (D) Live/dead images of (a) 7030, (b) 8020, and (c) COL bioinks, where live cells appear green and dead cells red. (d) Quantitative cell viability analysis of live/dead assay images. Reproduced with permission from ref. 173 Copyright © 2021 Frontiers.

constructs after several days of culture (Fig. 11D).[173] Results showed TCNF/ALG constructs exhibited inner meniscus-like characteristics, with higher COL2A1 expression and lower COL10A1 and MMP13 expression compared to collagen-based constructs. Immunofluorescence revealed human type I and II collagens in TCNF/ALG constructs.[173] In another work, cellulose nanocrystals (CNC), cellulose nanofibers (CNF), and microfibrillated cellulose (MFC) underwent one-pot oxidation and crosslinking with chitosan (1 : 5 mass ratio). The size and aldehyde content of oxidized NC samples were assessed to understand their impact on hydrogel properties.[260] Crosslinked hydrogels were characterized by field emission scanning electron microscopy (FESEM), swelling ability, Fourier transform infrared spectroscopy (FTIR), compression tests, thermal stability, and cell culture conditions. Oxidized-MFC hydrogel improved mechanical stability and swelling behavior but lacked stability in cell conditions due to low aldehyde content. Conversely, oxidized CNF and CNC formed suitable hydrogels for cell adhesion and MSC proliferation in 3D spheroids, with PO-CNF/chitosan hydrogel exhibiting antibacterial activity and MSC proliferation.[260] Furthermore, Abouzeid *et al.*[259] designed three-dimensional printed scaffolds by partially cross-linking TEMPO-oxidized cellulose nanofibril/alginate hydrogel with calcium ions, maintaining shape and filament integrity. Post-printing, full cross-linking with calcium ions enhanced hydrogel rigidity and long-term stability.[259] Rheological properties, including thixotropic behavior and viscosity recovery, were studied, revealing improved recovery with cellulose nanofibrils. Mineralization with simulated body fluid confirmed hydroxyapatite nucleation on the scaffold, indicating biomimetic properties. Compressive strength analysis demonstrated the scaffold's suitability for bone tissue engineering. The composite scaffold showed superior properties compared to pure alginate, suggesting promise for 3D printing applications in bone regeneration.[259]

2.3 Structural and mechanical properties of nanocellulose

Investigating the structural and mechanical characteristics of nanocellulose is crucial in the field of advanced materials research. Originating from plant or bacterial sources, nanocellulose displays a distinctive hierarchical structure at the nanoscale, which provides exceptional mechanical strength, flexibility, and biocompatibility.

2.3.1 Structural properties. Nanocellulose exhibits a primary crystalline allomorph that is essential to its structural integrity and functional properties. The primary crystalline structure of nanocellulose is typically classified into two main allomorphs: cellulose I and cellulose II.[261,262] Cellulose I is the predominant crystalline form found in nanocellulose, characterized by a repeating unit structure involving hydrogen-bonded chains. These chains are organized in a parallel fashion, forming tightly packed sheets. Within cellulose I, there are further subcategories such as Iα and Iβ, each with distinct arrangements of cellulose chains. Cellulose Iα features a triclinic unit with a single hydrogen bonding chain per unit cell, promoting parallel stacking of cellulose chains through van der Waals interaction.[263] In contrast, cellulose Iβ adopts a monoclinic unit with two hydrogen bonding chains per unit cell.[70] These two cellulose I forms coexist, their ratio varying based on the cellulose source. Cellulose from primitive organisms tends to be rich in Iα, while cellulose from higher woody plants is abundant in Iβ.[264] Cellulose II, although less common in nanocellulose, represents an alternative crystalline arrangement. It differs from cellulose I in terms of chain packing and hydrogen bonding. In cellulose II, the glucose chains are organized into a more ordered and stable structure, resulting in increased crystallinity. This crystalline arrangement is primarily characterized by an antiparallel alignment of cellulose chains, forming tightly packed sheets.[79,265] The presence of hydrogen bonds between adjacent chains further reinforces the crystalline structure, contributing to the material strength and rigidity. The transformation from cellulose I to cellulose II can be induced through various methods, including chemical treatments or mechanical processing.[262,266] Moreover, cellulose III and IV constitute less prevalent crystalline allomorphs of cellulose compared to the more commonly encountered cellulose I and II.[139,261] Cellulose III is derived through a process called mercerization, wherein cellulose undergoes treatment with strong alkali. This treatment induces alterations in the packing structure of cellulose, resulting in increased reactivity. The modification achieved through mercerization enhances the material suitability for various applications across industries.[265,267] Cellulose IV is synthesized through the amorphization of cellulose I, leading to improved solubility and reactivity. This modification broadens its applicability, particularly in contexts where enhanced solubility is advantageous.[268] Fig. 12 illustrates optimized crystal structures of cellulose allomorphs.

Understanding the characteristics of the primary crystalline allomorph is pivotal for tailoring nanocellulose to specific applications. CNCs primarily adopt the cellulose I crystalline allomorph. In this form, cellulose chains are organized in a parallel arrangement with a repeating unit structure.[270] The crystalline nature of CNCs contributes to their exceptional strength, stiffness, and thermal stability. The high aspect ratio and surface area of CNCs make them ideal reinforcements in nanocomposites, where they enhance mechanical properties.[60,110,271] CNFs can exhibit a combination of cellulose I and cellulose II crystalline forms, depending on the processing method. The mechanical treatment used during CNF production can induce a transformation from cellulose I to cellulose II.[272,273] The resulting crystalline

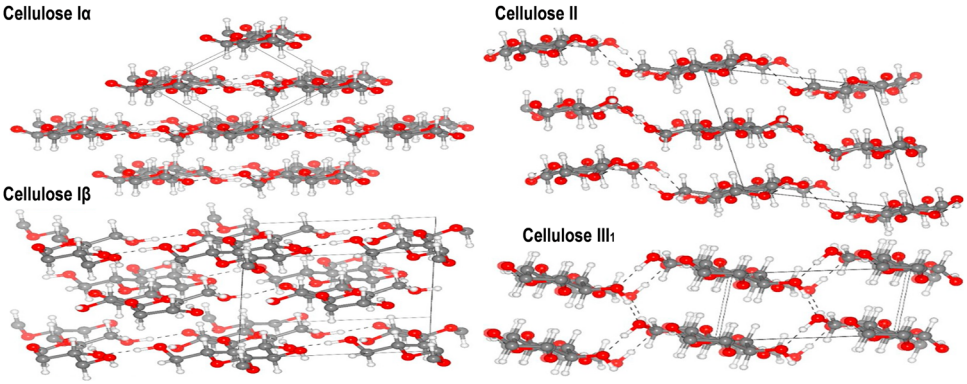

Fig. 12 Refined crystal structures of cellulose allomorphs Iα, Iβ, II, and III1 are shown, with carbon, oxygen, and hydrogen atoms depicted as gray, red, and white spheres, respectively. Hydrogen bonds are indicated by dashed lines. Reproduced with permission from ref. 269 Copyright © 2020 Elsevier.

structure impacts CNF properties such as flexibility, porosity, and surface area. This versatility allows CNFs to be tailored for diverse applications, including paper manufacturing, biocompatible materials, and reinforcing agents in composites.[8,24,108] BNC typically adopts the cellulose I crystalline allomorph, resembling the crystalline structure found in plant-derived cellulose.[274] BNC is produced by bacterial fermentation, leading to a highly pure and crystalline nanocellulose structure. The complex network of BNC fibers contributes to its remarkable mechanical properties, high purity and biocompatibility.[54,130] BNC found applications in biomedicine owing to its resemblance to the extracellular matrix and its ability to support cell growth.[56,118]

Crystallinity, a fundamental feature of nanocellulose can profoundly influence its mechanical, thermal, and chemical behaviors. This property quantifies the proportion of crystalline regions within the material, indicating the ordered arrangement of cellulose chains. For CNCs, a remarkable feature is their high degree of crystallinity, often surpassing 80%, contributing to their remarkable strength and stiffness.[60,275] This remarkable crystallinity is a result of their small size and the thorough isolation process. During isolation, CNCs are selectively derived from the most crystalline regions of cellulose, emphasizing their ordered structure and reinforcing their mechanical strength.[110,113] For CNFs, their crystallinity remains noteworthy, generally ranging from 60% to 80%. This range signifies a substantial degree of ordered cellulose chains within CNFs.[276,277] However, CNFs typically exhibit a lower crystallinity compared to CNFs. The structure of CNFs is characterized by a network of intertwined cellulose chains, resulting in a less ordered arrangement. The lower crystallinity contributes to the flexibility and deformability of CNFs, making them suitable for applications requiring enhanced flexibility and toughness. The amorphous regions within CNFs contribute to their ability to disperse more readily in certain matrices, enhancing their compatibility in composite materials.[87,278] In addition, the BNC variant is notably captivating, showcasing crystallinity levels typically falling within the range of 70% to 80%. This characteristic is complemented by a high degree of polymerization, spanning from 7000 to 16 000 glucose residues.[139,279] The crystallinity of BNC is attributed to the biosynthesis process by bacteria, which leads to a highly ordered arrangement of cellulose chains. BNC crystallinity is profoundly affected by the intricate interplay between genetic factors and environmental parameters, shaping its unique structure.[117,280] The crystalline structure of BNC is characterized by a well-organized network of cellulose nanofibers, forming a three-dimensional matrix. This high degree of crystallinity results in BNC possessing remarkable tensile strength, elasticity, and water-holding capacity. Its unique combination of strength, biocompatibility, and controllable porosity makes BNC an appealing choice for advancing research and innovation in regenerative medicine, tissue engineering, and drug delivery systems.[128,281]

Specific gravity, expressed as the ratio of a substance density to that of a reference material, commonly water, serves as a foundational property delineating material weightiness. Regarding nanocellulose, this parameter highlights the lightweight nature that distinguishes these materials. More precisely, the specific gravity of nanocellulose materials consistently falls within a confined range, typically ranging from 1.3 to 1.6 g cm^{-3}.[282–284] This specific range underscores the inherently low-density characteristic of nanocellulose, emphasizing its exceptionally lightweight quality.[282,283,285] The low specific gravity of nanocellulose materials is a result of their unique structural arrangement at the nanoscale. CNCs, CNFs, BNC possess highly organized nanostructures characterized by their intricate networks of cellulose chains. These structures are adept at minimizing the overall mass while maximizing the volume, contributing to the exceptionally low specific gravity values observed.[286,287] The lightweight nature of nanocellulose is crucial in applications requiring weight reduction, particularly in aerospace, automotive, and construction industries. In these sectors, material weight significantly impacts fuel efficiency, maneuverability, and structural integrity. Nanocellulose low specific gravity makes it an attractive option, allowing for reduced component weight without sacrificing strength or durability.[87,288] Moreover, in biomedical applications such as drug delivery systems and tissue engineering scaffolds, the lightweight nature of nanocellulose is essential. This characteristic minimizes the burden on biological systems while providing necessary support and functionality. Thus, nanocellulose emerges as a valuable material driving advancements in medical technologies.[21,289]

2.3.2 Mechanical properties. Nanocellulose exhibits a wide array of mechanical properties that render it highly attractive for diverse biomedical applications. These properties, such as stiffness, tensile and compressive strengths, Young's modulus, viscoelasticity, and rheological behavior, can vary significantly based on the source and production methods, making nanocellulose a versatile material in the field of advanced materials science.[60,139,290]

One of the key metrics used to evaluate the mechanical performance of nanocellulose is the elastic modulus, which measures its resistance to deformation under an applied load.[70,291–293] This property is profoundly influenced by the degree of crystallinity and the alignment of the nanofibrils within the material. The elastic modulus of nanocellulose can vary significantly, ranging from a few GPa to over 100 GPa, depending on factors such as cellulose source, processing methods, and nanocellulose dimensions and types.[91,294] For instance, CNFs exhibit anisotropic physical properties, with the elastic modulus reported to be about 150 GPa in the longitudinal direction and about 18–50 GPa in the transverse direction for highly crystalline CNF.[70,295] On the other hand, CNCs, generally obtained by acid hydrolysis of cellulose fibers, have high crystallinity and an elastic modulus reported to be between 100 and 150 GPa.[293,296] Furthermore, atomic force microscopy was employed in a study to determine the elastic modulus of BNC. The findings revealed a constant value of 78 ± 17 GPa over a fiber diameter range of 27–88 nm.[292] These characteristics position nanocellulose within the range of certain engineering reinforcement materials, highlighting its remarkable rigidity and structural integrity.[8,24,25] The high elastic modulus of nanocellulose is attributed to its well-defined crystalline structure and the efficient load-bearing capability of individual nanofibers or nanocrystals. This ability underscores the potential of nanocellulose for applications demanding superior mechanical strength, including reinforcing materials in advanced composites, manufacturing lightweight yet robust structural components, and developing innovative products in fields such as aerospace, automotive engineering, and bioengineering.[290,297,298]

Tensile and compressive strengths are also essential mechanical properties that define the ability of nanocellulose materials to withstand various mechanical loads. These features can significantly vary depending on parameters such as cellulose types, sources, the isolation techniques, crystallinity, and the size of individual nanofibers or nanocrystals.[86,299] CNCs are characterized by their remarkable mechanical properties. Their theoretical tensile strength reported ranges from 7.5 to 7.7 GPa, making them one of the strongest naturally occurring materials. Typically, the aspect ratio of CNCs, isolated from cellulosic materials like cotton, sisal, flax, and jute through acid hydrolysis, falls between 12 and 50.[300,301] Moreover, CNCs exhibit remarkable stiffness, with a Young's modulus ranging from 100 to 170 GPa, showcasing their ability to reinforce composites significantly.[88,89,302] On the other hand, CNFs boast high tensile strength, reaching up to 10 GPa, making them among the strongest natural fibers and highlighting their exceptional mechanical performance. CNFs characterized by high crystallinity (approximately 88%) exhibit notable strength, measuring approximately 1.6–7.7 GPa, along with a stiffness of around 150 GPa.[70,108,303] CNFs also exhibit a remarkable aspect ratio, ranging from 10 to 250, highlighting their slender and elongated structure.[304] The excellent mechanical properties of the nanofibers stem from the highly crystalline structure of native cellulose and the high aspect ratio achievable through nanofiber processing. Additionally, BNC in dry state exhibits remarkable mechanical strength, with tensile strength values ranging from 200 to 300 MPa and Young's modulus ranging from 15 to 35 GPa.[305] Mechanical attributes of cellulose have been extensively scrutinized through experimental and theoretical investigations, utilizing techniques such as X-ray diffraction, Raman spectroscopy, and atomic force microscopy.[86] Purely crystalline nanocellulose exhibits a crystalline structure. Similar to the modulus of elasticity, the tensile strength of nanocellulose is influenced by its anisotropic crystalline arrangement. Molecular modeling predicted a tensile strength ranging from 5 to 7 GPa along the chain direction, while the transverse strength is markedly lower at 0.3 to 0.9 GPa.[306] Computational predictions aligned well with experimental findings from sonication-induced fragmentation, reporting tensile strengths of 1.6 to 3 GPa for wood cellulose nanofibrils and 3–6 GPa for highly crystalline tunicate cellulose nanofibrils.[307] This underscores the cellulose crystal substantial stiffness and strength, with pronounced anisotropy at this level of structural hierarchy. Tensile strength, representing the maximum tensile stress a material can endure without fracturing, is a crucial parameter for materials used in applications requiring resistance to stretching or pulling forces.[308] This property is advantageous for mimicking load-bearing tissues like tendons and ligaments. The aligned and entangled nanofibrils within nanocellulose contribute to its superior tensile strength.[186] Conversely, compressive strength indicates a material capacity to withstand loads that push it together, compressing it. Compressive strength is vital for applications where tissues undergo compression, such as in cartilage and bone engineering.[309–311] Nanocellulose, with its porous structure and ability to form hydrogels, can provide a supportive environment for cells and promote tissue engineering in compression-loaded regions.[290] In addition, cellulose, with its inherent strength and versatility, serves as an excellent candidate for reinforcement strategies in composite materials.[108,147] By combining cellulose with other matrices, a synergistic effect can be achieved, enhancing the overall compressive strength of the composite. This strategy is particularly valuable in fields like construction, where the reinforced materials can contribute to the development of high-performance and durable structures.[312,313] The utilization of cellulose in composite materials opens up possibilities for innovative solutions across various industries, showcasing its potential as a sustainable and robust reinforcement agent. For instance, a recent study investigated the impact of incorporating nanocrystalline cellulose into cement mortars at varying concentrations (0.5%, 1.0%, and 1.5% by weight of cement).[314] The research assessed physical and mechanical properties, frost resistance, salt resistance, and microstructure. Results indicated that higher nanocellulose content correlates with reduced

weight loss in frost and salt tests. The addition of nanocrystalline cellulose led to a notable improvement in compressive strength (27.6%) and flexural strength (10.9%). Mortars with 1.5% nanocellulose exhibited a remarkable 98% enhancement in frost resistance after 50 freezing and thawing cycles.[314] Furthermore, the orientation and alignment of cellulose nanofibers or nanocrystals within cellulose-based hydrogels play a pivotal role in determining their tensile and compressive properties. When these nanomaterials are strategically oriented, it enhances the overall mechanical strength of the hydrogel. In the case of tensile properties, the aligned cellulose structures allow for better load distribution along the direction of force, resulting in improved tensile strength.[8,25] Similarly, in compression, the organized arrangement of cellulose chains contributes to heightened resistance against compressive forces. This controlled orientation at the nanoscale level imparts superior mechanical performance to cellulose-based hydrogels, making them promising materials for applications requiring robustness and structural integrity.[50,86] In a recent study, two composite hydrogels, featuring interpenetrating polymer networks, were fabricated by initiating free-radical polymerization of acrylamide within preformed physical networks of regenerated plant cellulose (PC) or bacterial cellulose (BC), both swollen in the reactive solution.[315] The mechanical responses of these hydrogels were investigated under compressive deformations of varying amplitudes. Results from compression tests revealed distinct mechanical behaviors between PC- and BC-based hydrogels. While both withstood single compressions up to 80% amplitude, cyclic compressions exposed a notable increase in stiffness for BC-based hydrogels beyond 60% deformation. This phenomenon suggested structural reorganization, potentially influenced by stress-induced reorientation of BC microfibrils.[315]

In addition to the previously mentioned mechanical attributes of nanocellulose-based materials, another significant property is viscoelasticity. This distinctive characteristic encapsulates the unique behavior of nanocellulose materials, combining both viscous and elastic properties.[243,316,317] This dual nature is pivotal for applications demanding materials to deform under stress and revert to their original shape upon stress removal, underpinning their versatility in various industrial sectors.[316,317] The viscoelastic properties of nanocellulose are meticulously tuned by several key parameters inclusding concentration, processing conditions and nanocellulose types.[318,319] The concentration of nanocellulose within a material can significantly influence its viscoelastic behavior. Higher concentrations often lead to increased viscosity, affecting the material flow and deformation properties.[320] For instance, in a recent investigation, a noteworthy enhancement in viscoelastic properties was observed by augmenting the concentration of CNCs within CNCs/collagen hydrogels. The study demonstrated a substantial increase in the rate of stress relaxation ($\tau_{1/2}$) and creep ($\gamma_{1/2}$), along with heightened values of storage modulus (G') and loss modulus (G''). The $\tau_{1/2}$ values for the hydrogels exhibited a range from approximately 29.2 to 261 seconds, with the frequency of the strain sweep measuring G' and G'' set at 1 Hz. Furthermore, within the linear viscoelastic region, the G' values of the hydrogels ranged from 10 to 30 kPa.[320] Moreover, Jiang *et al.*[321] developed a robust hydrogel system using dialdehyde cellulose nanocrystals (DAC) and gelatin (GEL) as bio-ink for 3D printing. To prepare the composite hydrogel, 4% CNC or 4% DAC suspension was blended with 8% GEL solution at a volume ratio of 1 : 1, yielding 4 : 8-CNC/GEL or 4 : 8-DAC/GEL hydrogel. The behavior of 4 : 8-DAC/GEL hydrogel was investigated under different conditions to optimize printability and structural integrity.[321] Rheological analysis revealed GEL and 4 : 8-CNC/GEL samples had $T_{sol-gel}$ values of 23.8 and 30.7 °C, respectively (Fig. 13a). However, 4 : 8-DAC/GEL showed no intersection of G' and G'' from 3 to 50 °C. While GEL and 4 : 8-CNC/GEL hydrogels were unsuitable for tissue engineering due to low $T_{sol-gel}$ values, 4 : 8-DAC/GEL exhibited promising results, with continuous improvement of gel structure, reaching a storage modulus (G') of 5297.23 Pa after 4 hours (Fig. 13b).[321] The viscosity of 4 : 8-DAC/GEL at 1, 2, 3 and 4 h was 5.71, 14.06, 29.11 and 152.98 Pa s, respectively (Fig. 13c). The hydrogel displayed shear-thinning behavior, with viscosity decreasing from 17.60 to 10.62 Pa s as shear rate increased from 20 to 60 s^{-1} (Fig. 13d). 3D printed scaffolds exhibited exceptional architectural precision and fidelity, thanks to precisely tailored printing parameters and the hydrogel intrinsic characteristics (Fig. 13e–j).[321]

In addition, the processing conditions, including temperature, pressure, and shear rate during the production process, play a crucial role in determining the viscoelastic response of nanocellulose-based materials.[322] Controlled processing conditions are essential for achieving desired mechanical properties. Variation in these conditions can result in materials with tailored viscoelastic characteristics suitable for specific applications. The viscoelastic properties of nanocellulose materials are also intricately influenced by temperature and shear rate, both playing pivotal roles in defining the material behavior under mechanical stress. Temperature affects the mobility and interactions of nanocellulose chains in the material, thereby altering its rheological responses. As temperature increases, the material may exhibit changes in viscosity, storage modulus (G'), and loss modulus (G''). Higher temperatures often lead to increased molecular mobility and reduced material stiffness, affecting both the elastic and viscous components of the composite response to mechanical stress. For example, research study conducted by Hassan *et al.*[323] demonstrated that varying temperatures induced changes in the mechanical properties of nanocellulose-based composites. The study investigated the impact of crosslinking with 1, 3, and 5% (w/w) citric acid in starch/cellulose composites on viscoelastic properties using dynamic mechanical thermal analysis from room temperature to 200 °C.[323] The storage modulus (E') of the starch/cellulose composites exhibited an initial increase with the rising concentration of citric acid up to 5% (w/w). However, further increments in citric acid concentration resulted in a subsequent decrease in the storage modulus. Across all samples, an elevation in temperature led to a consistent reduction in the storage modulus, indicating a progressive decline in stiffness.[323] Notably, the control starch/cellulose composite foam demonstrated

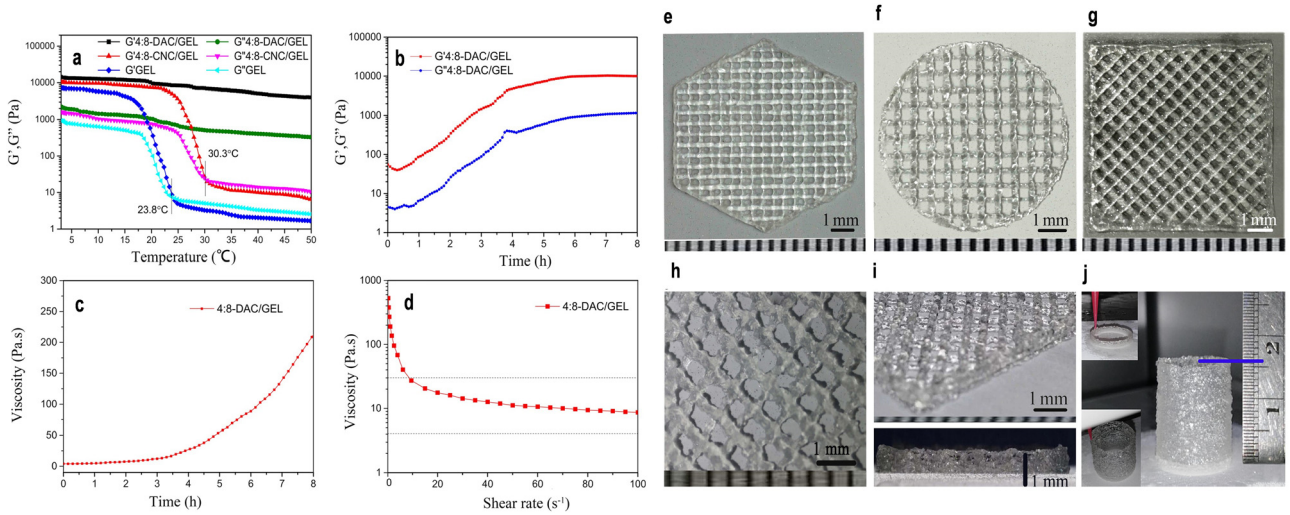

Fig. 13 (a) Graphical representation of the changes in storage modulus (G') and loss modulus (G'') observed in GEL, 4 : 8-CNC/GEL, and 4 : 8-DAC/GEL hydrogels as the temperature increases, showcasing their viscoelastic behavior. (b) Plot illustrating alterations in storage modulus (G') and loss modulus (G'') of the 4 : 8-DAC/GEL hydrogel concerning increasing incubation time, indicating the evolving mechanical properties during gelation. (c) Graph depicting variations in viscosity of the 4 : 8-DAC/GEL hydrogel over time, illustrating the changes in flow behavior with increasing incubation duration. (d) Relationship between viscosity and shear rate for the 4 : 8-DAC/GEL hydrogel, demonstrating its shear-thinning behavior, crucial for extrusion-based 3D printing processes. (e)–(g) Images of 4 : 8-DAC/GEL scaffolds fabricated in distinct geometric shapes, including regular hexagons, circles, and squares, highlighting the versatility in design possibilities. (h) Magnified photograph showcasing a detailed section of the scaffold, emphasizing its intricate structure and fidelity. (i) Oblique and side-view images offering detailed perspectives of the 4 : 8-DAC/GEL scaffold architecture, highlighting its intricate and well-defined nature. (j) Tubular construct printed utilizing the 4 : 8-DAC/GEL hydrogel, underscoring its potential for creating complex and functional tissue engineering constructs. Reproduced with permission from ref. 321 Copyright © 2018 Springer.

the lowest stiffness at all temperatures, while the starch/cellulose composite foam crosslinked with 5% (w/w) citric acid exhibited the highest storage modulus (E'). This trend aligned with the observed flexural moduli, emphasizing the temperature-dependent effect on the mechanical properties of the cellulose-based composites.[323] In addition, the viscoelastic properties of nanocellulose materials can also be significantly influenced by shear rate, a crucial parameter dictating the response of the material to mechanical forces. Shear rate refers to the rate at which adjacent layers of the material move relative to each other under applied shear stress.[324] In nanocellulose suspensions, varying shear rates can induce distinct rheological behaviors. At low shear rates, nanocellulose materials may exhibit more solid-like properties, with increased resistance to flow and pronounced elastic characteristics.[8,325] This behavior is attributed to the entanglement and alignment of nanocellulose entities under slower shear conditions. As shear rates escalate, nanocellulose structures may undergo alignment and disentanglement more rapidly, resulting in a transition to a more fluid-like response characterized by decreased viscosity and enhanced flow.[7,8,325] Futhermore, different types of nanocellulose, such as CNCs, CNFs, and BNC, exhibit distinct viscoelastic behaviors. CNCs, due to their rod-like shape and high aspect ratio, often contribute to materials with higher stiffness and viscosity.[326] CNFs, with their fibrillar structure, offer improved deformability, strength and flexibility.[327] BNC, characterized by its nanofibrous network, possesses unique viscoelastic properties, making it suitable for biomedical applications.[118]

3. Engineering biomimetic nanocellulose-reinforced hydrogels

Engineering biomimetic nanocellulose-reinforced hydrogels involves mimicking the intricate structure and properties of natural cellulose to fabricate advanced materials for various applications. By integrating nanocellulose into hydrogel matrices, scientists aim to enhance mechanical strength, biocompatibility, and bioactivity. These biomimetic hydrogels hold significant promise in tissue engineering, offering tailored scaffolds that closely mimic the extracellular matrix of living tissues.[7,8,24,25,52,328] Through precise control of nanocellulose dispersion and hydrogel crosslinking, these materials can replicate the hierarchical organization and mechanical resilience found in biological tissues, paving the way for innovative biomedical solutions.[20,329]

3.1 Physical and chemical technologies for processing nanocellulose-based hydrogels

The incorporation of nanocellulose into diverse matrices requires precise and innovative techniques to harness its unique properties effectively. Physical and chemical methods provide exceptional control and versatility in integrating nanocellulose into composite matrices, rendering them pivotal in a broad spectrum of applications.[26,227,330,331] The selection of a method for preparing nanocellulose-based hydrogels heavily depends on the intended application, balancing advantages and challenges (Table 2). Physical methods like solvent casting and mechanical mixing offer simplicity and scalability but may compromise hydrogel quality due to the use of potentially toxic

Table 2 Comparative overview of fabrication techniques for nanocellulose-based hydrogels

Methods	Description	Advantages	Disadvantages	Ref.
Physical methods				
Solvent casting	Casting nanocellulose in a solvent to form gel.	• Simple and cost-effective method. • Allows for control over hydrogel thickness and porosity. • Suitable for large-scale production	• May involve the use of toxic solvents. • Limited control over pore size and distribution. • May result in low mechanical strength of hydrogels.	332, 333, 343 and 344
Mechanical mixing	Dispersion of nanocellulose within a polymer matrix through mechanical agitation, such as stirring or high-shear mixing.	• Requires minimal equipment. • Can be easily scaled up for production. • Facilitates homogeneous dispersion of nanocellulose within the hydrogel matrix.	• Limited control over the orientation and distribution of nanocellulose. • May lead to uneven mechanical properties of the hydrogel.	217, 334 and 345
Freeze-casting	Freeze-casting, also known as ice-templating, involves the controlled freezing of a nanocellulose-based suspension followed by sublimation of the ice crystals to create a porous structure.	• Enables the fabrication of highly porous structures with aligned pores. • Allows for the control of pore size and morphology. • Preserves the hierarchical structure of nanocellulose within the hydrogel matrix.	• Requires specialized equipment for controlled freezing. • May lead to structural collapse during drying – Time-consuming process.	330 and 346
Electrospinning	Nanocellulose fibers are electrostatically spun into a gel matrix.	• Produces nanofibrous hydrogel scaffolds with high surface area and porosity. • Offers tunable fiber diameter and orientation. • Suitable for tissue engineering applications.	• Requires high voltage for electrospinning setup. • May involve the use of toxic solvents. • Limited scalability for large-scale production.	109, 347 and 348
3D printing	Nanocellulose-based inks are deposited layer by layer to fabricate complex 3D hydrogel structures.	• Offers precise control over the architecture and geometry of hydrogel constructs. • Allows for the incorporation of multiple materials for functionalization. • Enables patient-specific customization in biomedical applications.	• Requires specialized 3D printing equipment. • Limited availability of biocompatible printing materials. • May involve post-processing steps for cross-linking and sterilization.	8, 29, 349 and 350
Chemical methods				
Nanocellulose surface modification and functionalization	Chemical modification of nanocellulose surface to introduce desired functionalities and enhance its properties.	• Enhances the compatibility and stability of nanocellulose within the hydrogel matrix. • Enables the introduction of functional groups for targeted applications.	• May involve complex synthesis procedures. • Requires optimization to avoid cytotoxicity or alteration of native properties of nanocellulose. • Potential for batch-to-batch variability.	137, 221 and 238
Cross-linking approaches	Chemical cross-linking agents (*e.g.*, glutaraldehyde, epoxides, isocyanates) are used to form covalent bonds between nanocellulose chains to stabilize the hydrogel structure and improve its mechanical strength and stability.	• Improves the mechanical strength and stability of nanocellulose-based hydrogels. • Offers control over cross-link density and swelling behavior. • Enhances biocompatibility and resistance to enzymatic degradation.	• Some cross-linkers may be toxic or environmentally unfriendly. • Optimization required to achieve desired mechanical properties without compromising biocompatibility. • May lead to non-uniform cross-linking within the hydrogel matrix.	194, 331, 351 and 352
Polymer blending	Nanocellulose is blended with other polymers (such as polyethylene glycol, polyvinyl alcohol, or polyacrylic acid to form a composite hydrogel.	• Enables the incorporation of various polymers to modify the properties of nanocellulose-based hydrogels.	• Requires compatibility between nanocellulose and polymer matrices.	24, 25, 43, 158, 341 and 353

Table 2 (*continued*)

Methods	Description	Advantages	Disadvantages	Ref.
		• Offers tunable mechanical, thermal, and swelling properties. • Facilitates the creation of multifunctional hydrogel composites.	• May lead to phase separation or poor interfacial adhesion. • Optimization needed to achieve desired synergistic effects.	
Nanoparticle-functionalized nanocellulose hydrogels	Incorporation of functionalized nanoparticles (*e.g.*, silica, metal oxides, quantun dots) into nanocellulose hydrogels.	• Allows for the incorporation of functionalized nanoparticles to impart specific properties to the hydrogel. • Enhances mechanical strength, thermal stability, or responsiveness to external stimuli. • Offers potential for multifunctional applications.	• Synthesis and functionalization of nanoparticles may be complex and costly. • Requires optimization to ensure uniform dispersion within the hydrogel matrix. • May introduce additional processing steps and potential cytotoxicity concerns.	331, 340, 341 and 354
Layer-by-layer (LbL) Assembly	Alternating deposition of nanocellulose and oppositely charged polyelectrolytes onto a substrate, followed by cross-linking or drying to stabilize the multilayer structure.	• Provides precise control over the layer thickness and composition of nanocellulose-based hydrogels. • Allows for the incorporation of bioactive molecules, nanoparticles, or polymers in a step-wise manner. • Offers tailored properties for specific applications.	• Requires multiple deposition steps, leading to increased processing time. • May involve the use of toxic or environmentally harmful chemicals. • Limited scalability for large-area coatings or thick hydrogel constructs. • Optimization needed to achieve desired layer architecture and stability.	166, 342 and 355

solvents or limited control over nanocellulose distribution, respectively.[332–334] Advanced techniques like freeze-casting and electrospinning, while beneficial for creating structured and porous hydrogels suitable for applications like tissue engineering, face challenges like the need for specialized equipment and the potential use of harmful solvents.[51,53,330,332] 3D printing excels in customizability and precision in hydrogel structuring but is limited by equipment cost and material constraints.[29,328,335] On the chemical side, methods like surface modification and functionalization improve hydrogel stability and functionality, albeit at the cost of potentially complex synthesis and batch variability.[43,335,336] Cross-linking offers enhanced mechanical properties and stability; however, toxicity of cross-linkers remains a concern.[29,337] Polymer blending allows tailoring of hydrogel properties through the integration of various polymers, though compatibility issues may arise.[338,339] Incorporation of functionalized nanoparticles can impart specific advantageous properties but may introduce complexity in synthesis and concerns about uniformity and cytotoxicity.[331,340,341] Finally, the layer-by-layer (LbL) assembly provides precision in hydrogel design but suffers from scalability issues and lengthy processing.[166,342]

3.1.1 Physical methods. Advanced physical methods are frequently employed to seamlessly incorporate nanocellulose into various matrices, aiming to enhance material properties and functionalities while fabricating nanocellulose-based hydrogels with tailored characteristics.

3.1.1.1 Solvent casting. It is a fundamental technique in the fabrication of nanocellulose-based hydrogels for tissue engineering applications. In this process, nanocellulose is dissolved in a compatible solvent, forming a solution. The solution is then cast into specific molds or shapes and allowed to evaporate, leading to the formation of a hydrogel structure. During the evaporation process, nanocellulose particles become uniformly dispersed throughout the matrix, creating a nanocellulose-infused hydrogel.[344,356] The resulting cellulose-based hydrogel retains the morphology of the original solution and can be further crosslinked or modified to achieve desired properties such as mechanical strength, porosity, and biocompatibility.[221,269,351] This method offers several advantages. Firstly, the uniform dispersion of nanocellulose within the hydrogel ensures consistent mechanical properties, enhancing the overall strength and stability of the composite material.[290] Additionally, the presence of nanocellulose enhances the barrier functions of the hydrogel, making it suitable for applications where controlled substance release or protection against external agents is required.[333,344,357] In the literature, cellulose composites prepared using solvent casting have demonstrated improved mechanical properties for tissue engineering applications.[358,359] Utilizing favorable properties of cellulose and its derivatives, Pooyan *et al.*[358] developed a fully cellulose-based nanohybrid material by dispersing CNCs within a cellulose acetate propionate (CAP) matrix to fabricate a 3D percolating network, targeting small diameter vascular graft scaffolds in tissue engineering. CNCs from microcrystalline cellulose were dispersed in acetone to ensure uniform distribution.[358] Thin films were produced *via* solvent casting, exhibiting excellent mechanical performance at body temperature, with CNCs enhancing strength and rigidity

even at low concentrations (0.2 wt%), surpassing CAP alone.[358] In a subsequent study, CNC alignment within the CAP matrix using a weak external magnetic field (0.3 T) significantly improved mechanical and thermal properties up to 3 wt% nanofiller concentration.[359] Magnetic alignment enhanced filler interactions, dispersion, and filler-matrix contact. The composites showed a controlled porous structure conducive to cell seeding and proliferation, with aligned CNCs potentially guiding cell growth.[359] Furthermore, Ten *et al.*[360] developed bacterial polyester poly(3-hydroxybutyrate-*co*-3-hydroxyvalerate) (PHBV) reinforced with cellulose nanowhiskers (CNW) at concentrations of 1–5 wt% *via* solvent casting. CNW, derived from microcrystalline cellulose (MCC) through sulfuric acid hydrolysis, enhanced PHBV crystallization and mechanical properties.[360] Evaluation through polarized optical microscopy (POM), differential scanning calorimetry (DSC), dynamic mechanical analysis (DMA), and tensile and bulge tests revealed CNW effectiveness as a nucleation agent, increasing PHBV tensile strength, Young's modulus, and toughness. DMA showed enhanced storage modulus and restrained molecular mobility near CNW surfaces, indicating improved mechanical properties due to strong interphase interactions.[360]

3.1.1.2 Mechanical mixing. Mechanical mixing stands as a crucial technique in the fabrication of nanocellulose-based hydrogels. This method involves the application of high shear forces to achieve the uniform dispersion of nanocellulose within a host material, including polymers and composites.[8,10] The significance of mechanical mixing lies in its ability to ensure homogeneity, scalability, and the development of materials with enhanced mechanical properties. In tissue engineering, hydrogels function as scaffold materials providing structural support and a conducive environment for cell growth and tissue engineering.[8] By incorporating nanocellulose into matrix through mechanical mixing to fabricate hydroges, several advantages can be achieved. The high shear forces applied during the mixing process disperse the nanocellulose evenly, preventing clumping or agglomeration. This uniform distribution enhances the structural integrity of the hydrogel and promotes cell adhesion, proliferation, and differentiation.[8,10,361] A significant benefit of mechanical mixing in the fabrication of nanocellulose-based hydrogels lies in the enhancement of their strength, flexibility, and durability. By incorporating nanocellulose, which inherently possesses high tensile strength and stiffness, into the hydrogel matrix through mechanical mixing, the resulting material gains increased robustness and resilience, enabling it to withstand mechanical stresses more effectively.[362,363]

3.1.1.3 Freeze-casting. It is a technique that takes advantage of controlled freezing to organize nanocellulose chains in a structured manner. By subjecting a nanocellulose suspension to carefully controlled freezing conditions, the water within the solution forms ice crystals, guiding the alignment of the cellulose chains.[364,365] This unique process results in materials with hierarchical porosity, offering a sponge-like structure where interconnected pores at multiple size scales create a network, resembling natural tissues.[366,367] The porous structure of nanocellulose-based constructs is highly desirable for tissue engineering applications. The aligned porosity fosters cell adhesion and proliferation, promoting cellular activities as well as the exchange of nutrients and waste, which are vital for the proper functioning of artificial constructs.[23,290] Furthermore, this technology has been utilized in the development of advanced filtration membranes, where the precisely controlled porosity enhances filtration efficiency.[332]

3.1.1.4 Electrospinning. This technology showed great potential in fabricating cellulose-based hydrogels for tissue engineering applications.[347,348] In this process, a polymer solution containing nanocellulose is subjected to a high voltage electrical field, causing the solution to form a charged jet. As the jet travels towards a collector, solvent evaporation and polymer solidification occur, resulting in the formation of ultrafine nanofibers with diameters ranging from tens to hundreds of nanometers.[51,368] Electrospun cellulose-based hydrogels have been extensively used for tissue engineering.[227,347,348,369] Recently, uniaxially aligned cellulose nanofibers with embedded cellulose nanocrystals (CNCs) were produced *via* electrospinning, using a rotating drum as the collector. Scanning electron microscope images confirmed the alignment of most nanofibers.[52] Incorporating CNCs improved the uniformity and orientation of electrospun cellulose/CNCs nanocomposite nanofibers (ECCNN), enhancing their physical properties significantly. ECCNN nonwovens exhibited significantly enhanced physical properties, with 20% CNC loading increasing tensile strength and elastic modulus by 101.7% and 171.6%, respectively. ECCNN demonstrated biocompatibility in MTT tests and supported cell proliferation and organization, making them promising scaffold materials for tissue engineering.[52] In addition, these materials found applications in wound healing. In another study, a bilayer electrospun scaffold was fabricated, consisting of regenerated cellulose (RC)/quaternized chitosan (CS) as the primary layer and collagen/hyaluronic acid as the second layer. Both layers were chemically crosslinked with 1-ethyl-3-(3-dimethylaminopropyl) carbodiimide (EDC)/*N*-hydroxysuccinimide (NHS).[369] Cell adhesion, proliferation, and viability of electrospun scaffolds evaluated using L929 fibroblast cells showed increased spreading after 3 days compared to 1 day (Fig. 14A). Both layers underwent crosslinking, resulting in increased ultimate tensile strength (2.29 MPa for the bilayer scaffold compared to 1.82 MPa for the RC scaffold) (Fig. 14B).[369] *In vitro* studies with fibroblasts revealed enhanced gene expression of PDGF, VEGF-A, and COL1, indicating angiogenesis potential. Moreover, antimicrobial, antioxidant, and protease inhibitory activities were observed, demonstrating the bilayer scaffold potential in wound healing (Fig. 14C).[369] Moreover, in a recent investigation, core–shell fibers composed of poly(lactic acid) (PLA) as the core and cellulose acetate (CA) as the shell were fabricated through coaxial electrospinning. These fibers exhibited superior mechanical strength and biocompatibility compared to individual PLA and CA fibers and blend PLA/CA fibers.[370] Specifically, optimal core-to-shell flow rates produced defect-free fibers with high ultimate tensile strength (19.53 ± 1.68 MPa) and stiffness (0.62 ± 0.09 GPa), matching

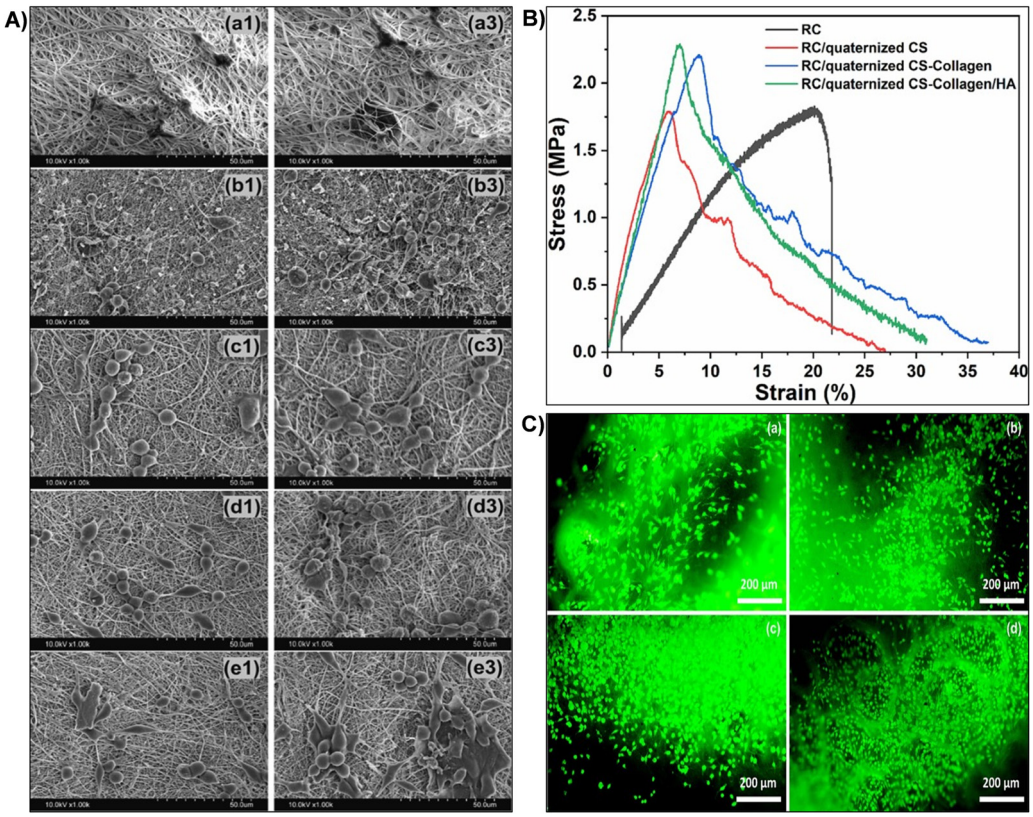

Fig. 14 (A) SEM images depicting cell-adhered electrospun scaffolds. RC: (a1) and (a3); RC/quaternized CS: (b1) and (b3); RC/quaternized CS-collagen: (c1) and (c3); RC/quaternized CS-collagen/HA: (d1) and (d3); EDC/NHS crosslinked RC/quaternized CS-collagen/HA: (e1) and (e3). Numbers denote culture time in days. (B) Mechanical properties shown by stress–strain curves of the electrospun scaffolds. (C) FDA-stained electrospun scaffolds after 3 days of culture with L929 cells: (a) RC; (b) RC/quaternized CS; (c) RC/quaternized CS-collagen; (d) RC/quaternized CS-collagen/HA scaffolds. Bilayer scaffolds were crosslinked. Reproduced with permission from ref. 369 Copyright © 2024 Elsevier.

native cancellous bone properties.[370] Enhanced mechanical strength resulted from higher PLA–core weight fraction and improved crystallinity. *In vitro* studies with human fetal osteoblasts confirmed improved cell attachment, proliferation, and alkaline phosphatase activity on these core–shell fibers, promising their use for bone tissue engineering.[370]

3.1.1.5 3D printing. 3D printing stands at the forefront of tissue engineering, offering unparalleled precision in scaffold design and fabrication. Through the layer-by-layer deposition of nanocellulose-based inks, this cutting-edge technology enables the manufacturing of intricate three-dimensional structures with remarkable control over geometry and internal architecture.[29,335,371] In tissue engineering, 3D-printed cellulose-based scaffolds played pivotal roles as biomimetic platforms offering promising and functional supports for cell growth and proliferation.[8,10,130,328,338] For instance, researchers have utilized nanocellulose-based hydrogels in 3D printing to fabricate scaffolds that closely resemble the native tissue environment.[34,349] These biomimetic hydrogels possessed excellent biocompatibility and mechanical properties. By precisely controlling the printing parameters, such as layer thickness and filament alignment, scientists engineered cellulose-based hydrogel scaffolds tailored to specific tissues like bone,[34] cartilage,[328,372] or skin.[371] Kamdem *et al.*[8] developed 3D printed hydrogel constructs using chitosan (CHI) and cellulose nanofibers (CNFs) (Fig. 15). The unique mechanical properties of native CNFs provided environmentally friendly high-performance composites. CHI served as a biocompatible matrix, while CNFs reinforced the hydrogel.[8] By means of extrusion-based printing functional hydrogel scaffolds were achieved with optimized concentrations of CHI and CNFs, exhibiting good mechanical performance (Young's modulus 3.0 MPa, stress at break 1.5 MPa, and strain at break 75%), anisotropic microstructure, and favorable biological response (Fig. 15).[8] Furthermore, 3D-printed hybrid biodegradable hydrogels, comprising cellulose nanocrystals, alginate and gelatin (CNC/Alg/Gel), were recently developed for bone tissue engineering. These scaffolds aimed to support cell proliferation, adhesion, nutrient exchange, and matrix mineralization.[373] They exhibited superior mechanical strength compared to pure polymer scaffolds. Assessment through various assays demonstrated enhanced cell proliferation, adhesion, and osteogenic differentiation on 1% CNC/Alg/Gel scaffolds. Moreover, increased expression of osteogenic-specific genes and improved bone formation in calvaria critical-sized defects model highlighted their potential for bone regeneration.[373]

Nanocellulose-based hydrogels have emerged as promising scaffolds for tissue regeneration due to their biocompatibility,

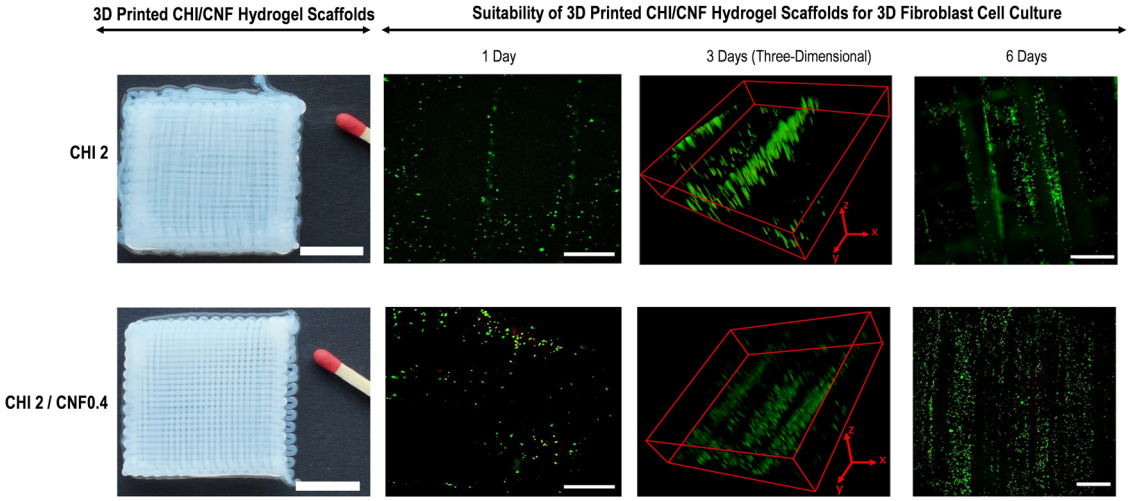

Fig. 15 (Left) 3D printed chitosan (CHI)/cellulose nanofiber (CNF) hydrogel scaffolds measuring 30 × 30 mm^2 with an interfilament distance of 0.85 mm. The scale bars in the top image represent 11.5 mm. (Right) Live/dead assay confocal laser scanning microscopy (CLSM) images after culturing NIH/3T3 fibroblast cells in 3D printed CHI or CHI/CNF hydrogel composite scaffolds. Live cells are indicated by green fluorescence, while dead cells are indicated by red fluorescence. Scale bars in the CLSM images represent 500 μm. Three-dimensional frames (3 days) scale: CHI2) $x \times y \times z$: 2.3 × 2.3 × 0.075 mm^3; CHI2/CNF0.4) $x \times y \times z$: 2.3 × 2.3 × 0.50 mm^3. Reproduced with permission from ref. 8 Copyright © 2021 MDPI.

biodegradability, mechanical robustness, and ability to mimic the ECM of native tissues.[22,374] One crucial aspect in the fabrication of nanocellulose-based hydrogels is the development of suitable inks for their precise deposition onto substrates, especially for fabricating complex structures with high fidelity.[8,29,338] Nanocellulose-based inks represent a class of printable materials with unique rheological, mechanical, and chemical properties that make them well-suited for 3D printing.[328,371] These inks typically consist of nanocellulose fibrils dispersed in a solvent or matrix, along with additives such as cross-linkers,[29] thickeners,[133,371,375] and bioactive agents[373] to enhance their printability and functionality. The key properties of nanocellulose-based inks influencing printability include viscosity, shear thinning behavior, surface tension, solid content, and compatibility with printing technologies.[376,377] The viscosity of nanocellulose-based inks plays a crucial role in their printability, affecting extrusion, droplet formation, and deposition onto substrates. Generally, these inks exhibit shear-thinning behavior, wherein their viscosity decreases under applied shear stress, facilitating smooth flow through printing nozzles and precise deposition onto target surfaces.[378,379] The rheological properties of nanocellulose-based inks can be tailored by adjusting factors such as nanocellulose concentration, solvent composition, and the presence of rheology modifiers, enabling control over printing parameters and structural fidelity of fabricated hydrogels.[378,379] In addition, surface tension influences the wetting behavior of inks on substrate surfaces, affecting droplet spreading, adhesion, and resolution during printing. Nanocellulose-based inks with optimized surface tension properties exhibit improved wetting on various substrates, including hydrophobic and hydrophilic surfaces, ensuring uniform deposition and adhesion of printed layers.[380] Surface modification techniques, such as plasma treatment or chemical functionalization, can be employed to tailor the surface properties of substrates, enhancing ink-substrate interactions and printability.[380,381] Furthermore, the solid content of nanocellulose-based inks dictates the mechanical properties and gelation kinetics of printed hydrogels, influencing their structural integrity and stability post-printing.[8] Higher solid content formulations result in stiffer hydrogels with enhanced mechanical strength, while lower solid content formulations may exhibit faster gelation kinetics and improved printability. Optimizing the solid content of inks is crucial to achieve a balance between printability, structural fidelity, and post-printing properties of fabricated hydrogels for tissue engineering applications.[8,382] Nanocellulose-based inks can be employed in various printing technologies, including extrusion-based printing,[8] inkjet printing,[224] and digital light processing,[383] each offering distinct advantages in terms of resolution, speed, and scalability for fabricating hydrogels with tailored architectures. Extrusion-based printing, for instance, enables layer-by-layer deposition of inks to create complex 3D structures,[384] while inkjet printing allows for precise droplet placement with high resolution.[385] Selecting an appropriate printing technology depends on the desired resolution, throughput, and material properties required for specific tissue engineering applications.[335,386] The printability of nanocellulose-based inks has enabled the fabrication of hydrogel scaffolds with intricate architectures and controlled porosity, mimicking the native ECM of various tissues such as cartilage,[34,328] bone,[133] skin,[206,371] and blood vessels.[387] These scaffolds served as platforms for cell adhesion, proliferation, and differentiation, promoting tissue regeneration and repair *in vitro* and *in vivo*.[8,10,133,328]

3.1.2 Chemical methods. The incorporation of nanocellulose into various matrices has opened new horizons in materials science, offering enhanced properties and functionalities across diverse applications. Several chemical techniques have been developed to facilitate the seamless incorporation of nanocellulose into different materials, paving the way for innovative solutions in fields like tissue engineering, nanotechnology, and sustainable packaging.

3.1.2.1 Nanocellulose surface modification and functionalization. Nanocellulose functionalization plays a pivotal role in enhancing its compatibility and performance in various applications, particularly in the biomedical field. Through techniques like carboxymethylation, phosphorylation, and silanization, specific chemical groups are introduced onto the nanocellulose surface. This functionalization enables tailored interactions with different materials, including polymers and metals, ensuring uniform dispersion and robust interfacial bonding.[26,137,388] In biomedical applications, nanocellulose-based hydrogels, modified and functionalized using these techniques, find extensive use. For instance, carboxymethylated nanocellulose hydrogels were employed in wound dressings due to their excellent water absorption properties.[206,389] Furthermore, carboxymethylation of cellulose has garnered interest for its role in constructing adhesive hydrogels with potential in chronic diabetic wound repair. A mussel-inspired hydrogel, composed of catechol modified carboxymethyl cellulose (CMC-DA) and tannic acid, demonstrated rapid shape adaptability, wet adhesion, and antioxidant properties.[390] The hydrogel, with injectability and self-healing ability, adhered strongly to tissues (45.9 kPa) and retained adhesion even on wet surfaces, with adhesion strength remaining at 14.9 kPa. It offered efficient wound healing, hemostasis, and antibacterial effects, showing promise for diabetic wound management.[390] Moreover, phosphorylated nanocellulose hydrogels served as drug delivery carriers, offering controlled release mechanisms for pharmaceuticals.[159] In tissue engineering, phosphorylation of cellulose received attention due to its ability to enhance bone cell differentiation and calcification. In this context, surface-phosphorylated cellulose nanofibers (P-CNFs) were developed as eco-friendly scaffolds for bone tissue engineering.[211] These P-CNFs, with adjustable phosphate group content, showed improved zeta-potential and formed stable, uniform scaffolds. Notably, osteoblasts cultured on P-CNFs exhibited better adherence, proliferation, and osteogenic differentiation compared to those on native CNFs, particularly at optimal phosphate levels. This research underscored the potential of bio-based P-CNFs in simulating bone components and regulating osteoblast activity.[211] Similarly, in another study, a novel three-dimensional composite scaffold was successfully fabricated for bone tissue repair using a strategy that incorporated cellulose as a backbone and alginate to expand pore size.[209] The cellulose underwent bisphosphonate modification through oxidation with sodium periodate and a Schiff-base reaction with sodium alendronate, followed by biomimetic mineralization.[209] The resultant scaffolds were porous and exhibited a chemical structure and morphology that closely mimicked natural bone, including crystallite size and Ca/P ratio. The phosphorylated scaffolds showed no cytotoxicity and supported excellent cell attachment, highlighting their potential for bone tissue engineering applications.[209] In addition, silanized nanocellulose hydrogels found applications in tissue engineering, providing scaffolds that supported cell growth and proliferation.[146,148] In a study, Vinatier *et al.*[146] developed an injectable and self-setting hydrogel consisting of hydroxypropyl methylcellulose grafted with silanol groups (Si-HPMC) for cartilage repair. The authors tested its cytocompatibility and its ability to maintain a chondrocyte-specific phenotype. Primary chondrocytes from rabbit and human cell lines were cultured within Si-HPMC.[146] Results confirmed that the hydrogel supported chondrocyte viability, proliferation, and allowed growth while maintaining the cell ability to produce key cartilage components such as type II collagen and sulfated glycosaminoglycans. This suggests that Si-HPMC is a promising scaffold for the three-dimensional culture and transfer of chondrocytes in cartilage tissue engineering.[146]

3.1.2.2 Chemical cross-linking approaches. These methods have revolutionized the field of nanocellulose-based materials, particularly in the development of advanced hydrogels tailored for biomedical applications. By employing cross-linkers such as epoxides, isocyanates, and multifunctional acrylates, covalent bonds are formed in nanocellulose-based hydrogels, creating robust networks that significantly enhance the material structural integrity and mechanical properties.[20,138,357] A noteworthy utilization of cross-linked nanocellulose hydrogels resides in the generation of biocompatible scaffolds. These scaffolds function as three-dimensional matrices, closely emulating the natural extracellular matrix.[210,337,391] This emulation facilitates cell adhesion, growth, and proliferation, proving conducive for the engineering of compromised or diseased tissues. Such applications render these scaffolds indispensable in the advancement of functional organs and tissues.[29,331] Furthermore, the cross-linking of nanocellulose to fabricate hydrogels enables the mechanical reinforcement of the resulting hydrogels, enhancing their suitability for biomedical applications. Porous structures with controlled pore size, mechanical robustness, and biocompatibility are crucial for tissue engineering.[323,392] A recent investigation proposed a novel approach using bacterial cellulose (BC) and eco-friendly additives for enhanced properties. Glucose, vanillin, and citric acid served as non-toxic cross-linkers, while γ-aminopropyltriethoxysilane was used to modify cellulose surface OH groups.[393] Modified BC sponges exhibited 80–90% open porosity, with cross-linked glucose and citric acid variants showing 150% and 120% higher strength-to-weight ratios. *In vitro* assessments confirmed biocompatibility and lack of inflammatory response.[393] Moreover, responsive hydrogels, representing an innovative application, exhibit sensitivity to external stimuli such as pH, temperature, or specific biomolecules. The introduction of cross-linking in nanocellulose-based hydrogels enhances their responsiveness, positioning them as optimal candidates for controlled drug delivery systems. These intelligent hydrogels demonstrated the capability to release therapeutic agents in response to physiological cues, ensuring precision and targeted drug delivery.[394,395] For instance, in the field of cancer therapy, responsive nanocellulose-based hydrogels exhibited the capacity to selectively release chemotherapy drugs within tumor sites, thereby minimizing damage to healthy tissues and improving treatment efficacy.[396,397] Moreover, cross-linked nanocellulose-based hydrogels have found utility in the fabrication of robust coatings for medical devices. These coatings have elevated the biocompatibility of implants and devices, consequently reducing the risk of adverse reactions within the living organisms.[398,399] Illustratively, orthopedic implants derived from nanocellulose

hydrogels have demonstrated heightened integration with surrounding tissues, thereby reducing the likelihood of implant rejection and promoting enhanced *in vivo* tissue recovery.[400–402] In a study, to overcome the biological inertness of pristine bacterial cellulose (BC) for bone regeneration, a strategy was devised to crosslink short-cut BC nanofibers with Ca^{2+}, yielding a macroporous BC scaffold (MPBC@Ca) with enhanced bioactivity.[402] This scaffold exhibited improved structural stability and facilitated hydroxyapatite (HAp) deposition, mimicking the bone tissue extracellular matrix microenvironment. Hydroxyapatite-deposited MPBC@Ca scaffolds (HAp-MPBC@Ca) demonstrated excellent cytocompatibility and enhanced osteogenic differentiation of stem cells *in vitro*.[402] *In vivo* tests confirmed the scaffold osteoinductivity and ability to accelerate cranial bone tissue regeneration, suggesting its potential for repairing large cranial bone defects. This study highlights the importance of crosslinking cellulose for creating biomimetic scaffolds with enhanced bioactivity and regenerative potential.[402] Furthermore, cross-linked cellulose hydrogels have been successfully used for tendon tissue engineering. For instance, fibers based on alginate (Alg) and hydroxyethyl cellulose (HEC) were developed *via* wet-spinning to mimic the fibrous ECM sheath. Blends of 1% Alg and 4% HEC (25 : 75, 50 : 50, 75 : 25) were cross-linked with $CaCl_2$ and glutaraldehyde to enhance physical and mechanical properties.[403] Characterization revealed molecular interactions and favorable mechanical strength comparable to collagenous fibers. Lower HEC concentrations exhibited good degradability and mechanical features, while increased cross-linking altered mechanical behavior. The fibers demonstrated excellent biocompatibility, tenocyte proliferation, and migration, suggesting their potential as tendon substitutes.[403] Additionally, the versatility of cross-linked nanocellulose hydrogels has allowed for their modification with bioactive molecules. For instance, the incorporation of growth factors or antimicrobial agents within the hydrogel structure has augmented their therapeutic potential. In applications related to wound healing, cross-linked nanocellulose hydrogels have been loaded with growth factors, accelerating tissue engineering and proving valuable in the management of chronic wounds.[336] In a research work, carboxymethyl chitosan (CMCS)/hydroxyethyl cellulose (HEC) hydrogel films were developed to address challenges in fibroblast growth factor 2 (FGF-2) delivery for wound healing. These films, with a porous structure and high swelling capacity, facilitated controlled release of FGF-2, enhancing its bioavailability.[404] They promoted cell proliferation, protected FGF-2 from degradation, and sustained its release. In animal burn treatment, FGF-2-loaded hydrogel films accelerated wound healing, stimulating re-epithelialization, granulation tissue formation, and angiogenesis, while reducing hypertrophic scarring. This innovative approach suggests CMCS/HEC hydrogel films as promising wound dressings, potentially revolutionizing burn treatment with enhanced FGF-2 delivery and wound healing outcomes.[404]

3.1.2.3 Polymer blending. This technique represent advanced methods for integrating nanocellulose into various polymeric matrices, yielding advanced materials with exceptional properties.[405,406] By blending nanocellulose with polymers, such as biodegradable poly(lactic acid) (PLA)[407] or biocompatible polyethylene glycol (PEG),[408] researchers have developed hybrid materials that combined the unique attributes of nanocellulose with the desirable properties of the host polymers. In biomedical applications, nanocellulose-based hydrogels were recognized as prominent examples of these advanced materials.[21,329] Hydrogels are 3D networks that can hold large amounts of water while maintaining their structural integrity. Nanocellulose high surface area and excellent water-absorption capacity made it an ideal candidate for hydrogel formulations.[409] When incorporated into hydrogel matrices through blending, nanocellulose imparted mechanical strength, and responsiveness to the resulting hydrogels.[7,8,24] One notable application of composite nanocellulose-based hydrogels is in tissue engineering. These hydrogels served as scaffolds that mimic the natural extracellular matrix, providing a supportive environment for cells to adhere, proliferate, and differentiate.[20,29] The mechanical properties of nanocellulose hydrogels can be tailored to match specific tissues, making them invaluable for engineering functional tissues. Moreover, the biocompatibility of nanocellulose ensures that these hydrogels are well-tolerated by living tissues, reducing the risk of adverse reactions.[7] Bacterial cellulose (BC) for instance holds promise for wound healing, but its limited malleability hinders applications. Blending with non-cellulosic polysaccharides like dextran (D) and xyloglucan (XG) could enhance wound healing and flexibility.[410] A study introduced a novel *in situ* method to create BC-based hybrid hydrogels containing dextran (BC–D) and xyloglucan–dextran (BC–XG–D), with unique mechanical properties. Structural analysis revealed dextran forming micron-sized particles bound loosely to cellulose fibers.[410] Xyloglucan acted as a lubricant, reducing Young's modulus to 4 MPa and increasing maximum tensile strain to 53%. BC–XG–D hydrogels exhibited improved wound healing and skin maturation in animal models. These findings advanced functional BC-based materials for wound healing.[410] In another study, an injectable hydrogel mimicking the bone microenvironment and supporting bone regeneration was developed and characterized. The hydrogel, comprising chitosan (CS) and cellulose nanofibers/nanocrystals (CNFs/CNCs), exhibited enhanced mechanical properties. Fig. 16A(a) and (b) highlights schematic illustration of interactions in composite hydrogels prepared in this study.[411] Cellulose nanocrystals (CNCs) notably improved gelation kinetics (from ~24 s to 7 s) and mechanical strength (from ~28 kPa to ~379 kPa) of the chitosan hydrogel. Scanning electron microscopy imaging confirmed the CNCs incorporation into the chitosan network, resulting in a densely crosslinked structure.[411] Fourier-transform infrared spectroscopy analysis revealed increased hydrogen bonding, enhancing mechanical reinforcement. FTIR also confirmed chemical interactions between chemical groups of chitosan and those of cellulose (Fig. 16A(c)–(f)). The hydrogel was biocompatible, promoting high cell viability, and altered cell morphology, making it a promising biomaterial for bone regeneration (Fig. 16B).[411] In drug delivery, nanocellulose-based hydrogels offer unique advantages. Their high water content enables the encapsulation and controlled release of drugs,[159,395] proteins,[412] or growth

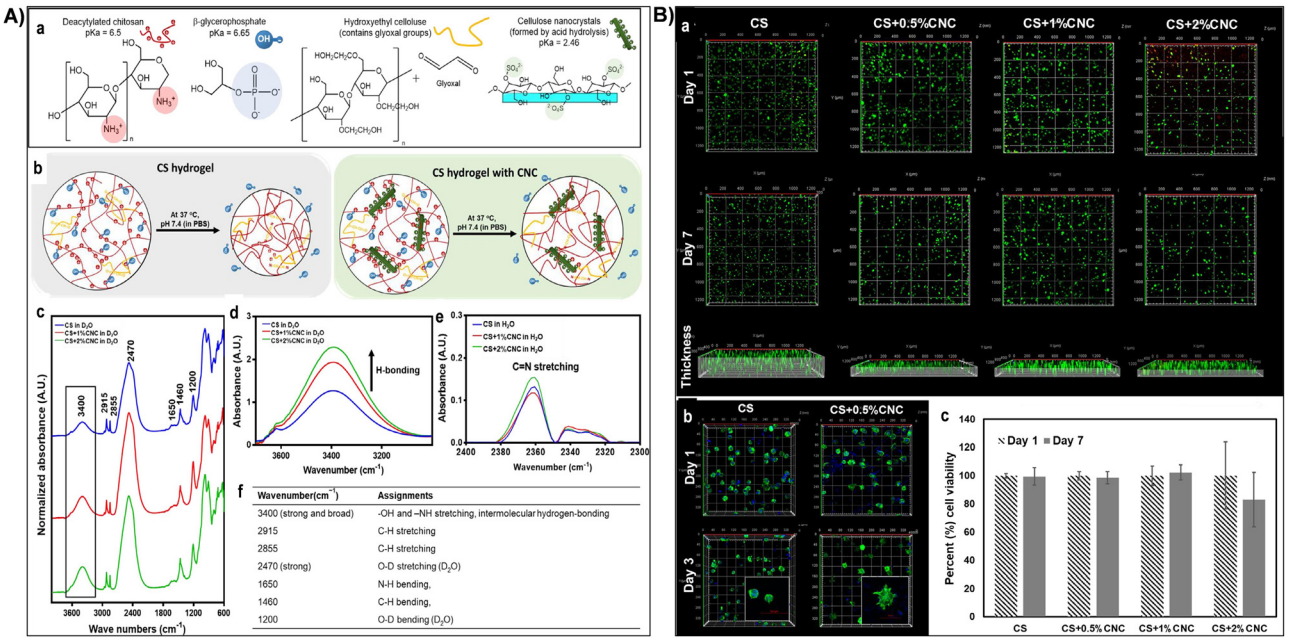

Fig. 16 (A) Chemical interactions within hydrogel systems. (a) Chemical structures and pK_a values of hydrogel compositions: chitosan (CS), β-glycerophosphate (BGP), hydroxyethyl cellulose (HEC), and CNCs. (b) Hydrogel formation mechanism comparison between CS and CS-CNC networks. (c) FTIR spectra of various CS hydrogel formulations in deuterium oxide, with inset showing absorbance related to intermolecular hydrogen bonding. (d) Overlay FTIR spectra from inset of c demonstrating increased absorbance at 3400 cm^{-1} in CS-CNC hydrogels compared to CS hydrogels in deuterium oxide. (e) Overlay FTIR spectra of different CS hydrogel formulations in water, indicating absorbance at 2360 cm^{-1} corresponding to C═N stretch resulting from interactions between glyoxal molecules from HEC and chitosan amine groups. (f) FTIR assignments of various chitosan hydrogel formulations in deuterium oxide (D_2O). (B) *In vitro* cell-based assays of encapsulated cells in hydrogels: (a) Z-stacking confocal images of MC3T3-E1 cells encapsulated in different hydrogel formulations, with live cells stained green and dead cells stained red. (b) Morphology of MC3T3-E1 cells encapsulated in different hydrogel formulations, stained for cytoskeletons and nuclei. (c) Percentage cell proliferation on day 7 compared to day 1 in each hydrogel formulation using cell counter ImageJ analysis. Reproduced with permission from ref. 411 Copyright © 2020 Elsevier.

factors.[404] Researchers achieved precise control over drug release rates by modulating the composition and structure of the hydrogels and enhancing their properties through blending nanocellulose with other polymers, making them suitable for long-term therapeutic applications.[13,329] Furthermore, nanocellulose-based hydrogels can find utility in wound healing and regenerative medicine. They can be loaded with antimicrobial agents to prevent infections and accelerate wound closure.[337,413] Recently, poly(vinyl alcohol)/cellulose acetate (PVA/CA) films were fabricated using a novel method blending principles of solvent casting and phase inversion. Films with varying PVA/CA ratios were produced for flexibility. Dopamine was employed to anchor the antimicrobial peptide (AMP) LL37 onto the films.[414] LL37-modified films exhibited potent antibacterial activity against *Staphylococcus aureus*, *Staphylococcus epidermidis*, and *Escherichia coli*, with approximately 75% inhibition for *Staphylococcus aureus*, 85% for *Staphylococcus epidermidis*, and 60% for *Escherichia coli*, irrespective of PVA/CA ratio.[414] Presence of albumin reduced bacterial inhibition due to binding of protein molecules to antimicrobial agents. LL37-treated films also accelerated clotting time (≈10 min), surpassing vancomycin and bare surfaces, indicating effective activation of the coagulation cascade.[414]

3.1.2.4 Nanoparticle-functionalized nanocellulose hydrogels. This represents a groundbreaking avenue in the field of advanced materials, particularly in biomedical applications. Serving as a versatile platform, nanocellulose offers a stable foundation for the functionalization by diverse nanoparticles, facilitating the creation of innovative nanocomposites with multifaceted functionalities.[415,416] One of the key applications lies in targeted drug delivery systems. Nanocellulose, with its high surface area and biocompatibility, can be modified to carry therapeutic agents, such as anticancer drugs[417–419] or antibiotics.[159,420] By attaching drug-loaded onto nanocellulose surfaces, these nanocomposites can navigate the body biological barriers more effectively, delivering medications directly to specific cells or tissues. This targeted approach minimizes side effects and enhances the overall efficacy of treatments.[175,421] Recently, two morphological structures, blending polylactic acid (PLA) with nanocellulose (NC) and self-assembled copolymer (M-PLA-*co*-NC), were synthesized with Fe_3O_4 NPs incorporated into both. These magnetic nanocomposites served as carriers for anti-cancer drugs 5-fluorouracil (5-FU) and curcumin (CUR).[417] Both carriers showed similar 5-FU loading, but M-PLA-*co*-NC doubled CUR loading compared to PLA/M-NC, indicating copolymeric micelle superiority. M-PLA-*co*-NC/5-FU/CUR exhibited slower release and higher antibacterial and antitumor efficacy than PLA/M-NC/5-FU/CUR, suggesting it as a promising nanomedicine for bacterial infections and cancer treatment.[417] Another study investigated pH-responsive drug

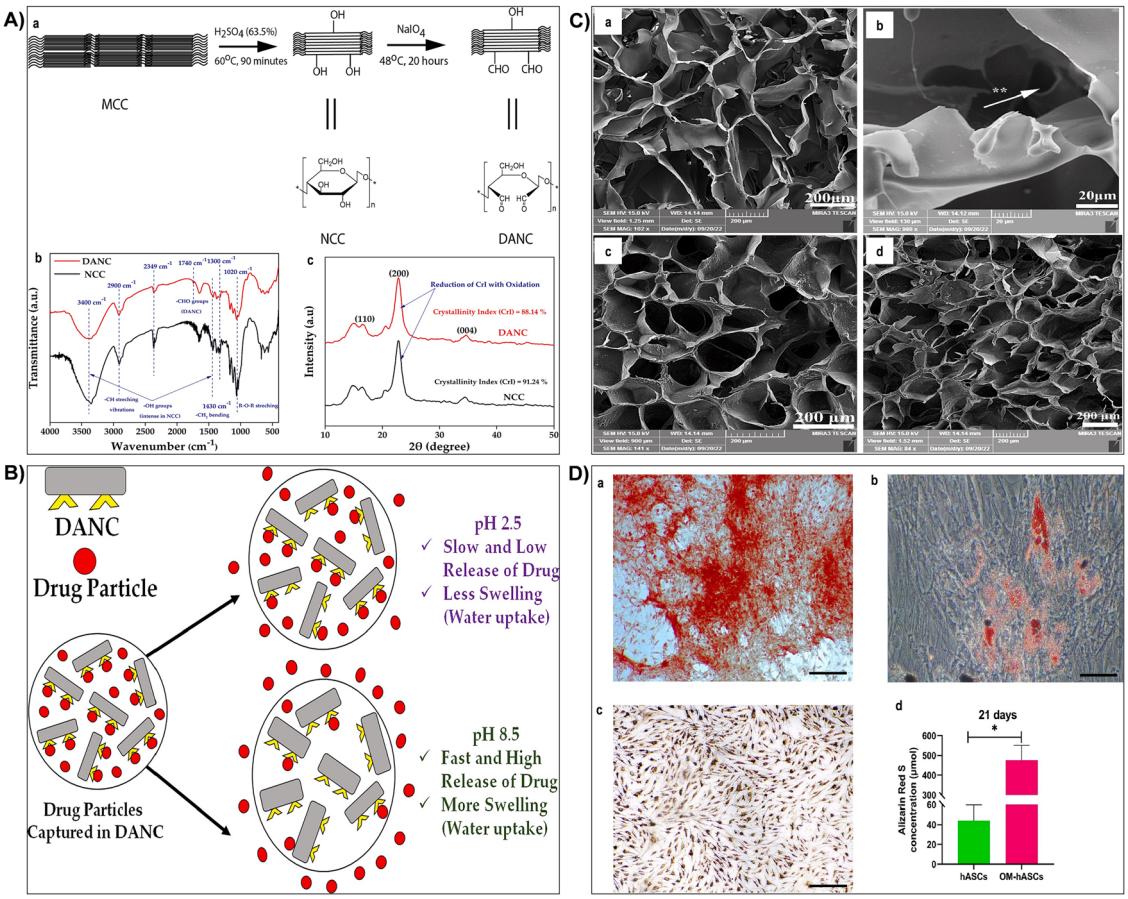

Fig. 17 (A) (a) Synthesis scheme and structures of DANC from MCC *via* NCC. Characteristic peaks in FTIR spectra (b) and characteristic plane in XRD analysis (c) of NCC and DANC. Reproduced with permission from ref. 422 Copyright © 2024 Elsevier (B) release of ciprofloxacin hydrochloride from DANC matrix at pH 2.5 and pH 8.5. Reproduced with permission from ref. 422 Copyright © 2024 Elsevier (C) SEM images showing composite scaffold morphology: (a) SF scaffold (scale bar: 200 μm), (b) interconnected pores in SF scaffolds (scale bar: 20 μm), (c) BC/SF composite scaffolds (scale bar: 200 μm), (d) BC/SF/BGNPs composite scaffolds (scale bar: 200 μm). Reproduced with permission from ref. 423 Copyright © 2024 Elsevier (D) osteogenic and adipogenic differentiation assay of hASCs over 21 days: (a) mineralized nodules stained with Alizarin Red S after 21 days, (b) lipid vacuoles stained with Oil Red after 21 days, (c) hASCs cultured in osteogenic differentiation media and stained with ARS after 21 days, (d) quantitative analysis of ARS staining on hASCs after 21 days (n = 4/group; scale bar = 200 μm). OM-hASCs refers to hASCs cultured in osteogenic differentiation media. Reproduced with permission from ref. 423 Copyright © 2024 Elsevier.

release from various cellulose forms: micro-, nano-, and functionalized cellulose. Nanocrystalline cellulose (NCC) was derived from microcrystalline cellulose (MCC) *via* sulfuric acid hydrolysis (Fig. 17A(a)).[422] Selective oxidation introduced aldehyde groups at carbon-2 and carbon-3 positions, yielding di-aldehyde nanocellulose (DANC). Chemical, spectroscopic and cristallographic analyses confirmed the conversion (Fig. 17A(b) and (c)). DANC exhibited higher drug binding capacity (200.8 mg g^{-1}) than NCC (138.3 mg g^{-1}) and MCC (120.2 mg g^{-1}).[422] Drug release increased with pH from 2.5 to 8.5. At pH 2.5, slow release occurred, while equilibrium (84.8% drug release) was reached within 10 minutes at pH 8.5 (Fig. 17B). Higuchi and Korsmeyer–Peppas kinetic models accurately described drug release, suggesting potential for pH-responsive drug delivery applications with functionalized cellulose.[422] In addition, nanocellulose-based hydrogels incorporating functionalized nanoparticles found extensive use in biomedical imaging. Quantum dots, for instance, can be conjugated with nanocellulose to create luminescent probes. These probes emit specific wavelengths of light when exposed to external energy sources, enabling highly sensitive and precise imaging of biological structures.[340,341] Such imaging techniques are invaluable in diagnosing diseases, monitoring cellular activities, and understanding complex biological processes.[340,341] In addition, nanoparticle-functionalized nanocellulose hydrogels are emerging as promising materials for tissue engineering applications. By incorporating nanoparticles such as bioactive glass nanoparticles[423] or metal oxides[424] into nanocellulose-based hydrogels, researchers aim to enhance their mechanical properties, biocompatibility, and bioactivity. These hybrid materials offer a versatile platform for controlling cell behavior, promoting tissue regeneration, and delivering therapeutic agents. In a recent study, blend polymers comprising natural polymers were investigated for their mechanical and biological properties. Composite scaffolds of bacterial cellulose (BC)/silk fibroin (SF) with bioactive glass nanoparticles (BGNPs) were developed to promote osteogenesis in human adipose-

derived stem cells (hASCs).[423] SEM analysis revealed spherical BGNPs with sizes ranging from 15 to 30 nm. Incorporating BC and BGNPs reduced pore diameter (as shown by SEM images of composites (Fig. 17(C)), increased compressive strength, and modulus of SF scaffolds. Flow cytometry validated hASC surface markers. Adipogenic and osteogenic differentiation were confirmed by Alizarin Red S and Oil Red O staining, showing calcium deposition and lipid vacuole formation after 21 days (Fig. 17D(a) and (b)).[423] Treatment with osteogenic medium for 21 days led to calcified nodule formation, indicating differentiation into bone cells (Fig. 17D(a)). Conversely, cells cultured in regular medium did not form mineral nodules (Fig. 17D(c)). Quantitative analysis revealed a significant increase in calcified nodule concentration with osteogenic differentiation medium (Fig. 17D(d)), highlighting its efficacy in promoting hASC differentiation into bone cells. Gene expression studies indicated osteogenic potential. Enhanced cell adhesion, viability, and differentiation in BC/SF and BC/SF/BGNPs scaffolds demonstrated their therapeutic potential for bone defects.[423] In another study, Ghanbari *et al.*[424] fabricated a 3D nanocomposite scaffold was developed using green-synthesized magnesium oxide nanoparticles (MgONPs) and bacterial cellulose (BC) nanofibers for bone regeneration. Camellia sinensis extract was utilized for MgONP synthesis.[424] The scaffold showed improved mechanical strength and porosity due to MgONPs, enhancing osteoblast proliferation and osteogenic gene expression. The MgONP-BC scaffold demonstrated higher calcium deposition and alkaline phosphatase activity compared to pure BC, indicating enhanced osteogenic potential. This study highlights the benefits of blending cellulose with MgONPs for creating biocompatible scaffolds with promising therapeutic potential in bone tissue engineering.[424] Moreover, in another study, a biomimetic Ag/bacterial cellulose/hydroxyapatite (Ag/BC@HAp) hydrogel mesh was designed for temporary cranioplasty with guided bone regeneration.[425] The hydrogel featured a double-sided functionalized structure, with one layer dense and covered with Ag nanoparticles, while the other was porous and anchored with HAp through mineralization for varying durations.[425] This design endowed the hydrogel with distinguished antibacterial activities and guided bone regeneration effects, while maintaining biocompatibility with preosteoblasts. *In vivo* experiments showed optimal guided bone regeneration with 7-day mineralization, while the hydrogel exhibited low swelling and strong mechanical strength, ensuring protection of soft brain tissues without increasing intracranial pressure.[425]

3.1.2.5 Layer-by-layer (LbL) assembly. LbL assembly is a remarkable technique that has gained significant attention for the fabrication of nanocellulose-based hydrogels, particularly for biomedical applications.[342,355] In this method, nanocellulose is meticulously deposited in alternating layers with other polyelectrolytes, creating a structurally controlled and multifunctional composite material. The driving force behind this assembly lies in electrostatic interactions between the positively and negatively charged components, ensuring the precise arrangement of layers.[342,426,427] LbL assembly empowers researchers to design and engineer nanocellulose-based hydrogels with tailored properties. By choosing specific polyelectrolytes and controlling the number of layers, the resulting hydrogel mechanical, chemical, and biological characteristics can be precisely customized. This level of control is especially advantageous for biomedical applications, where the hydrogel must meet specific requirements, such as tissue compatibility, drug delivery, or cell adhesion.[428,429] One of the remarkable aspects of LbL assembly is its ability to control the film thickness with exceptional precision. This feature is pivotal in biomedical applications, where the hydrogel thickness can influence factors like drug release rates, cellular interactions, or barrier properties. Researchers can fine-tune the films thickness by simply adjusting the number of layers deposited, ensuring the hydrogel aligns with the intended application.[430,431] Nanocellulose-based hydrogels produced through LbL assembly have shown immense promise in various biomedical applications. For example, they can be engineered to serve as drug delivery carriers, with the controlled release of therapeutic agents over time.[355] In tissue engineering, these hydrogels can provide structural support for cell growth and engineering, mimicking the extracellular matrix.[432] Recently, a magnetically-guided oxygen-propelled CoPt/gold nanosheet motor (NSM) was fabricated as an active self-propelled platform for anticancer doxorubicin drug (DOX) delivery to cancer cells. Microcapsules, serving as drug carriers, were fabricated using layer-by-layer (LbL) coating of chitosan and carboxymethyl cellulose layers, with gold and magnetite nanoparticles incorporated.[433] Two sorts of nanoparticles (NPs) including magnetite (Fe_3O_4) and gold (Au) NPs were incorporated into the microcapsule shells by the LbL procedure for different functions. DOX loading efficiency reached 77%. NSMs successfully delivered DOX-loaded magnetic multilayer microcapsules to target cancer cells *via* external magnetic guidance.[433] Under near-infrared irradiation, gold nanoparticles induced rapid drug release. Cytotoxicity studies demonstrated minimal side effects of NSMs and multilayer microcapsules across all tested concentrations.[433] Moreover, they have been explored in wound dressings to enhance the healing process, benefiting from their biocompatibility and tunable properties. The multilayered nanocellulose-based hydrogels produced through LbL assembly exhibited an inherent biological compatibility, making them suitable for biomedical applications.[434] The precisely designed layers can promote cell adhesion, proliferation, and tissue integration. In addition, their porous structure allows for the efficient diffusion of nutrients and oxygen, contributing to improved biocompatibility.[355,432,434] A layer-by-layer (LbL) transdermal patch was crafted using bacterial cellulose (BC) *via* a Schiff base reaction. Ethylene diamine-modified carboxymethylated BC and aldehyde-modified pectin were assembled through this method. The presence of imine bonds facilitated self-healing upon scratching in pH 7.4 buffer solution, as observed through optical and atomic force microscopy.[434] Field-emission scanning electron microscopy confirmed the assembly formation. Water swelling and deswelling tests demonstrated efficient water retention. Incorporation of silver nanoparticles (AgNPs) was verified, exhibiting antimicrobial activity against *Staphylococcus aureus* and *Escherichia coli*. The patch cytotoxicity

and wound healing properties were assessed on NIH 3T3 fibroblast and A549 epithelial cell lines, showing positive effects.[434]

3.2 Crosslinking strategies for enhancing mechanical properties of nanocellulose based-hydrogels

Fabricating robust and mechanically stable hydrogels is crucial in tissue engineering applications to ensure the structural integrity and long-term functionality of implanted constructs.[435–437] Biomimetic hydrogels reinforced with nanocellulose offer a promising avenue for tissue engineering due to their biological and tunable properties. To enhance the mechanical stability of these hydrogels, various crosslinking strategies are commonly employed, each tailored to meet specific requirements and applications.[140,438] The chemical and structural properties of a hydrogel significantly influence the crosslinking mechanism, which can be categorized into physical (non-covalent) and chemical (covalent) bonding, as shown in Fig. 18A. In hydrogels, physical crosslinking is often complemented by chemical crosslinking, as physical bonds alone are insufficient to maintain hydrogel integrity. Specific crosslinking techniques are illustrated in Fig. 18B.

Table 3 provides an overview of various cross-linking methods commonly used for nanocellulose-based hydrogel fabrication, highlighting their principles, advantages, disadvantages, and properties of the resulting hydrogels. Depending on specific application requirements, the choice of cross-linking method can be tailored to achieve desired properties and performances.

3.2.1 Chemical crosslinking. Chemical crosslinking serves as a pivotal technique in enhancing the mechanical stability of nanocellulose-based hydrogels, ensuring their suitability for diverse biomedical applications. This method involves the utilization of specific chemical agents to establish covalent bonds between polymer chains, creating a robust network within the hydrogel matrix.[446] Concerning nanocellulose-based hydrogels, common crosslinkers such as glutaraldehyde,[447] genipin,[337,448] and carbodiimides[352] are frequently employed. Glutaraldehyde is a widely used crosslinker known for its efficiency in promoting covalent bonds, reinforcing the hydrogel structure. It facilitates strong intermolecular interactions, enhancing the mechanical strength of the hydrogel.[449,450] Recently, the impact of glutaraldehyde and calcium cations as covalent and ionic crosslinkers was explored on chitosan/cellulose nanocrystal scaffolds for bone tissue engineering. Four scaffolds with varied crosslinking methods were fabricated *via* freeze-drying. Structural and chemical analysis revealed porous networks with connected pores. Glutaraldehyde-crosslinked scaffolds exhibited the highest compressive strength, while uncrosslinked scaffolds showed the highest swelling ratio. Glutaraldehyde-containing scaffolds had lower cell viability compared to others, despite supporting cell proliferation and adhesion. In addition, genipin has gained significant attention in biomimetic hydrogels due to its biocompatibility and mild crosslinking conditions. Unlike glutaraldehyde, genipin offers a more biologically friendly option. It preserves the bioactivity of encapsulated cells and growth factors, making it particularly valuable in tissue engineering and regenerative medicine applications.[451] Additionally, through chemical crosslinking with agents like genipin, nanocellulose-based hydrogels are endowed with enhanced mechanical properties. In a study, chitosan hydrogels crosslinked with genipin and reinforced with cellulose nanocrystals (CNCs) were developed for future biomedical applications. Chitosan/CNC nanocomposite hydrogels with varying CNC concentrations (0%, 2%, 4%, and 6% w/w) were fabricated, and genipin served as the crosslinking agent.[452] Mechanical tests revealed a 36% increase in maximum stress with 6% CNC compared to neat chitosan. Enhanced mechanical properties were attributed to increased crosslinking and intermolecular interactions between CNC and chitosan.[452] Moreover, genipin cross-linked nanocellulose hydrogels were successfully used as ideal matrices for applications such as drug delivery systems, wound healing dressings, and tissue engineering scaffolds.[337,448] In a recent study, Erdagi *et al.*[337] synthesized and assessed neomycin-loaded hydrogels for wound healing. Gelatin-interpenetrated nanocellulose hydrogels, crosslinked

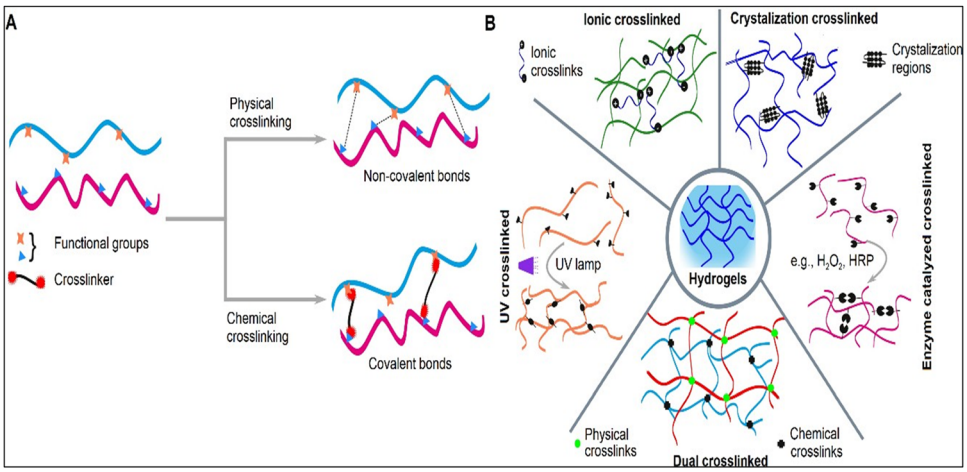

Fig. 18 Illustration depicting (A) the influence of physical and chemical crosslinking on bond formation and (B) various examples of distinct crosslinking techniques. Reproduced with permission from ref. 438 Copyright © 2021 MDPI.

Table 3 Overview of common cross-linking methods for nanocellulose-based hydrogel fabrication

Cross-linking methods	Principles	Advantages	Disadvantages	Properties and features of hydrogels	Ref.
Chemical cross-linking	Chemical reactions between functional groups on nanocellulose and cross-linking agents.	• High cross-linking density can be achieved. • Tunable mechanical properties. • Enhanced stability.	• May involve toxic chemicals. • Potential alteration of nanocellulose properties.	• High mechanical strength. • Improved stability and durability. • Tunable swelling behavior. • Potential toxicity concerns depending on the cross-linking agents used.	351 and 439
Physical cross-linking	Entanglement or physical interactions such as hydrogen bonding or hydrophobic interactions between nanocellulose chains.	• Simple and environmentally friendly. • No chemical agents required.	• Lower mechanical strength compared to chemical cross-linking. • Limited stability.	• Moderate mechanical strength. • Responsive to environmental stimuli (*e.g.*, temperature, pH). • Biocompatible and suitable for biomedical applications. • May undergo reversible gel–sol transitions.	392 and 440
Ionic cross-linking	Interaction between oppositely charged ions, often involving polyelectrolytes and counterions.	• Mild conditions and simple preparation. • Can achieve tunable mechanical properties.	• Limited stability in certain environments. • Sensitivity to pH and ionic strength variations.	• Variable mechanical properties depending on ionic interactions. • Responsive to environmental changes, such as pH and ionic strength. • Suitable for controlled release applications due to ion exchange capabilities.	10 and 72
UV cross-linking	Initiation of cross-linking reactions by ultraviolet (UV) radiation-induced radicals.	• Rapid cross-linking process. • Precise spatial and temporal control.	• Requires photo-initiators which may have toxicity concerns. • Limited penetration depth of UV light.	• Quick gelation and cross-linking. • Possibility of achieving spatially controlled cross-linking. • High mechanical strength and stability. • Applicable for patterning and 3D printing of hydrogels.	441 and 442
Enzymatic cross-linking	Enzyme-mediated formation of cross-links between nanocellulose chains.	• Biocompatible and environmentally friendly. • High specificity and mild reaction conditions.	• Relatively slower reaction kinetics. • Limited availability of suitable enzymes.	• Biocompatible and suitable for biomedical applications. • Controlled and precise cross-linking. • Retention of native nanocellulose properties. • Potential for functionalization through enzyme engineering.	244, 439 and 443
Doubly cross-linked hydrogels	Combination of two or more cross-linking methods to enhance hydrogel properties.	• Synergistic combination of advantages from different cross-linking methods. • Enhanced mechanical strength and stability.	• Complex synthesis process. • May require optimization of cross-linking conditions.	• Superior mechanical properties compared to single cross-linking methods. • Enhanced stability and durability. • Tunable properties by adjusting the ratio of cross-linking methods. • Suitable for applications requiring high mechanical strength and stability.	444 and 445

with genipin, were fabricated. The hydrogels exhibited good swelling capacity and gel yield.[337] They demonstrated antibacterial activity against *E. coli* and *S. aureus*, with inhibition ranging from 50% to 88%. *In vitro* studies showed high cytocompatibility and drug release (>80% and >90% after 24 hours, respectively). Overall, these hydrogels showed promising antibacterial properties, suggesting their potential for wound dressing and healing applications, highlighting the interest of glutaraldehyde in

enhancing mechanical properties.[337] In addition, carbodiimides such as 1-ethyl-3-(3-dimethylaminopropyl) carbodiimide (EDC) and *N*-hydroxysuccinimide (NHS), have been successfully employed to chemically cross-link nanocellulose-based hydrogels in various biomedical and materials science applications.[352,453] In the context of hydrogel formation, carbodiimides serve as coupling agents, facilitating the covalent bonding between carboxyl groups on the nanocellulose and amine groups on other components of the hydrogel system.[352,453,454] The cross-linking process typically involves the activation of carboxyl groups on the nanocellulose surface by EDC, forming an *O*-acylisourea intermediate. This activated intermediate then reacts with NHS, creating a stable NHS-ester. These activated nanocellulose molecules can subsequently form covalent bonds with amine-containing entities, such as polymers or other nanocellulose chains, resulting in a chemically cross-linked hydrogel network.[455,456] The versatility of carbodiimide chemistry makes it a valuable tool in tailoring nanocellulose hydrogels for biomedical applications.[457] In a recent investigation, a 3D composite scaffold was developed using bioprinting technology, comprising cellulose nanofibrils (TCNFs), chitosan, and casein to address traumatic hemorrhage. Casein bioconjugated TCNFs, cross-linked by carbodiimide, were bioprinted to fabricate customizable 3D scaffolds. *In situ* cross-linking was achieved through green ionic complexation.[457] The covalent conjugation of TCNF, casein, and chitosan was confirmed by various analytical techniques. The 3D composite scaffold exhibited superior swelling behavior and faster blood clotting compared to TCNF scaffold and commercial dressings. It promoted higher thrombin content and stable blood clot formation, essential for faster coagulation. Furthermore, it showed enhanced efficiency in entrapping red blood cells, crucial for inducing clotting. *In vitro* cytocompatibility studies demonstrated cell growth and proliferation, vital for wound healing.[457] In another study, novel composite scaffolds were developed for wound dressing and tissue engineering by electrospinning keratin/bacterial cellulose fibers and electrospraying hydrogel particles. The hydrogel particles, based on nonionic triblock copolymers conjugated with Tragacanth gum, were cross-linked *via* carbodiimide chemistry.[458] This process improved hydrogel embedding into the fibrous network without altering its structure or fiber diameter. Composite modification significantly enhanced hydrophilicity (by ~23%), elasticity modulus (by ~31%), tensile strength (by ~35%), and ductility (by ~23%). *In vitro* biocompatibility studies with L929 fibroblast cells confirmed improved biocompatibility, cell adhesion, and proliferation on the modified scaffolds.[458]

3.2.2 Physical crosslinking. Physical crosslinking methods play a pivotal role in the formulation of advanced hydrogels. In these methods, the hydrogel structure is strengthened through non-covalent interactions, encompassing hydrogen bondings, van der Waals forces, and hydrophobic interactions.[20,361] A noteworthy application of physical crosslinking is observed in the development of temperature-sensitive hydrogels. These hydrogels possess a distinctive property, undergoing gelation at physiological temperatures, ensuring compatibility with biological systems.[176,440,459] This feature is particularly crucial in biomedical applications, where hydrogels need to respond to the body natural temperature, facilitating seamless integration with surrounding tissues.[460] Recently, cellulose-polyvinyl alcohol (PVA) hydrogels were prepared *via* physical cross-linking, forming hydrogen bonds between PVA and cellulose chains during the formation of hydrogels. Suspensions of cellulose at concentrations of 3 vol%, 1.5 vol%, and 0.75 vol% were blended with PVA (5 w/v%) dissolved at 80 °C. After freezing at −20 °C for two hours, samples underwent six freeze–thaw cycles.[461] Following physical crosslinking, samples were dried at 30 °C. The resulting hydrogels exhibited structural integrity. The cellulose concentration and size affected the hydrogel properties, with hydrogen bonding facilitating stronger PVA–cellulose interactions.[461] In addition to temperature, several other parameters can be manipulated to achieve physically crosslinked cellulose-based hydrogels, offering a versatile approach to tailor their properties. One critical factor is pH, as it influences the ionization state of cellulose and other components in the hydrogel system.[462] By adjusting pH, researchers can modulate the degree of ionization of cellulose chains and the interactions between polymer chains, thereby controlling the gelation process and the mechanical properties of the resulting hydrogel. Moreover, the concentration of cellulose and other polymers in the solution plays a crucial role in gel formation. Higher polymer concentrations typically lead to denser networks and stronger gels due to increased entanglement and intermolecular interactions.[7,8] Additionally, the presence of salts or additives in the solution can impact gel properties by altering the ionic strength, solvation, and electrostatic interactions in the hydrogel matrix.[463,464] Furthermore, the choice of solvent or solvent mixture affects cellulose dissolution, chain conformation, and subsequent gel formation kinetics. Solvents with different polarities or hydrogen bonding capabilities can induce variations in cellulose hydration and aggregation, influencing gel structure and mechanical strength.[465–467] However, cellulose-based hydrogels developed through physical cross-linking processes often encounter limitations in their mechanical properties when compared to those obtained *via* chemical cross-linking methods.[140,444,468] Physical cross-linking relies on non-covalent interactions, such as hydrogen bonding or hydrophobic interactions, to form the network structure of the hydrogel. While this approach offers advantages in terms of biocompatibility and environmental friendliness, it typically results in weaker mechanical strength and lower elasticity compared to chemical cross-linking.[469] The mechanical properties of physical cross-linked cellulose hydrogels are influenced by several factors. Firstly, the type and strength of the non-covalent interactions involved in cross-linking play a significant role. Hydrogen bonding, for example, is relatively weaker compared to covalent bonds formed in chemical cross-linking, leading to lower mechanical strength.[470] Secondly, the density of cross-linking points within the hydrogel network affects its mechanical properties. Physical cross-linking may result in fewer cross-links, leading to larger mesh sizes and decreased mechanical integrity.[140,470,471]

3.2.3 Enzymatic crosslinking. Enzymatic crosslinking stands as a noteworthy approach employed in the development of hydrogels, including those reinforced with nanocellulose, for diverse biomedical applications.[244,472,473] This method capitalizes on the catalytic activity of enzymes, such as transglutaminase and horseradish peroxidase, to facilitate the formation of covalent bonds within the hydrogel network. Enzymatic crosslinking distinguishes itself through precision, biocompatibility, and the mild conditions under which it operates, rendering it particularly valuable in the context of tissue engineering and regenerative medicine.[439,472] The horseradish peroxidase (HRP) enzyme proves instrumental in crosslinking nanocellulose with other polymers to fabricate nanocellulose-reinforced hydrogels.[244] In this method, HRP catalyzes the oxidative coupling of phenolic compounds in the presence of hydrogen peroxide (H_2O_2). This reaction results in the formation of covalent bonds between phenolic groups on the nanocellulose surface and other polymers, establishing a robust and stable network within the hydrogel.[244] In addition, transglutaminase-mediated crosslinking can be precisely controlled, allowing for tailored adjustments to the hydrogel properties.[474,475] Through its enzymatic action, transglutaminase catalyzes the formation of covalent bonds between amino acid residues, enabling the cross-linking of polymer chains in hydrogel matrices.[474,475] The enzymatic cross-linking confers enhanced mechanical strength, stability, and biocompatibility to the resulting composite hydrogels. Dong *et al.*[472] prepared gelatin/CNCs composite hydrogels (Gel–TG–CNCs) using microbial transglutaminase (mTG) as a crosslinking catalyst and CNCs as nanoreinforcements. Dynamic rheological measurement and uniaxial compression tests assessed the effects of mTG and CNC contents on storage modulus and breaking strength. Results showed significant enhancements in mechanical properties, with Gel–TG–CNCs (2%) exhibiting a breaking strength of 1000 g at 25 °C, 30 times greater than pure gelatin hydrogels.[472] MTT tests confirmed excellent biocompatibility of enzymatically-crosslinked hydrogels. These findings highlighted potential applications of these hydrogels in biomedicine as wellas the dual reinforcing effect of CNCs and mTG in enhancing mechanical strength and biocompatibility in composite hydrogels.[472] The enzymatic crosslinking approach offers several advantages, encompassing mild reaction conditions, biocompatibility, and the ability to create nanocellulose-reinforced hydrogels under physiological conditions.[472,473] Additionally, the resultant hydrogels exhibit heightened mechanical properties and stability, rendering them suitable for a spectrum of biomedical applications, including tissue engineering and drug delivery systems.[476] A key advantage of enzymatic crosslinking is its capability to preserve the viability of encapsulated cells, crucial when designing hydrogel constructs for tissue engineering, especially those hosting living cells. The process, executed under mild physiological conditions, ensures that the crosslinking does not harm or compromise the embedded cells. This facilitates the creation of cell–laden hydrogel constructs, where cells can proliferate and differentiate, contributing to tissue engineering.[477,478] In the field of cartilage engineering, Trachsel *et al.*[479] have utilized enzymatic crosslinking with sortase A to develop biocomaptible double network (DN) hydrogels containing CNFs. These matrices exhibited superior mechanical properties compared to single-network hydrogels and supported high cell viability of encapsulated human auricular chondrocytes (hACs). Incorporating CNFs improved rheological properties for extrusion-based 3D printing.[479] Incorporating hACs resulted in sustained viability for 3 weeks, indicating suitability for tissue engineering. DN–CNF mixtures showed good printability and fidelity as well as rapid crosslinking. Bioprinted DN–CNF grids maintained over 90% viability for a week, demonstrating their potential for advanced cell–laden constructs in tissue engineering.[479] Enzymatic crosslinking provides meticulous control over reactions, enabling researchers to fine-tune hydrogel properties like mechanical strength and crosslink density through enzyme concentration and reaction duration adjustments. This precision is crucial for tailoring hydrogels to diverse tissue engineering needs, ensuring optimal alignment of mechanical stability, porosity, and degradation rates with specific tissue requirements.[244,472,474]

3.2.4 Hybrid crosslinking strategies (dual crosslinking). They encompass the innovative amalgamation of multiple crosslinking methods to leverage their unique advantages, yielding hydrogels with superior mechanical properties and enhanced stability. This approach allows for the exploitation of synergistic benefits arising from the complementary nature of various crosslinking techniques.[480] The integration of chemical and physical crosslinking methods exemplifies a powerful synergy. Chemical crosslinking introduces covalent bonds between polymer chains, ensuring robustness, while physical crosslinking mechanisms, such as hydrogen bonding or van der Waals forces, fortify the hydrogel network through weaker yet dynamic interactions. This hybrid approach is particularly valuable in tissue engineering applications, where tailoring hydrogel properties to specific requirements is indispensable. By selectively combining chemical and physical crosslinking, researchers can fine-tune the mechanical strength, elasticity, and stability of hydrogels according to the needs of diverse tissues.[480,481] For example, injectable hydrogels, while advantageous in biomedical contexts, often suffer from weak mechanical and functional properties. In a study, *in situ*-gelling nanocomposite hydrogels based on poly(oligoethylene glycol methacrylate) (POEGMA) and rigid rod-like CNCs were developed using both physical and chemical crosslinkings to address this issue.[482] By physically incorporating CNCs into hydrazone cross-linked POEGMA hydrogels, macroscopic properties such as gelation rate, swelling kinetics, and mechanical strength were enhanced.[482] Double cross-linking *via* strong adsorption of POEGMA precursor polymers onto CNCs significantly improved mechanical properties, with up to 35-fold increases in storage modulus observed. These enhancements, coupled with maintained cell viability, indicate the potential of POEGMA–CNC nanocomposite hydrogels for tissue engineering and cell growth platforms.[482] In addition, double ionic and covalent crosslinking strategies can be also synergistically employed to enhance mechanical and functional properties of resulting hydrogels, offering a robust platform for various biomedical and industrial

applications.[483] By incorporating both types of crosslinks, hydrogels can achieve superior strength, toughness, and stability compared to their single-crosslink counterparts. The ionic interactions provide reversible bonds, imparting dynamic properties and responsiveness to environmental stimuli, while covalent bonds offer long-term structural integrity.[483,484] In a recent research study, Xu *et al.*[484] prepared doubly cross-linked (DC) nanocellulose hydrogels, featuring both ionic and chemical crosslinks. DC-Hydrogels demonstrated superior mechanical properties compared to singly cross-linked counterparts. Fe^{3+} cross-linked and chemically cross-linked nanocellulose hydrogels fractured at 117 kPa (strain = 80%) and 17 kPa (strain = 40%) respectively.[484] DC nanocellulose hydrogels displayed remarkable compressive strength (>450 kPa) and strain (90%) without fracturing, broadening their application scope. Additionally, these hydrogels exhibited optical transparency and high swelling, meeting practical demands.[484] Moreover, the limited mechanical strength of hydrogels historically hindered their biomedical and industrial applications. To overcome this issue, Zhang *et al.*[483] developed a nanocomposite network of poly(acrylic acid-*co*-acrylamide) (PAAAM), sequentially cross-linked by quaternized tunicate cellulose nanocrystals (Q-TCNCs) and Fe^{3+}. Q-TCNCs served as both reinforcing agents and cross-linkers, facilitating loose cross-linking in the nanocomposite hydrogels, while Fe^{3+} coordinated with $-COO^-$ groups of PAAAM, creating compact cross-linking.[483] The resulting dual cross-linked hydrogel exhibited excellent toughness, 340 times greater than mono-cross-linked hydrogel and 10 times that of PAAAM hydrogel. Notably, the nanocomposite hydrogels displayed remarkable self-recovery after stretching when treated with $FeCl_3$ aqueous solution.[483] These study highlighted the efficacy of double cross-linking in creating tough nanocomposite hydrogels reinforced with nanocellulose, offering a versatile approach for enhancing hydrogel properties.[483,484]

4 Nanocellulose-based hydrogels for tissue engineering applications

Nanocellulose-based hydrogels have revolutionized the field of tissue engineering and regenerative medicine, owing to their exceptional versatility and biocompatibility.[21,29,30,51,401] In this section, the latest applications of these hydrogels in regenerating different biological tissues are described and discussed. The recent progress in employing cellulose-based hydrogels for tissue engineering applications is outlined in Table 4. Nanocellulose is frequently combined with other biomaterials and polymers to fabricate customized hydrogels tailored to meet the specific challenges presented by different tissue types. By encapsulating biological cues and incorporating diverse functionalities, these hydrogels demonstrate mechanical strength and biological activities essential for effective tissue engineering. Vital tissues in living organisms, such as skin, cartilage, bone, cardiac muscle, nerves, and vasculature, play critical roles in their structural integrity, function, and overall well-being.[20,49,335] However, injuries, diseases, or congenital conditions can compromise the integrity of these tissues, leading to pain, reduced mobility, impaired organ function, or life-threatening situations. Consequently, the imperative to repair, regenerate, or replace damaged tissues has driven significant advancements in regenerative medicine.[485–487] Nanocellulose hydrogels have emerged as remarkable materials, offering interesting properties that facilitate tissue repair. Fig. 19 summarizes key properties and various tissue engineering applications of nanocellulose-based hydrogels.

As highlighted in Table 4, the utilization of nanocellulose-based hydrogels highlights a significant advancement in the field of tissue engineering. Through meticulous design and innovative processing techniques, these hydrogels have demonstrated remarkable mechanical and biological properties essential for the engineering of various tissues, including skin, cartilage, bone, heart, and nerve, among others. The data in Table 4 provides a comprehensive overview of nanocellulose-based hydrogel compositions, processing methods, and the achieved mechanical and biological outcomes. These findings underscore the promising potential of nanocellulose-based hydrogels in revolutionizing tissue engineering therapies, offering tailored solutions for diverse clinical applications. The use of nanocellulose-based hydrogels represents a significant step forward in the pursuit of innovative and effective strategies to repair and regenerate damaged tissues, ultimately improving the quality of life for patients in need of such treatments.

4.1 Skin tissue engineering

Skin acts as a barrier protecting the body from pathogens and regulating temperature. Skin injuries, whether due to wounds, burns, or chronic ulcers, can lead to severe complications. Nanocellulose hydrogels provide a biocompatible and supportive scaffold, promoting cell adhesion, proliferation, and wound healing. Their high water content maintains a moist environment, enhancing tissue engineering and minimizing scarring.[207,520] For instance, in a recent study, a biocompatible and biodegradable hydrogel system was developed by combining curcumin (Cur) solubilization with pluronic F-127, polyvinyl alcohol (PVA) gelation, and porosity enhancement by TEMPO-oxidized cellulose nanofiber (TOCN). This physically cross-linked TOCN-PVA-Cur hydrogel, prepared *via* freeze-thawing, effectively released Cur, enhancing wound healing. *In vitro* studies demonstrated the uptake of curcumin by fibroblast cells. Application of TOCN-PVA-Cur to rat full-thickness skin wounds increased wound closure, stimulated neoepidermis and granulation tissue formation, and encouraged collagen fiber accumulation, highlighting the hydrogel potential for promoting natural wound healing (Fig. 20A and B).[521] In addition to the compelling findings presented in Table 4 regarding the use of nanocellulose-based hydrogels as functional matrices for repairing skin tissues, it's worth noting that certain microbial infections can damage skin tissue. In this regard, cellulose hydrogels have also demonstrated intriguing antibacterial properties and proven biocompatibility, thus supporting the regeneration of skin tissues.[219,517,522] In a recent study conducted by Hu *et al.*,[522] ε-polylysine (ε-PL), known for its biocompatibility and antibacterial properties, was integrated

Table 4 Summary of recent research studies focused on use of nanocellulose-based hydrogels for achieving the engineering of various tissues, including skin, cartilage, bone, heart, nerve and vasculature

Regenerated tissues	Hydrogel composition	Results	Ref.
Skin	Bacterial cellulose/acrylic acid hydrogel	• *In vitro* tests confirmed hydrogel supported keratinocytes and fibroblasts attachment. • Hydrogel maintained cell viability and facilitated cell transfer without excess migration. • *In vivo* studies showed hydrogel alone and with cells accelerated wound healing. • Hydrogel with cells outperformed hydrogel alone in healing, shown by gross appearance. • Masson's trichrome staining highlighted better performance of hydrogel with cells.	488
Skin	Chloramphenicol (CAP) loaded 2,3 dialdehyde cellulose (DABC) hydrogel membranes	• Bacterial cellulose transformed into DABC using sodium metaperiodate oxidation. • DABC membranes released 99–99.5% of CAP within 24 hours, no burst effect. • Both CAP-loaded BC and DABC showed prolonged antibacterial activity for 3 days. • CAP-loaded DABC enhanced fibroblast adhesion and proliferation *versus* CAP-loaded BC. • Fibroblast support confirmed by MTT tests.	489
Skin	Bacterial cellulose/polyacrylamide hydrogel microparticles	• Microparticles showed cytocompatibility with L929 cells. • Non-irritating in dermal irritation tests. • Hydrogel improved wound contraction and epithelialization. • Accelerated fibroblast proliferation; resulted in complete wound repair. • Confirmed biocompatibility and effectiveness as wound dressing material.	490
Skin	Carboxymethyl cellulose/hydroxyethyl cellulose/LAPONITE®/acetylated distarch phosphate/berberine	• The biocomposite effectively controlled oxidative stress and inflammation in chronic wounds. • It reduced keratinocyte hyperproliferation by 25%, aiding wound healing. • Berberine and hydrogel synergy notably enhanced material properties. • The biocomposite is highly promising for dermatological applications, promoting wound healing.	491
Skin	A series of hydrogels (CMC-ADH/PEG-FBA) was developed by chemically linking carboxymethyl cellulose-*graft*-adipic dihydrazide (CMC-ADH) with 4-formylbenzoic acid-terminated poly(ethylene glycol) (PEG-FBA)	• The hydrogels sustained drug release and showed effective antibacterial properties *in vitro*. • *In vivo* studies confirmed their hemostatic and wound-healing effects. • They accelerated wound healing and exhibited superior hemostatic effects. • The hydrogels adhered well to irregular wounds and enhanced angiogenic capabilities. • Their performance attributes include stopping bleeding, creating a protected wound environment, releasing ciprofloxacin, reducing inflammation, and promoting tissue engineering.	413
Skin	Boronic acid was grafted onto carboxyethyl cellulose (CMC) to create boronic acid grafted CMC (CMC-BA). Subsequently, a self-healing hydrogel was produced by crosslinking with polyvinyl alcohol (PVA) through dynamic boronic ester bonds.	• The CMC-BA/PVA hydrogel displayed excellent biocompatibility and degradability. • It was susceptible to cellulase both *in vitro* and *in vivo*. • Rapid formation of hydrogel enabled localized injection, suitable for irregular wounds. • *In vivo* experiments demonstrated airtight adhesion, reducing blood loss. • The hydrogel acted as a drug carrier, minimizing acute *in vivo* toxicity. • It preserved the antitumor efficacy of doxorubicin through controlled release.	492
Skin	Hydrogel fabricated using TEMPO-oxidized bacterial cellulose (TBC) combined with tannic acid-modified metal–organic framework (TA@ZIF-8 [TZ]), and loaded with MXene (TBC-TA@ ZIF-8-MXene [TTZM]).	• The hydrogel exhibited strong antibacterial effects and sped up wound healing. • Under near-infrared light, Zn^{2+} and MXene agents synergistically inhibited bacterial metabolism. • TTZM hydrogel stimulated blood vessel growth and regulated inflammation for wound healing. • In bacteria-infected wounds, NIR-responsive TTZM hydrogel accelerated closure and eliminated infections.	493
Skin	A bilayer material was prepared by electrospinning a hybrid of PVA and bacterial cellulose (BC NFs) atop a highly interconnected porous 3D gelatin-PVA hydrogel obtained by freeze-drying.	• FTIR confirmed cross-linking of layers, SEM showed porous structure, random and aligned NFs. • Water contact angle indicated a hydrophilic surface for the bilayer material. • Swelling analysis indicated high swelling, while degradation analysis showed good stability. • The bilayer material released Ag-sulfadiazine in a sustained and controlled manner, exhibiting antibacterial activity. • *In vitro* studies on fibroblasts and human embryonic kidneys showed desirable cell viability and adhesion. • The synergistic effect of NFs and hydrogel resulted in a potential wound dressing material.	494
Skin	Multimodal antibacterial cellulose wound dressing (MACD) with photothermal therapy (PTT) was developed	• The developed hydrogels showed remarkable antibacterial properties. • Ionic liquids and quaternary ammonium salts contributed to photothermal conversion ability.	495

Table 4 (*continued*)

Regenerated tissues	Hydrogel composition	Results	Ref.
	by graft polymerizing an imidazolium ionic liquid. monomer containing an iron complex anion structure.	• Hydrogel dressings exhibited 99.57% antibacterial efficacy against *S. aureus*. • They also demonstrated 99.16% efficacy against *E. coli*. • Minimal hemolysis (<5%) and high cell viability (>85%) were observed. • *In vivo* experiments confirmed accelerated wound healing.	
Skin	Bacterial cellulose (BC) dressings incorporating ε-polylysine (ε-PL), cross-linked with a biocompatible and mussel-inspired polydopamine (PDA).	• BC membranes were coated with PDA and treated with ε-PL. • Modified membranes exhibited robust antibacterial properties *in vitro* and *in vivo*. • Membranes showed excellent hemocompatibility and cytocompatibility. • Functionalized membranes significantly improved wound healing in rats. • Complete wound closure occurred with functionalized membranes. • Histological analysis showed thicker, smoother skin with modified membranes.	496
Skin	Water-responsive hybrid hydrogels based on carboxymethyl cellulose (CMC) and poly(vinyl alcohol) (PVA) using citric acid (CA) as the cross-linking agent were developed.	• Hydrogels were designed with flexible swelling properties through molecular mass and degree of functionalization. • Swelling degrees ranged from 100% to 5000%, with gel fraction from 40% to 80%. • Highly absorbent hydrogels were produced, influenced by CA crosslinker concentration and presence of PVA. • Crosslinking mechanism involved ester bonds formed between CA, CMC, and PVA polymers. • Hydrogels presented hydrophilicity, permeability and structural features dependent on crosslinking and composition. • Hydrogels showed cytocompatibility with *in vitro* cell viability responses over 90%, promising for skin repair.	497
Cartilage	Hydrogel composite comprising cross-linked thiolated chitosan (TCS) and carboxymethyl cellulose (CMC) (TCS/CMC).	• Rheological analysis confirmed TCS/CMC hydrogels strength exceeding 2.5 kPa elastic modulus. • Crosslinking impacted network distribution, surface morphology, pore size, gelation time, and degradation. • Hydrogels maintained 90% weight and shape for 21 days, releasing TGF-β1. • *In vitro* experiments showed accelerated BMSC growth with TGF-β1-loaded hydrogels. • *In vivo* rat knee studies for 8 weeks demonstrated hydrogel effectiveness in cartilage repair.	498
Cartilage	Injectable hydrogels based on chitosan (CS), cellulose nanocrystals (CNCs) and pectin were designed	• Injectable hydrogels of CS, CNCs, and pectin exhibited significant internal structure. • Pectin and CS-based hydrogels mimicked ECM, but their low mechanical strength limited cartilage repair. • CNCs were added to reinforce natural polysaccharide-based hydrogels, aiming to enhance mechanical properties. • Varying weight ratios of CNCs improved network structure, reduced swelling, and enhanced degradation resistance. • CNC incorporation increased chondrocyte proliferation, suggesting potential for cartilage tissue regeneration.	499
Cartilage	Double-network microcrystalline cellulose hydrogels	• A chemical-physical multi-step cross-linking strategy was used to fabricate hydrogels. • Hydrogels biomimetic macroporous shape and high water content suited chondrocyte adhesion and proliferation. • Hydrogels met cartilage tissue engineering scaffold requirements with high compressive strength (4.53 MPa). • *In vitro* findings showed hydrogels enhanced cell adhesion and proliferation safely. • Hydrogels demonstrated stability, slow degradation, and strong histocompatibility *in vivo* implantation.	500
Cartilage	Azide and alkyne functional groups were incorporated into citric acid-modified hydroxyethyl cellulose (HEC) utilizing a bioorthogonal click chemistry approach.	• Lyophilized samples exhibited interconnected microstructure suitable for cartilage tissue engineering. • Crosslinking improved scaffold stability. • The click sample retained high water uptake (~650% swelling degree). • Click sample showed Young's modulus ~10 MPa, tensile strength ~0.43 MPa, resembling natural cartilage. • *In vitro* assays confirmed click sample biocompatibility, chondrogenic potential, and bioorthogonal characteristics.	391
Cartilage	Composite hydrogels comprising methacrylated gelatin (GelMA) and bacterial cellulose (BC) were successfully fabricated.	• The morphology of GelMA/BC hydrogels was analyzed with SEM. • Hydrogels displayed interconnected porous structure, pore sizes decreased with BC content. • Characterization included swelling experiments, XRD, TGA, rheology, and compressive tests.	501

Table 4 (*continued*)

Regenerated tissues	Hydrogel composition	Results	Ref.
		• Composite hydrogels showed enhanced mechanical properties compared to pure GelMA. • Preliminary biocompatibility assessment with chondrocytes showed cell proliferation and phenotype maintenance.	
Cartilage	Bacterial cellulose-chitosan (BCC) and alginate-gelatin (AG) were synergistically utilized to fabricate 3D hydrogel scaffolds.	• Composite scaffolds featured robust 3D architecture with average pore diameters. • BCC–AG scaffolds exhibited substantial compressive strength, stability, and biocompatibility. • Mesenchymal stem cells (hMSCs) mixed with hydrogel, cultured in chondrogenic medium. • Hydrogel scaffold supported cell proliferation, leading to glycosaminoglycan and collagen accumulation at 6.26% and 6.71% (w/w), respectively, after 42 days of incubation. • BCC–AG scaffolds show potential for cartilage tissue engineering applications.	16
Cartilage	Alginate dialdehyde–gelatin (ADA–GEL)/nanofibrillated cellulose (NFC) hydrogel	• Nanofibrillated cellulose (NFC) introduced into ADA–GEL matrix to improve physicochemical properties. • Fourier transform infrared spectra show no chemical interaction between NFC and ADA–GEL. • Scanning electron microscopy reveals NFC fibers embedded in hydrogel matrix, confirming fiber-reinforced composite. • NFC-reinforced ADA–GEL (AG-N) composite hydrogels exhibited increased stiffness, up to 19.6 $\pm$ 3.0 kPa. • Cell viability, proliferation, and chondrogenic differentiation assessed, suggesting potential osteochondral plug application.	502
Cartilage	Poly(vinyl alcohol) grafted glycidyl methacrylate/cellulose nanofiber (PVA-*g*-GMA/CNF) injectable hydrogels were developed.	• PVA-*g*-GMA lacked mechanical properties and cell proliferation. • Cellulose nanofibers (CNF) were chosen as reinforcement to enhance properties. • UV curing formed hydrogels with interconnected microporosity and pore size diameters of 3–68 μm. • Hydrogels exhibited high physicochemical properties: gel fraction (81–82%), porosity (83–94%), water content (73–87%), and swelling (272–652%). • Increasing CNF concentration improved water content, swelling, compressive strength, and modulus while reducing porosity. • 0.7% CNF hydrogels showed superior cell proliferation, indicating potential for meniscus tissue engineering.	503
Bone	New hydrogel scaffolds were developed for bone tissue engineering, incorporating inorganic calcium in the form of calcium phosphate, both alone and in combination with $CaCO_3$, within bacterial cellulose (BC) matrices.	• Fourier transform infrared and thermogravimetric analyses confirmed BC and inorganic calcium presence. • Scanning electron microscopy revealed porous structures ranging from 50 to 200 μm. • Swelling studies showed notable capacity in calcium phosphate-filled and calcium phosphate & $CaCO_3$-filled scaffolds. • Compressive strength of calcium-filled scaffolds ranged from 0.24 to 0.60 MPa, comparable to trabecular bone. • Significant cell viability persisted for up to 72, 120, and 168 hours.	504
Bone	Cellulose hydrogels were crosslinked using citric acid.	• Cellulose hydrogels were crosslinked using non-toxic citric acid. • Citric acid induced –COOH functional groups, enhancing hydrophilicity and roughness. • Physiochemical, morphological, and mechanical analyses were conducted before and after crosslinking. • Human mesenchymal stem cell responses were influenced by surface chemistry and roughness.	505
Bone	Well-defined porous silk fibroin/cellulose hydrogels were successfully designed.	• Cellulose enhanced mechanical properties and stiffness of silk fibroin (SF) material. • Atmospheric humidity regenerated cellulose framework, followed by SF assembly. • Hydrogels exhibited β-sheet conformation in surface-near layers, decreasing in deeper layers. • Cellulose framework boosted mechanical properties; SF matrix supported cell growth. • MC3T3-E1 cells on SF/cellulose hydrogels showed accelerated osteocyte differentiation.	506
Bone	Nanocomposite scaffold of semi-interpenetrating network cellulose-*graft*-polyacrylamide/nano-hydroxyapatite was synthesized using free radical polymerization.	• Scaffolds fabricated *via* freeze-drying with compressive strength of 4.80 MPa. • Elastic modulus measured at 0.29 GPa under optimal conditions. • Scaffolds exhibited 47.37% porosity. • Apatite-forming ability assessed by immersion in simulated body fluid (SBF). • Apatite particles observed on scaffold surface after 14 days in SBF.	507

Table 4 (*continued*)

Regenerated tissues	Hydrogel composition	Results	Ref.
Bone	Cellulose nanofiber (CNF)-reinforced oxidized alginate (OSA)/gelatin (Gel) hydrogel	• OSA/Gel/CNF sample displayed notable compressive modulus (up to 361.3 kPa). • Gelation time ensured excellent injectability (~150 s). • Self-healing efficiency reached up to 92%, allowing dynamic adjustments and personalized therapies. • OSA/Gel/CNF hydrogel exhibited excellent biomineralization (Ca/P ratio ~1.69). • Enhanced preosteoblast cell (MC3T3-E1) viability, proliferation, and osteogenic differentiation observed (over 96%).	508
Bone	Citric acid-cross-linked carboxymethyl cellulose (C3CA) scaffolds were fabricated using freeze-drying	• Citric acid-cross-linked carboxymethyl cellulose scaffolds were developed *via* freeze-drying at −20, −40, or −80 °C. • Scaffold pore sizes differed, with −20 °C scaffolds having larger pores (74 ± 4 μm) compared to −40 and −80 °C. • Saos-2 osteoblast cell line proliferation and differentiation were supported, with significant matrix mineralization observed in −40 °C scaffolds. • Subcutaneous implantation in rats showed matrix formation as early as 14 days in −40 °C scaffolds, compared to 28 days in −20 and −80 °C.	509
Heart	Electroconductive, thermosensitive, and injectable hydrogel composed of chitosan, pluronic, and gold-decorated cellulose nanofibers was developed.	• The hydrogels possessed porous structures with open pore channels ranging from 50 to 200 μm. • Shear rate sweep measurements demonstrated reversible sol-to-gel phase transitions within 5 minutes. • These hydrogels exhibited shear-thinning behavior, with a shear modulus ranging from 1 to 12 kPa. • Electrical conductivity studies revealed a conductance of 6×10^{-2} S m^{-1} at 75 mM Au concentration. • *In vitro* cytocompatibility assays with H9C2 cells showed high biocompatibility and strong cell adhesion. • The developed hydrogel showed significant potential as injectable biomaterials in cardiac tissue engineering.	510
Heart	Cellulose acetate (CA)/regenerated cellulose (RC) hydrogel scaffolds were developed.	• CA and RC surfaces promoted cardiac cell growth, enhanced cell connectivity, and improved electrical functionality. • CA scaffolds provided optical clarity and non-autofluorescent properties, enabling accurate optical measurements in cell constructs. • These scaffolds were moldable to intricate shapes, crucial for tissue engineering design. • Cellulose scaffolds offered excellent adhesion, nanoscale molding capabilities, and controlled biodegradability for *in vitro* cardiac construct growth.	511
Heart	Carboxymethyl cellulose–alginate interpenetrating hydroxy ethyl methacrylate crosslinked polyvinyl alcohol reinforced hybrid hydrogel templates	• Two superabsorbent hydrogels developed using interpenetration chemistry displayed superior physiochemical features. • *In vitro* degradation showed acceptable weight composure and pH changes for both hydrogels. • Both hydrogels demonstrated hemocompatibility and biocompatibility. • Hydrogels facilitated anterograde and retrograde migration of H9c2 cells. • Coculture with swine epicardial adipose tissue cells and cardiac fibroblasts showed synchronous cell growth. • Hydrogels containing H9c2 cells promoted extracellular matrix production.	512
Heart	TEMPO-oxidized cellulose nanofibrils (TOCNs) and sulfonated carbon nanotubes (SCNTs) used to prepare TOCN–SCNT composite hydrogels.	• TOCN–SCNT hydrogels showed conductivity between 5.2×10^{-6} to 6.2×10^{-2} S cm^{-1} by adjusting SCNT content from 0 to 5 wt%. • 1 wt% SCNT incorporation promoted adhesive cell growth and proliferation. • Hydrogel exhibited higher Connexin 43 and cardiac troponin-T proteins, suggesting myocardial tissue engineering scaffold potential.	513
Nerve	Cellulose nanofibers (CNFs)/polypyrrole (PPy)	• CNFs were electrospun from cellulose acetate. • CNFs were surface-modified *via in situ* PPy polymerization. • PPy particles adhered to nanofiber surface, increasing conductivity 105-fold. • No cytotoxic effects observed *in vitro*. • SH-SY5Y human neuroblastoma cells exhibited enhanced adhesion on PPy-coated CNFs. • Cell viability sustained for up to 15 days of differentiation. • Cells adopted neuron-like morphology on PPy-coated CNFs.	53
Nerve	Cellulose acetate (CA)/poly(ε-caprolactone) (PCL)/graphene oxide (GO)	• A novel electroactive biocompatible nanofibrous scaffold consisting of CA, PCL and GO was prepared using electrospinning. • An optimum sample containing 0.5 wt% of GO exhibited a diameter of 280 nm. • The electrical conductivity of the sample was approximately 75 μS m^{-1}. • Chemical analysis showed no reaction during the distribution of GO within the nanofibers.	514

Table 4 (*continued*)

Regenerated tissues	Hydrogel composition	Results	Ref.
		• The optimized sample displayed a water contact angle of 39 and a tensile strength of 2.5 MPa. • Electrical activity, assessed by cyclic voltammetry, was higher in the presence of GO. • Cell viability, adhesion, and differentiation were significantly enhanced in the presence of GO.	
Nerve	Nanoporous cellulose gels (NCG) were coated with PPy nanoparticles, creating electroconductive materials.	• The NCG/PPy composite hydrogels, turned into aerogels using supercritical CO_2 drying, demonstrated remarkable properties. • They had a density of 0.41–0.53 g cm^{-3} and nitrogen adsorption surface areas ranging from 264 to 303 m^2 g^{-1}. • Additionally, they showed robust mechanical strength and electrical conductivity up to 0.08 S cm^{-1}. • *In vitro* studies indicated improved adhesion and proliferation of PC12 cells. • Electrical stimulation led to PC12 cells attaching and extending longer neurites.	515
Nerve	Chitosan–cellulose nanofiber (CS–CNF) composite self-healing hydrogels	• Incorporating cellulose nanofibers (CNFs) into chitosan (CS) improved hydrogel properties. • CNF-modified hydrogels showed enhanced self-healing, dynamic bonding, and strain sensitivity. • Neural stem cells in CS–CNF hydrogels exhibited improved oxygen metabolism and differentiation. • Metabolic changes in hydrogels aligned with neural stem cell differentiation. • Optimized CS–CNF hydrogel with 0.09 wt% CNFs showed 50% better neural engineering. • Improved hydrogel outperformed pristine CS hydrogel in zebrafish brain injury model.	516
Vasculature	Functional bacterial cellulose (BC) hydrogel incorporating silver-loaded zeolitic imidazolate framework-8 (ZIF-8) antibacterial agent.	• The biopolymer dressing exceeded 1 MPa in tensile strength. • *In vitro* tests showed antibacterial efficacy, with 0.85% survival for *E. coli* and 0.39% for *S. aureus*. • Cell culture experiments demonstrated excellent biocompatibility and notable angiogenic potential. • *In vivo* studies on rats exhibited remarkable wound healing and skin re-epithelialization. • This study introduced a high-performing dressing with potent antibacterial properties.	517
Vasculature	Multifunctional hydrogel (CCS/CCHO-Ag) was developed by incorporating silver (Ag) into catechol-modified chitosan (CCS) and aldehyde-modified cellulose nanocrystals (CCHOs).	• Cellulose nanocrystals (CNCs) in liquid crystal phase enhanced vascularization. • CCS/CCHO-Ag hydrogels had *in situ* formation, satisfactory strength, controlled Ag release. • Hydrogels exhibited antibacterial properties and biocompatibility. • They seamlessly covered and adhered to irregular wounds, reducing reinjury risk. • CCS/CCHO-Ag hydrogels promoted neovascularization and tissue engineering. • *In vitro* and *in vivo* experiments confirmed their effectiveness.	518
Vaculature	Regenerative cellulose hydrogel matrix and photo-polymerized poly(hydroxyethyl methacrylate) filler	• Biomimetic approach inspired by native blood vessels enabled fabrication of cellulose-based small-diameter artificial blood vessels (SDABV). • Gradient distribution of poly(hydroxyethyl methacrylate) in cellulose network created composite gel tube mimicking native blood vessels. • Cellulose-based SDABV hydrogels exhibited similar mechanical performance to native counterparts: tensile strength (1.4 MPa), strain (93%), Young's modulus (2.98 MPa), toughness (1040 kJ m^{-3}). • Materials demonstrated excellent suture retention, burst pressure, *in vitro* biocompatibility, low fibrinogen adsorption, and platelet adhesion. • *In vivo* experiments on rabbits confirmed material safety with no blood vessel blockages or inflammatory responses after three months.	519

into a cellulose/γ-polyglutamic acid (γ-PGA) hydrogel, creating a double-network hydrogel termed CGLH (Fig. 20C).[522] Its elastic modulus increased from 0.097 ± 0.015 MPa to 0.441 ± 0.096 MPa, and swelling ratio from 382.7 ± 24.3% to 611.2 ± 8.6%. CGLH showed promising results in preclinical models, demonstrating biocompatibility and antibacterial activity, aiding in healing infected and critical-size wounds within 12 days. It also enhanced collagen synthesis, vascularization and cell proliferation.[522]

Additionally, cellulose-based hydrogels have shown promising outcomes in skin tissue regeneration. Nanocellulose-based hydrogels have been thoroughly assessed in murine models, examining wound healing kinetics, inflammatory responses, and tissue remodeling. Metrics including wound closure rates, collagen deposition, and angiogenesis are meticulously quantified, providing valuable insights into the hydrogel effectiveness in advancing skin tissue engineering.[523] A recent

Fig. 19 Key properties and tissue engineering applications of nanocellulose-based hydrogels.

investigation showcased the expedited healing of full-thickness wounds through the application of bacterial cellulose-based multilayer composites. This innovative strategy involved employing a wound dressing composed of bacterial cellulose (BC) hydrogel, gelatin/alginate (Gel/Alg) hydrogel, and polycaprolactone (PCL) nanofibers loaded with ciprofloxacin (CIP) to facilitate *in vivo* healing.[524] The developed dressings exhibited notable water absorption and an adequate water vapor transmission rate within the initial week, confirming their effective wound exudate absorption. The drug-containing dressing demonstrated a significant release of CIP in the first four hours, followed by a gradual reduction and stabilization from hours 4 to 24, persisting until day 9.[524] This controlled CIP release effectively inhibited both positive and negative bacterial strains while ensuring the normal morphology and metabolic activity of fibroblasts. Additionally, *in vivo* experiments showcased the remarkable efficacy of CIP-loaded multilayer dressings in accelerating full-thickness wound healing within a 14-day timeframe. The dressings not only reduced inflammation but also stimulated re-epithelialization and enhanced skin engineering.[524] In an another study, bacterial cellulose nanocrystals (BCNCs) were employed to reinforce regenerated chitin (RC) fibers, forming BCNC/RC filaments. Mechanical assessments revealed a significant enhancement in the strength of the BCNC/RC filament compared to RC. A yarn of 30 BCNC-loaded fibers exhibited satisfactory mechanical performance with a knot-pull tensile strength of 9.8 ± 0.6 N.[525] *In vivo* experiments on mice demonstrated that suturing with BCNC/RC yarn promoted wound healing without adverse effects. Animal models were divided into four groups: a negative control (Group I), a positive control with commercial polyamide (PA) sutures (Group II), and two novel sutures twisted and coated BCNC/RC yarn (Group III) and twisted but uncoated BCNC/RC sutures (Group IV). Images showing the wound healing process are highlighted in Fig. 21A. Histopathology analysis revealed complete tissue morphology in Groups II, III, and IV at three and ten days post-surgery, contrasting with the unsutured Group-I mice (Fig. 21B). No decay or inflammatory lesions were observed, and collagen around the suture increased over an extended recovery period. BCNC/RC sutures promoted effective wound healing without adverse effects, comparable to commercial PA sutures after 10 days (Fig. 21B).[525]

4.2 Cartilage tissue engineering

Cartilage, crucial for joint mobility, can deteriorate due to injuries or degenerative diseases, causing pain and impaired movement. Nanocellulose hydrogels, when combined with chondrocytes or stem cells, could mimic the natural cartilage matrix. These hydrogels provide mechanical support, facilitate cell adhesion, and offer sustained release of growth factors, aiding in cartilage engineering and mitigating joint-related discomfort.[16,391] For example, 3D hierarchical porous bacterial cellulose (BC)/decellularized cartilage extracellular matrix (DCECM) scaffolds, mimicking cartilage microenvironment,

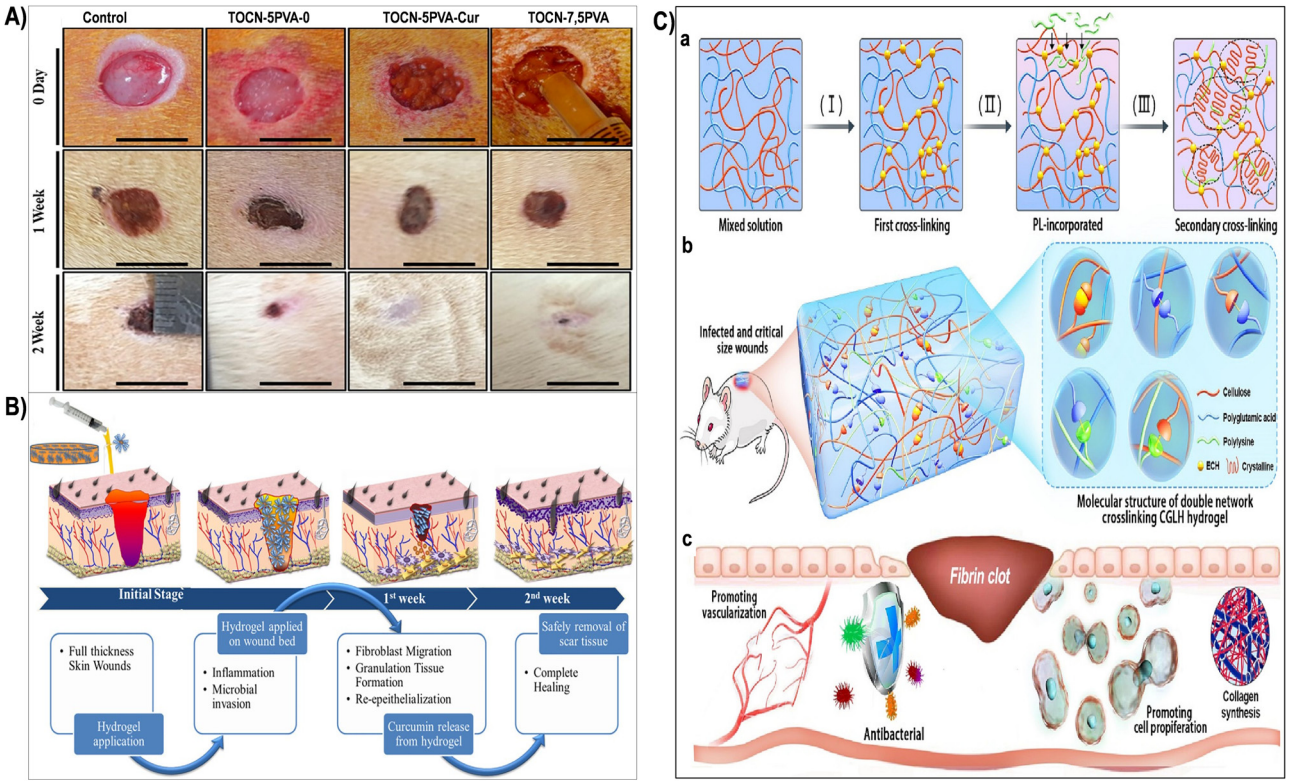

Fig. 20 Wound healing stages are illustrated (A), showing enhanced neoepidermis formation using TOCN-5PVA-0, TOCN-5PVA-Cur and TOCN-7.5PVA-Cur hydrogel samples (B). Reproduced with permission from ref. 521 Copyright © 2020 Elsevier. (C) Schematic depiction of the preparation process and biomedical utilization of double-network CGLH. (a) Sequential chemical (primary) and physical (secondary) crosslinking led to CGLH formation. (b) Emphasizing the biomolecular structure and crosslinking sites within CGLH. (c) Illustrating CGLH capability to expedite wound healing by eradicating bacteria and enhancing vascularization, cell proliferation, and collagen deposition. Reproduced with permission from ref. 522 Copyright © 2023 Elsevier.

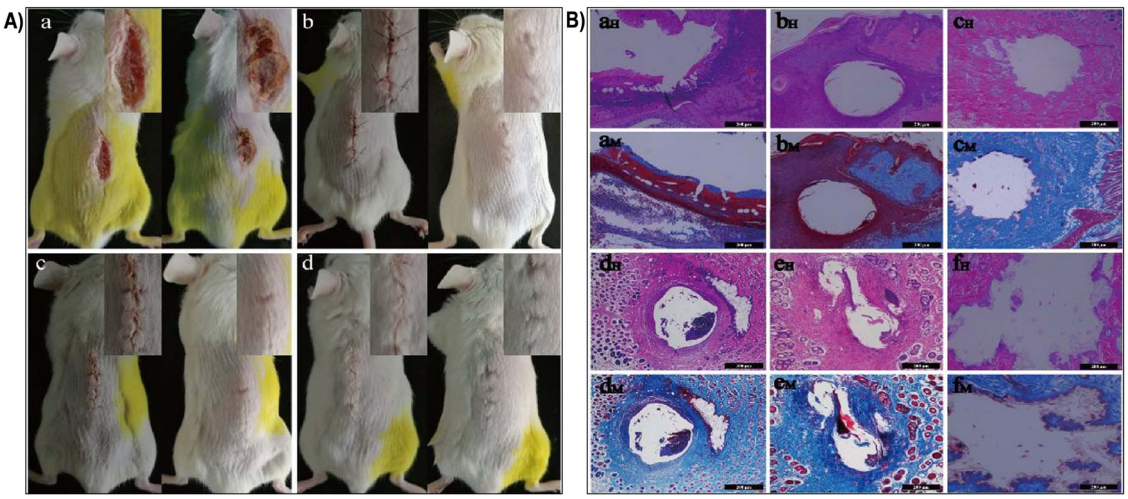

Fig. 21 (A) Wound healing process images after 3 days (left) and 10 days (right) for (a) suture-less mice (Group-I), (b) mice with polyamide sutures (Group-II), (c) mice sutured with coated BCNC-10 mL/RC yarns (Group-III), and (d) mice sutured with uncoated BCNC-10 mL/RC yarns (Group-IV). Insets show enlarged views of the wound area. (B) Histological analysis with HE staining (a_H) –(f_H) and Masson's trichrome staining (a_M)–(f_M) for Group-I at 10 days (a_H) and (a_M), Group-II at 3 days (b_H) and (b_M), Group-II at 10 days (c_H) and (c_M), Group-III at 3 days (d_H) and (d_M), Group-III at 10 days (e_H) and (e_M), and Group-IV at 10 days (f_H) and (f_M). Scale bars: 200 μm. Reproduced with permission from ref. 525 Copyright © 2018 Elsevier.

were fabricated.[526] A schematic of the experimental design used this work is shown in the Fig. 22A. These scaffolds demonstrated exceptional mechanical strength, water absorbency, and shape-memory properties. Enhanced cell adhesion and proliferation were observed in the fabricated scaffolds (Fig. 22B). *In vitro* and *in vivo* studies showed successful neocartilage tissue

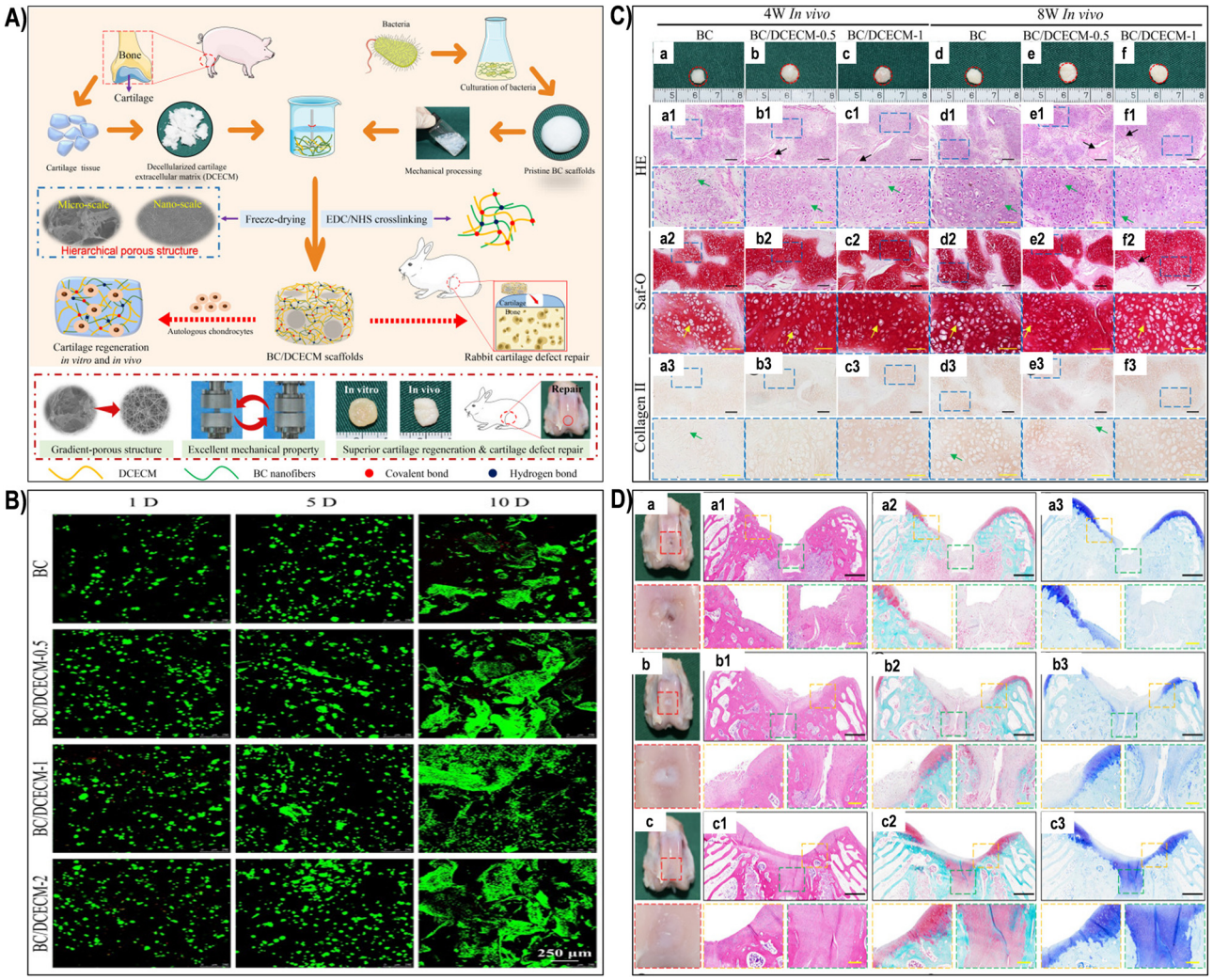

Fig. 22 (A) Illustration of the fabrication process for 3D hierarchical porous scaffolds mimicking cartilage microenvironment for tissue engineering applications. (B) Live/dead staining of chondrocytes after 1, 5, and 10 days of culture. (C) Gross, histological, and immunohistological views of cell-scaffold constructs after 4 and 8 weeks *in vivo*. Gross images show engineered constructs at 4 and 8 weeks (a)–(f). Histological stains include HE for cells and extracellular matrix (a1)–(f1), Saf-O for GAG (a2)–(f2), and Collagen II for type II collagen (a3)–(f3). (D) *In vivo* assessment of scaffold therapeutic efficacy for cartilage defects at 8 weeks post-surgery. Macroscopic images of defects (a: BC control; b: BC/DCECM-0.5; c: BC/DCECM-1). Histological stains depict regenerated tissues (a1)–(c1), (a2)–(c2), (a3)–(c3). Scale bars: black, 200 μm; yellow, 100 μm. Reproduced with permission from ref. 526 Copyright © 2021 Elsevier.

engineering with natural appearance and cartilage-specific lacuna formation (Fig. 22C). The BC/DCECM scaffolds led to superior repair outcomes, forming hyaline cartilage-like tissue within defect sites (Fig. 22D). This study marked significant progress in utilizing BC for cartilage tissue engineering.[526]

Moreover, nanocellulose-based hydrogels have showcased significant potential for *in vivo* cartilage tissue regeneration. Studies utilizing small animal models, such as mice and rabbits, have explored the effectiveness of these hydrogels in repairing cartilage defects. Current treatments for cartilage damage, such as autologous chondrocyte implantation (ACI) and microfracture surgery, often pose challenges, leading researchers to explore innovative solutions. In a recent study, researchers developed a novel hydrogel by oxidizing methylcellulose with sodium periodate, yielding dialdehyde methylcellulose (DAC). This DAC was then combined with succinyl-chitosan (SUC) to form an *in situ* DAC-SUC hydrogel, characterized by its stiffness, elasticity, and porosity as observed through advanced microscopy and rheological analysis. Notably, the DAC-SUC13 hydrogel exhibited excellent compatibility with cells, particularly bone marrow mesenchymal stem cells (BM-pMSCs), showcasing their chondrogenic potential.[527] To assess the hydrogel efficacy, researchers created osteochondral defects in porcine knee joints, injecting BM-pMSC/DAC-SUC hydrogel after joint irrigation with sterile isotonic saline (Fig. 23A). After a 6-month observation period, the defect site treated with BM-pMSC/DAC-SUC hydrogel showed significant engineering, characterized by distinct reddish-white tissue filling the defect area, contrasting sharply with the irregular and depressed defect sites in the sham group (Fig. 23B). Moreover, histological analysis revealed that the DAC-SUC13

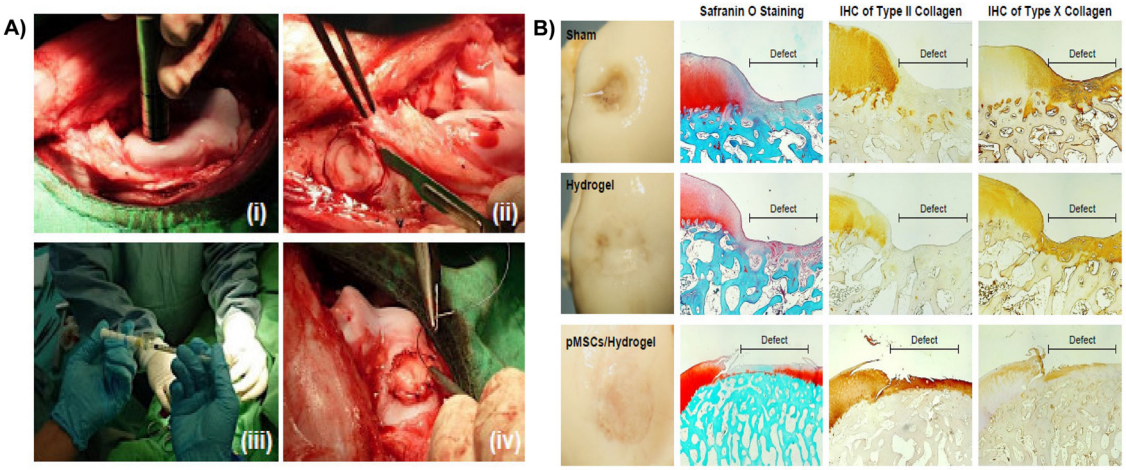

Fig. 23 (A) Surgical procedure: (i) OCD generated using an electric drill; (ii) 6.5 mm × 5 mm OCD area obtained; (iii) pMSC-hydrogel scaffold implanted into OCD; (iv) patella relocated, and the wound sutured in layers. (B) Histological evaluation: microscopic views and histological sections of repaired sites at 6 months post-implantation. Macroscopic image of femoral condyle with pMSC in hydrogel implants. Paraffin-embedded sections stained with Safranin O, type II collagen, and type X collagen. The detailed examination provided insights into the regenerative potential of the implanted pMSC-hydrogel constructs. Reproduced with permission from ref. 527 Copyright © 2022 MDPI.

hydrogel acted as an efficient stem cell carrier, stimulating the synthesis of glycosaminoglycans and type II collagen in porcine knee osteochondral defects.[527]

4.3 Bone tissue engineering

Bone provides structural support, protects organs, and maintains mineral balance. Bone injuries resulting from trauma or diseases like osteoporosis require effective engineering to maintain skeletal integrity.[528] Nanocellulose hydrogels, combined with osteogenic factors and nanomaterials, can create a conducive environment for osteoblast differentiation and bone tissue engineering. These hydrogels aid in bone defect repair and enhance overall skeletal stability.[210,506] In a recent work, bacterial cellulose (BC) was treated with TEMPO-mediated oxidation (TO-BC) and maleic acid (MA-BC) to fabricate BC dispersions for bone engineering scaffolds (Fig. 24A). Both MA-BC and TO-BC-based 3D scaffolds exhibited distinct pore structures, with MA-BC showing regular, loose, and well-arranged lamellar patterns (Fig. 24B).[529] MA-BC, combined with gelatin, demonstrated enhanced rheological properties and compression modulus for 3D printing, promoting osteogenic marker gene expression and mineralized nodule formation *in vitro*. Moreover, MA-BC-based gelatin scaffolds exhibited superior rat calvaria engineering, displaying higher bone mineral density and trabecular thickness *in vivo*, making them promising for biomedical applications.[529]

In vivo evaluation of nanocellulose-based hydrogels is pivotal, particularly in the field of bone and cartilage engineering. Animals serve as indispensable models for assessing the efficacy and safety of these hydrogels, serving as a bridge between laboratory investigations and clinical applications. In a recent investigation, cellulose nanofibrils (CNF) were employed in scaffold fabrication, leveraging their biocompatibility and capacity to form robust 3D porous networks from aqueous suspensions. A method enhancing their bioactivity for bone formation resulted in highly interconnected 3D networks.[44] These materials exhibited optimal morphological and mechanical features, fostering hydroxyapatite formation and releasing essential ions crucial for *in vivo* bone repair. The scaffold porosity and roughness supported various cellular functions, and the released ions influence gene expression associated with cell differentiation. The controlled release of ions played a pivotal role in stimulating the production of bone morphogenetic protein 2 (BMP-2) from cells within the fractured area, expediting *in vivo* bone repair. Comprehensive biocompatibility assessments revealed no adverse effects on vital organs, such as the liver and kidneys. These findings signified a significant stride toward the facile development of advanced, high-performance CNF-based scaffolds tailored for bone tissue engineering applications.[44] In addition, cutting-edge imaging technologies such as micro-computed tomography (micro-CT) and magnetic resonance imaging (MRI), have been strategically employed for non-invasive visualization of bone engineering progression in animal models subjected to nanocellulose-based hydrogels. These techniques provide quantitative assessments of critical parameters such as bone volume, density, and microstructure, delivering valuable insights into the hydrogel efficacy in facilitating bone healing.[530] In a notable study,[400] bacterial cellulose (BC) was combined with gold (Au) nanoparticles (GNPs) through *in situ* fermentation, with BC possessing attributes like biocompatibility, high porosity, robust mechanical strength, and a large surface area. GNPs are known for their remarkable osteogenic differentiation capability. Based on cellular assays, the Au/BC-III sample, which had the highest GNP content, exhibited superior *in vitro* osteogenic differentiation potential.[400] It was subsequently chosen for *in vivo* bone engineering evaluation in a rabbit femoral defect model (Fig. 24C(a)). After 2 months, femurs were harvested and evaluated using micro-computed tomography (micro-CT) to

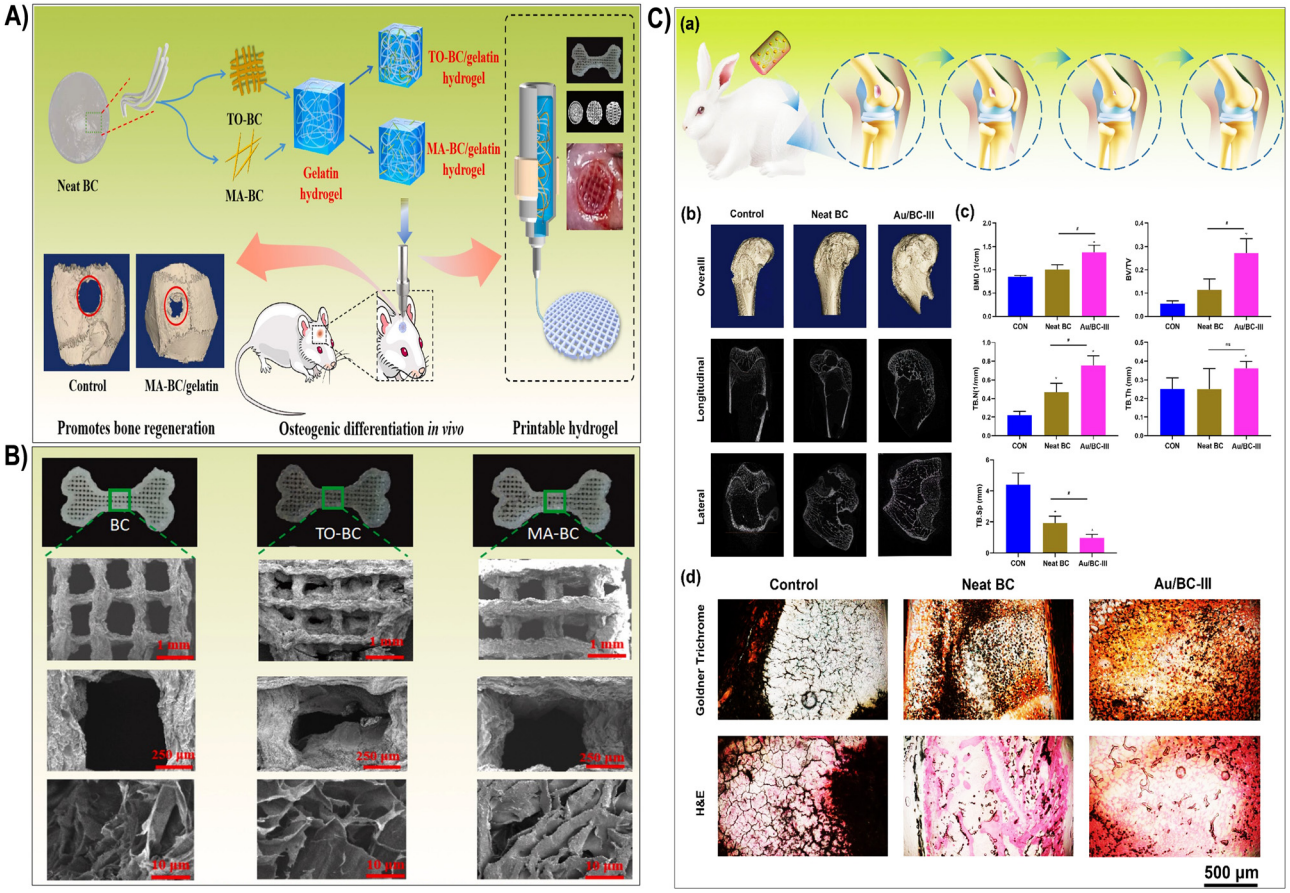

Fig. 24 (A) Schematic depicting the preparation of printable bacterial cellulose-gelatin gel for *in vivo* osteogenic engineering. (B) Scanning electron microscopy images showcasing printed scaffolds. Reproduced with permission from ref. 529 Copyright © 2021 Elsevier. (C) *In vivo* osteogenic assessment of Au/BC hydrogels. (a) Illustration outlining the experimental procedure. (b) 3D micro-CT reconstructions and cross-sectional images of the femoral condyle treated with neat BC and Au/BC-III hydrogels, respectively. (c) Quantitative evaluation of the regenerated area using micro-CT parameters: BMD, BV/TV, TB·N, TB·Sp, and TB·Th. (d) Staining images with Goldner Trichrome and H&E, depicting bone defects implanted with neat BC and Au/BC-III hydrogels, respectively. Asterisks denote statistically significant differences between the control and experimental groups (*$p < 0.05$; **$p < 0.01$; ****$p < 0.001$). Reproduced with permission from ref. 400 Copyright © 2023 Elsevier.

assess structural changes. The 3D-reconstruction and cross-sectional images of femurs (Fig. 24C(b)) revealed significant bone defects in the control and neat BC hydrogel groups.[400] Conversely, the femurs treated with Au/BC-III hydrogel showed more newly formed bone in the defect areas, indicating its capacity for *in vivo* bone engineering. Quantitative assessments, including bone mineral density (BMD), bone volume fraction (BV/TV), and bone trabecular parameters (TB·N, TB·Th, and TB·Sp), further characterized the differences in osseous tissue formation within the defect areas (Fig. 24C(c)). BMD in the defect areas treated with neat BC hydrogel and Au/BC-III hydrogels increased by 1.19-fold and 1.62-fold, respectively, compared to the control group, emphasizing the role of BC hydrogel as a platform for osteogenic cell adhesion and mineralization. Furthermore, treatment with Au/BC-III hydrogel led to significant increases in BV/TV, TB·N, and TB·Th, while reducing TB·Sp when compared to the control group and the neat BC hydrogel group. These results confirmed that Au/BC-III, due to the inclusion of GNPs, had a positive impact on *in vivo* bone engineering. Histological analysis using Masson-Goldner's trichrome staining (Fig. 24C(d)) revealed a substantial empty area in the newly formed osteoid region of the control group. In contrast, the groups with BC-based hydrogel implants displayed more newly formed bone adhering to the bone surface. Remarkably, the osteoid in the Au/BC-III group exhibited alignment and compactness, closely resembling healthy bone tissue. Similar trends were observed in H&E staining images, collectively highlighting Au/BC-III as the most effective in enhancing bone formation within the defect areas.[400]

Furthermore, in the pursuit of attaining optimal mechanical and biological characteristics in engineered cellulose-based hydrogels for bone tissue regeneration, it is common practice to integrate various components such as bioactive glasses and ceramics into cellulose inks, thereby crafting composite materials.[44,531] Ceramics are inorganic, non-metallic materials characterized by their high melting points, hardness, and brittleness. In tissue engineering, ceramics like hydroxyapatite (HA) and tricalcium phosphate (TCP) are favored due to their similarity to the mineral component of bone, facilitating integration with native tissue. They provide a scaffold for cell attachment, proliferation, and differentiation, promoting bone

regeneration.[532,533] For instance, cellulose scaffolds incorporated with nano- or micro-hydroxyapatite (nHA or μHA) were created through cellulose regeneration and mechanical immobilization of inorganic particles, followed by freeze-drying. Micro-computed tomography revealed highly interconnected porous structures in both scaffolds, with mean pore diameters of 490 ± 94 μm for cellulose/nHA and 540 ± 132 μm for cellulose/μHA.[533] *In vitro* and *in vivo* studies were conducted, with osteoblastic cell cultures and a rabbit calvarial defect model, respectively. Results showed enhanced cell adhesion, metabolic activity, and osteoblastic gene expression in cellulose/nHA scaffolds compared to cellulose/μHA and the control. Furthermore, greater mineralized tissue formation was observed in defects loaded with cellulose/nHA, indicating promising potential for bone regeneration applications.[533] In another study, Matinfar *et al.*[534] fabricated porous scaffolds of chitosan (CS) and carboxymethyl cellulose (CMC), strengthened with whisker-like biphasic and triphasic calcium phosphate fibers *via* freeze drying. They evaluated the effects of CMC addition, fiber type, and content on mechanical, physicochemical, and biological properties.[534] The synthesized fibers, containing hydroxyapatite (HA), monetite, β-tricalcium phosphate, and calcium pyrophosphate, were characterized. Composite scaffolds showed high porosity (61–75%) and interconnected pores (35–200 μm). CMC addition significantly improved mechanical properties (up to 150%) without affecting water uptake or biocompatibility. Both fiber types enhanced *in vitro* cell proliferation, attachment, and mineralization, with triphasic fibers showing superior reinforcement and cell viability. Scaffold reinforcement with 50 wt% triphasic fibers demonstrated superior mechanical and biological properties, suggesting their potential in bone tissue engineering, albeit requiring further mechanical enhancement.[534]

Bioactive glasses, on the other hand, possess a unique ability to bond with host tissue through the formation of a hydroxycarbonate apatite layer on their surface when in contact with bodily fluids. This bioactivity triggers cellular responses, such as enhanced osteogenic differentiation and angiogenesis, crucial for bone regeneration.[535,536] In bone tissue engineering, various types of bioactive glasses are utilized, including silicate-based glasses, phosphate-based glasses, and borate-based glasses. Silicate-based glasses, such as 45S5 Bioglass, are among the most extensively studied and are known for their ability to promote osteogenesis and bond to bone tissue. Phosphate-based glasses offer enhanced bioactivity and degradation rates, while borate-based glasses exhibit excellent mechanical properties and bioactivity, making them suitable for load-bearing applications.[535,537] In the study conducted by Li *et al.*[538] 3D bioactive glass/lignocellulose (BG/cellulose) composite scaffolds were successfully produced using 3D printing. The scaffold physical structure, morphology, mechanical properties, hydroxyapatite growth, and cell response were analyzed. Scanning electron microscopy revealed uniform macropores and rough surfaces in the BG/cellulose scaffolds. They demonstrated superior mechanical strength compared to pure cellulose scaffolds, meeting human trabecular bone strength requirements.[538] BG enhanced hydroxyapatite formation, confirmed by mineralization in simulated body fluid (SBF). The scaffolds exhibited low cytotoxicity to human bone marrow mesenchymal stem cells (hBMSCs), with maximum cell viability observed at a cellulose to BG weight ratio of 2. These findings suggested promising applications for 3D-printed BG/cellulose scaffolds in bone tissue engineering.[538] Additionally, surface functionalization of orthopedic implants was extensively explored to enhance bone-to-implant contact and expedite bone healing. In the study conducted by Chen *et al.*,[167] a hybrid coating, comprising 45S5 bioactive glass (BG) individually enveloped and linked with fibrous cellulose nanocrystals was applied onto 316L stainless steel *via* one-step electrophoretic deposition.[167] Zeta-potential and scanning electron microscopy clarified the codeposition mechanism. *In vitro* assessment in simulated body fluid showcased rapid mineralization of BG particles on the coating, forming a hydroxyapatite layer within 0.5 days. Comparative trials and characterization elucidated mineralization dynamics. Cell culture trials with MC3T3-E1 cells demonstrated enhanced cell behavior and matrix mineralization, affirming CNC role in augmenting BG bioactivity for improved bone implant coatings.[167]

4.4 Cardiac tissue engineering

Heart muscle damage, frequently resulting from myocardial infarctions, has profound implications for cardiac function. Nanocellulose hydrogels, when laden with cardiac-specific cells and frequently supplemented with growth factors, play a pivotal role in orchestrating the engineering of myocardial tissue. These hydrogels serve a dual purpose in this context. Firstly, they offer essential mechanical support to the damaged cardiac tissue, helping to structurally reinforce the compromised areas of the heart. Secondly, the hydrogels can create a microenvironment conducive to the survival and proliferation of cardiac cells, fostering the engineering process. By providing mechanical support and enhancing cell survival, nanocellulose-based hydrogels actively contribute to the recovery of heart function post-injury.[511,539] This approach holds promise in addressing the challenges associated with myocardial damage, potentially offering innovative solutions for cardiac tissue engineering and functional recovery. In a specific study, an electroconductive cardiac patch was developed using bacterial cellulose (BC) infused with polypyrrole (Ppy) nanoparticles to mimic the natural myocardial environment. For assessing mechanical properties and cell experiments, BC materials prepared with Py concentrations of 1–10 mM were selected, denoted as BP1 (1 mM), BP3 (3 mM), BP5 (5 mM), and BP10 (10 mM).[540] The properties of BC-Ppy composites were adjustable by varying precursor concentration. BC films changed from transparent white to opaque yellow-black with increasing monomer concentration. Scaffold thickness increased with Ppy functionalization, reaching ~140 μm at 100 mM Py. Flexibility persisted up to 10 mM Py, but higher concentrations resulted in fragility (Fig. 25A).[540] Comprehensive experiments involving cardiac fibroblasts and H9c2 cells highlighted the exceptional biocompatibility of BC-Ppy composites, enhancing cell viability and attachment, and fostering favorable cardiomyoblast morphology (Fig. 25B). Biochemical analyses unveiled diverse cardiomyocyte phenotypes and maturation

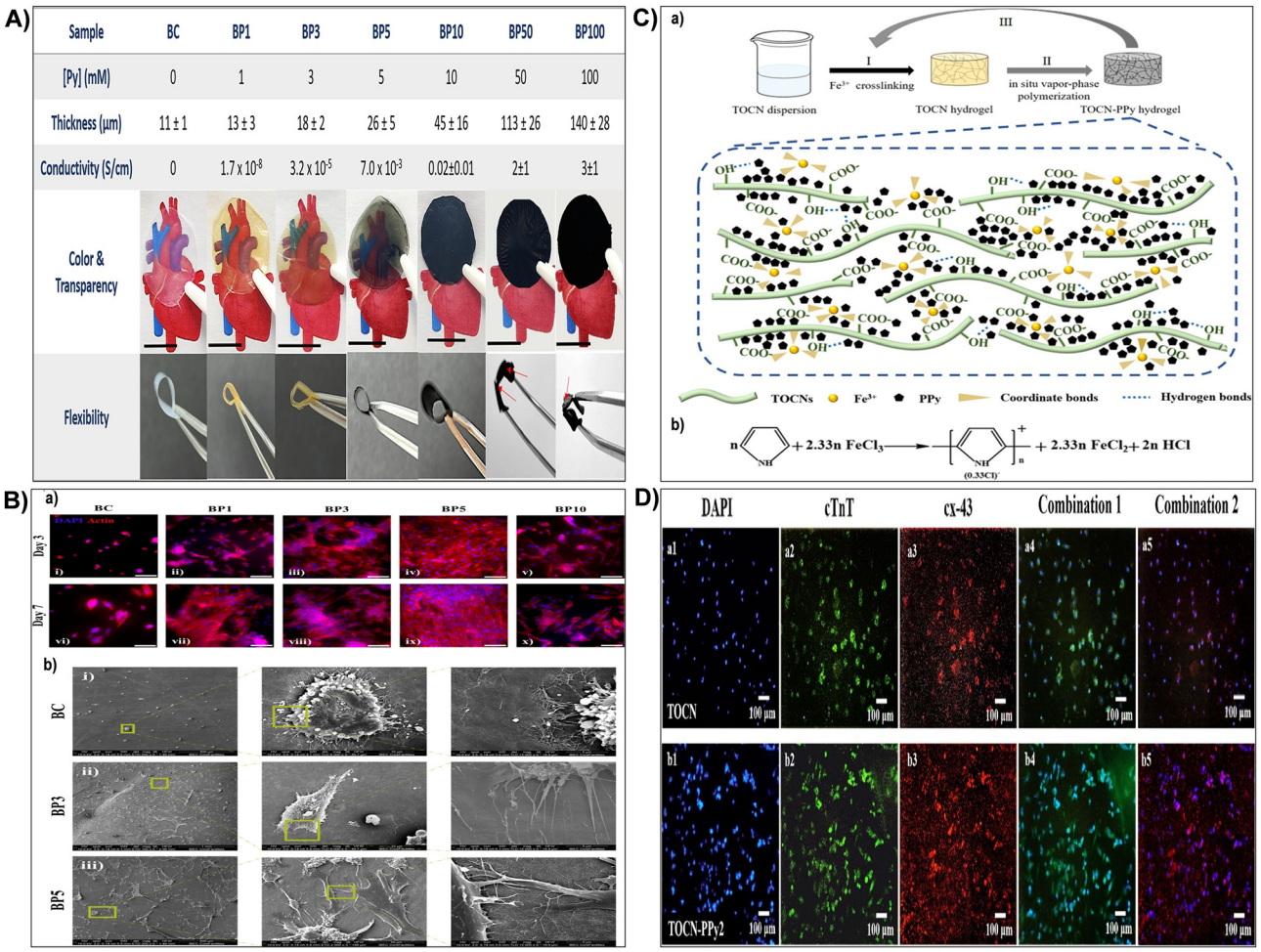

Fig. 25 (A) Impact of Py concentration on scaffold properties. Bacterial nanocellulose (BC) and bacterial nanocellulose-polypyrrole nanocomposites (BC-Ppy) at varying pyrrole (Py) concentrations and their property alterations. Scale bars: 1 cm. Reproduced with permission from ref. 540 Copyright © 2023 American Chemical Society. (B) H9c2 cell attachment to BC and BC-Ppy scaffolds. (a) Fluorescence microscopy images showing H9c2 cell populations on nanocellulose composites after 3 and 7 days of culture. Scale bars: 100 μm. (b) SEM images illustrating H9c2 attachment and morphology after 7 days of culture on BC, BP3, and BP5 materials. Reproduced with permission from ref. 540 Copyright © 2023 American Chemical Society. (C) Preparation process of nano-cellulose/polypyrrole conductive hydrogel. (a) Sequential cross-linking of TOCN dispersion with Fe^{3+} ions, followed by vapor-phase pyrrole monomer polymerization to form TOCN-PPy1 composite hydrogel, repeated to generate TOCN-PPy2 and TOCN-PPy3 composite hydrogels. (b) Schematic representation of pyrrole polymerization with $FeCl_3$. Reproduced with permission from ref. 541 Copyright © 2024 Springer. (D) Immunofluorescent staining of cells on pure TOCN and TOCN-PPy2 hydrogels. DAPI (a1) and (b1), cTnT protein (a2) and (b2), cx-43 protein (a3) and (b3), (a4) combination diagram of a1 and a2, (a5) combination diagram of a1 and a3, (b4) combination diagram of b1 and b2, (b5) combination diagram of b1 and b3. Reproduced with permission from ref. 541 Copyright © 2024 Springer.

levels in H9c2 cells, correlated with Ppy content. Furthermore, the BC-Ppy composites induced partial differentiation of H9c2 cells towards a cardiomyocyte-like phenotype.[540] In addition, Ma *et al.*[539] developed photocrosslinkable composite hydrogels mNCC-MeGel (mNG) by integrating TEMPO-modified nanocrystalline cellulose (mNCC) into methacrylated gelatin (MeGel) backbone. Encapsulated human adipose-derived mesenchymal stem cells (HADMSC) exhibited valve interstitial cell phenotypes over 14 days in both normal and osteogenic media.[539] Compared to MeGel, mNG reduced αSMA expression and increased vimentin and aggrecan expression, supporting a quiescent fibroblastic phenotype. Under osteogenic conditions, mNG lowered expression of osteogenic genes, resisting calcification. Bioprinted tall tubular structures with sustained cell viability demonstrated mNG potential for tissue-engineered heart valves.[539] In another study, Hou *et al.*[541] synthesized crosslinked TEMPO-oxidized cellulose nanofibers (TOCN), polymerized with pyrrole monomer, yielding polypyrrole nanocellulose composite hydrogel scaffolds for myocardial tissue engineering (Fig. 25C). The hydrogel displayed mechanical properties (50–75 kPa) and electrical conductivity (5×10^{-5}–1×10^{-3} S cm^{-1}) akin to natural myocardial tissue, with high biocompatibility (relative growth rate >90%) and non-cytotoxicity.[541] Cells cultured on TOCN-PPy scaffold exhibited increased expression of myocardial-specific proteins like connexin 43 and cardiac troponin T, suggesting its potential in myocardial tissue engineering (Fig. 25D).[541]

4.5 Nerve tissue engineering

In the context of nerve injuries or neurological disorders, which can lead to sensory or motor impairments, nanocellulose hydrogels can serve as promising scaffolds to repair damaged nerve tissues.[388,516,542] These hydrogels serve a dual purpose, offering both physical and biochemical cues that foster an environment conducive to guided nerve engineering. They facilitate controlled delivery of neurotrophic factors, supporting and enhancing axonal growth while establishing a supportive matrix for functional reinnervation.[543,544] This multifaceted approach facilitates nerve tissue repair, contributing to improved functional recovery. Additionally, the neurotrophic factors delivered by nanocellulose hydrogels are crucial signaling molecules that promote the survival, growth, and differentiation of neurons.[516,542] Recently, Chang *et al.*[544] sought to improve *in vitro* and *in vivo* survival and neuronal differentiation of otic neuronal progenitors (ONPs) by creating a stem cell niche. They used 3D human embryonic stem cells (hESC)-derived ONP spheroids with a nanofibrillar cellulose hydrogel and sustained-release neurotrophic factor delivery.[544] Results showed transplanted hESC-derived ONP spheroids survived, differentiated into otic neuronal lineages, and extended neurites towards the cochlea bony wall after 90 days, without immunosuppressants. This robust protocol established viable *in vivo* transplantation of hESC-derived ONPs to the inner ear, potentially enabling further integration and functional auditory neuron generation.[544] In addition, as illustrated by several recent research studies presented in Table 4 focused on the use of nanocellulose-based hydrogels for neural tissue engineering, nanocellulose-based hydrogels have emerged as promising matrices for neural tissue engineering due to their remarkable biocompatibility and tunable properties.[388,514] Nanocellulose, derived from renewable sources, possesses inherent biocompatibility and interesting mechanical properties, making it suitable for a wide range of biomedical applications. Its exceptional mechanical properties provide hydrogels with robust performances, offering physical cues that influence and guide the growth of cells in hydrogels during regenration process of neural tissues.[514,515] Moreover, the nanostructured morphology of nanocellulose provides a significantly high surface area for cell adhesion and proliferation, which is crucial for supporting neural cell growth and differentiation.[516,542] One significant advancement in this field lies in the ability to functionalize nanocellulose hydrogels with electroconductive polymers, enabling the development of electroconductive nanocellulose hydrogels. By incorporating electroconductive polymers like polypyrrole[53,515] or graphene[514] into nanocellulose matrices, these hydrogels gain the capacity to facilitate electrical signal propagation, effectively mimicking the natural electroconductive environment of neural tissues. This electroconductivity is vital for neural tissue engineering, as it allows neural cells to communicate effectively and propagate electrical signals necessary for proper tissue function.[53,514,515]

4.6 Vascular tissue engineering

The vascular system, comprising arteries, veins, and capillaries, is indispensable for delivering oxygen and nutrients to tissues throughout the body.[545–547] Disruptions in vascular function, such as those caused by atherosclerosis, can lead to critical conditions like heart attacks and strokes due to impaired blood flow.[548] In addressing these challenges, the use of nanocellulose hydrogels in vascular tissue engineering offers a promising solution. These hydrogels are engineered to mimic the structural and mechanical properties of native blood vessels, making them ideal candidates for developing vascular grafts.[517,518] The utilization of nanocellulose hydrogels for blood vessel fabrication presents a compelling avenue for addressing critical challenges in vascular tissue regeneration. Each approach outlined in the reviewed research studies highlighted in Table 4 offers unique contributions and insights into the potential applications of nanocellulose-based materials in this context. Firstly, the functional bacterial cellulose hydrogel incorporating a silver-loaded antibacterial agent demonstrated exceptional mechanical strength exceeding 1 MPa, alongside potent antibacterial efficacy against common pathogens such as *E. coli* and *S. aureus*.[517] Moreover, cell culture experiments underscored the remarkable biocompatibility and angiogenic potential of this dressing, while *in vivo* studies on rats showcased its efficacy in promoting wound healing and skin re-epithelialization, highlighting its clinical relevance.[517] Similarly, the multifunctional hydrogel incorporating silver into catechol-modified chitosan and aldehyde-modified cellulose nanocrystals exhibited enhanced vascularization, controlled silver release, and seamless coverage of irregular wounds, highlighting its versatility and efficacy in promoting neovascularization and tissue engineering.[518] Lastly, the biomimetic approach employed in fabricating cellulose-based small-diameter artificial blood vessels showcased impressive mechanical performance comparable to native vessels, coupled with excellent biocompatibility and safety profiles validated through comprehensive *in vitro* and *in vivo* experiments.[519] Overall, these findings collectively underscore the significant potential of nanocellulose hydrogels in advancing vascular tissue engineering by offering robust mechanical properties, antibacterial efficacy, and enhanced tissue regeneration capabilities, thereby paving the way for innovative therapeutic interventions in tissue repair.

5 Conclusion, challenges and future propects

Biomimetic nanocellulose-based hydrogels play a pivotal role in tissue engineering. These advanced materials are designed to mimic the functions and architecture of native tissues and are characterized by their exceptional biocompatibility, robust mechanical strength, and customizable biofunctionalities. The unique attributes of cellulose-based hydrogels render them exceptionally well-suited for a broad spectrum of tissue engineering applications, offering promising solutions for the field of regenerative medicine.

However, nanocellulose-based hydrogels, while gaining significant attention for their biocompatibility, biodegradability, and tunable mechanical strength, face several challenges that hinder their widespread biomedical applications. Achieving

optimal mechanical strength, which matches that of native tissues, remains elusive due to variations in fabrication methods, crosslinking techniques and processing conditions, which significantly impact their structural integrity and mechanical properties. Moreover, ensuring biological compatibility and biofunctionality is critical. Although nanocellulose possesses inherent biocompatibility, the inclusion of modifications and additives during the fabrication process of nanocellulose-based hydrogels can disrupt its interactions with cells and tissues. This disruption can have significant effects on cell viability, proliferation, and differentiation in the hydrogel matrix, which are essential factors for successful tissue regeneration. Additionally, nanocellulose-based hydrogels should degrade at a rate compatible with tissue regeneration while maintaining structural integrity during the healing process. Balancing biodegradation and stability is challenging and requires precise control over hydrogel composition, crosslinking density, and degradation kinetics. Rapid degradation may lead to premature loss of mechanical support, while slow degradation can impede tissue remodeling and integration. On the practical side, scaling up the production of nanocellulose-based hydrogels to meet clinical demands in a cost-effective manner involves complex processing techniques and significant investment in infrastructure and equipment, with the cost of raw materials and purification processes adding to the overall expense. The immunogenicity and potential inflammatory responses, especially *in vivo*, also need careful assessment as variations in nanocellulose sources, purification methods, and surface modifications can influence immunological properties of resulting hydrogels. Addressing potential immune reactions is crucial to ensure the long-term safety and efficacy of these hydrogels.

Despite the challenges faced, ongoing research endeavors aim to surmount existing limitations and propel the utilization of nanocellulose-based hydrogels for tissue engineering forward. This includes the development of multifunctional hydrogels tailored to possess enhanced mechanical strength, controlled biodegradation, and bioactive functionalities. Integration of bioactive molecules and therapeutic agents into the hydrogel matrix can stimulate specific cellular responses, fostering tissue regeneration. Additionally, exploration of advanced fabrication techniques such as 3D bioprinting and electrospinning offers precise control over hydrogel architecture and properties, enabling customizable scaffold designs for complex tissue regeneration. Looking ahead, the utilization of nanocellulose-based hydrogels in organ-on-chips presents promising prospects for biomedical applications. Organ-on-chip technology seeks to replicate human organ structure and function in microfluidic devices, facilitating physiologically relevant models for drug screening and disease modeling. Nanocellulose hydrogels offer advantages including biocompatibility, tunable mechanical properties, and support for cell growth and differentiation, enhancing biomimicry of the microenvironment in organ-on-chip systems. Future research directions may involve optimizing nanocellulose-based hydrogel formulations for specific organ models and integrating advanced fabrication techniques to create complex organ systems. Efforts to enhance hydrogel functionality through biofunctionalization and biochemical cue incorporation could further enhance their relevance for organ-on-chip applications, ultimately advancing biomedical research and improving human health outcomes.

Author contributions

Arnaud Kamdem Tamo: conceptualization, methodology, investigation, data curation, supervision, funding acquisition, writing – original draft, writing – review & editing.

Data availability

No data was used for the research described in the article.

Conflicts of interest

The author declares there is no conflict of interest. The author declares that they have no known competing financial interests or personal relationships that could have appeared to influence the work reported in this article.

Acknowledgements

The German Academic Exchange Service (DAAD) is acknowledged for financial support.

References

1 M. M. Farag, *J. Mater. Sci.*, 2023, **58**, 527–558.
2 F. Han, J. Wang, L. Ding, Y. Hu, W. Li, Z. Yuan, Q. Guo, C. Zhu, L. Yu, H. Wang, Z. Zhao, L. Jia, J. Li, Y. Yu, W. Zhang, G. Chu, S. Chen and B. Li, *Front. Bioeng. Biotechnol.*, 2020, **8**, 83.
3 S. Verma, V. Khanna, S. Kumar and S. Kumar, *ACS Omega*, 2023, **8**, 47322–47339.
4 J. M. Colazo, B. C. Evans, A. F. Farinas, S. Al-Kassis, C. L. Duvall and W. P. Thayer, *Tissue Eng., Part B*, 2019, **25**, 259–290.
5 C. Mandrycky, K. Phong and Y. Zheng, *MRS Commun.*, 2017, **7**, 332–347.
6 D. Shopova, A. Yaneva, D. Bakova, A. Mihaylova, P. Kasnakova, M. Hristozova, Y. Sbirkov, V. Sarafian and M. Semerdzhieva, *Bioengineering*, 2023, **10**, 287.
7 I. Doench, M. Torres-Ramos, A. Montembault, P. Nunes De Oliveira, C. Halimi, E. Viguier, L. Heux, R. Siadous, R. Thiré and A. Osorio-Madrazo, *Polymers*, 2018, **10**, 1202.
8 A. Kamdem Tamo, I. Doench, L. Walter, A. Montembault, G. Sudre, L. David, A. Morales-Helguera, M. Selig, B. Rolauffs, A. Bernstein, D. Hoenders, A. Walther and A. Osorio-Madrazo, *Polymers*, 2021, **13**, 1663.
9 M. Brovold, J. I. Almeida, I. Pla-Palacín, P. Sainz-Arnal, N. Sánchez-Romero, J. J. Rivas, H. Almeida, P. R. Dachary, T. Serrano-Aulló, S. Soker and P. M. Baptista, in *Novel Biomaterials for Regenerative Medicine*, ed. H. J. Chun, K. Park, C.-H. Kim and G. Khang, Springer Singapore, Singapore, 2018, vol. 1077, pp. 421–449.

10 A. K. Tamo, T. A. Tran, I. Doench, S. Jahangir, A. Lall, L. David, C. Peniche-Covas, A. Walther and A. Osorio-Madrazo, *Materials*, 2022, **15**, 6039.
11 A. Sood, A. Gupta and G. Agrawal, *Carbohydr. Polym. Technol. Appl.*, 2021, **2**, 100067.
12 N. Desai, D. Rana, S. Salave, R. Gupta, P. Patel, B. Karunakaran, A. Sharma, J. Giri, D. Benival and N. Kommineni, *Pharmaceutics*, 2023, **15**, 1313.
13 S. Das, B. Ghosh and K. Sarkar, *Sens. Int.*, 2022, **3**, 100135.
14 A. E. Eldeeb, S. Salah and N. A. Elkasabgy, *AAPS PharmSciTech*, 2022, **23**, 267.
15 D. S. Kohane and R. Langer, *Pediatr. Res.*, 2008, **63**, 487–491.
16 P. P. Phatchayawat, A. Khamkeaw, S. Yodmuang and M. Phisalaphong, *Biochem. Eng. J.*, 2022, **184**, 108476.
17 P.-H. Chen, H.-C. Liao, S.-H. Hsu, R.-S. Chen, M.-C. Wu, Y.-F. Yang, C.-C. Wu, M.-H. Chen and W.-F. Su, *RSC Adv.*, 2015, **5**, 6932–6939.
18 D. M. Alshangiti, T. K. El-damhougy, A. Zaher, M. Madani and M. Mohamady Ghobashy, *RSC Adv.*, 2023, **13**, 35251–35291.
19 R. Li, Y. Zhao, Z. Zheng, Y. Liu, S. Song, L. Song, J. Ren, J. Dong and P. Wang, *RSC Adv.*, 2023, **13**, 7153–7167.
20 C. Chen, Y. Xi and Y. Weng, *Polymers*, 2022, **14**, 3335.
21 R. Curvello, V. S. Raghuwanshi and G. Garnier, *Adv. Colloid Interface Sci.*, 2019, **267**, 47–61.
22 H. P. S. A. Khalil, F. Jummaat, E. B. Yahya, N. G. Olaiya, A. S. Adnan, M. Abdat, N. A. M. Nasir, A. S. Halim, U. S. U. Kumar, R. Bairwan and A. B. Suriani, *Polymers*, 2020, **12**, 2043.
23 F. V. Ferreira, C. G. Otoni, K. J. De France, H. S. Barud, L. M. F. Lona, E. D. Cranston and O. J. Rojas, *Mater. Today*, 2020, **37**, 126–141.
24 I. Doench, T. Tran, L. David, A. Montembault, E. Viguier, C. Gorzelanny, G. Sudre, T. Cachon, M. Louback-Mohamed, N. Horbelt, C. Peniche-Covas and A. Osorio-Madrazo, *Biomimetics*, 2019, **4**, 19.
25 S. Marquez-Bravo, I. Doench, P. Molina, F. E. Bentley, A. K. Tamo, R. Passieux, F. Lossada, L. David and A. Osorio-Madrazo, *Polymers*, 2021, **13**, 1563.
26 S. Tortorella, V. Vetri Buratti, M. Maturi, L. Sambri, M. Comes Franchini and E. Locatelli, *IJN*, 2020, **15**, 9909–9937.
27 F. Rol, M. N. Belgacem, A. Gandini and J. Bras, *Prog. Polym. Sci.*, 2019, **88**, 241–264.
28 Z. Wei, C. Wu, R. Li, D. Yu and Q. Ding, *Cellulose*, 2021, **28**, 7497–7520.
29 M. Monfared, D. Mawad, J. Rnjak-Kovacina and M. H. Stenzel, *J. Mater. Chem. B*, 2021, **9**, 6163–6175.
30 D. K. Patel, S. D. Dutta, W.-C. Shin, K. Ganguly and K.-T. Lim, *RSC Adv.*, 2021, **11**, 7466–7478.
31 A. Kantaros and T. Ganetsos, *IJMS*, 2023, **24**, 15748.
32 E. Merotto, P. G. Pavan and M. Piccoli, *Biomedicines*, 2023, **11**, 1742.
33 A. Lall, A. Kamdem Tamo, I. Doench, L. David, P. Nunes De Oliveira, C. Gorzelanny and A. Osorio-Madrazo, *IJMS*, 2020, **21**, 5602.
34 L. Lin, S. Jiang, J. Yang, J. Qiu, X. Jiao, X. Yue, X. Ke, G. Yang and L. Zhang, *IJB*, 2022, **9**, 637.
35 A. Osorio-Madrazo, M. Eder, M. Rueggeberg, J. K. Pandey, M. J. Harrington, Y. Nishiyama, J.-L. Putaux, C. Rochas and I. Burgert, *Biomacromolecules*, 2012, **13**, 850–856.
36 X. He and Q. Lu, *Carbohydr. Polym.*, 2023, **301**, 120351.
37 A. Kamdem Tamo, I. Doench, A. Morales Helguera, D. Hoenders, A. Walther and A. O. Madrazo, *Polymers*, 2020, **12**, 1522.
38 W. Chimpibul, T. Nakaji-Hirabayashi, X. Yuan and K. Matsumura, *J. Mater. Chem. B*, 2020, **8**, 7904–7913.
39 T. Agarwal, S. N. G. H. Narayana, K. Pal, K. Pramanik, S. Giri and I. Banerjee, *Int. J. Biol. Macromol.*, 2015, **75**, 409–417.
40 M. G. Bekaroğlu, Y. İşçi and S. İşçi, *Mater. Sci. Eng., C*, 2017, **78**, 847–853.
41 L. Ning, C. You, Y. Zhang, X. Li and F. Wang, *Composites Commun.*, 2021, **26**, 100739.
42 M. Y. Leong, Y. L. Kong, M. Y. Harun, C. Y. Looi and W. F. Wong, *Carbohydr. Res.*, 2023, **532**, 108899.
43 V. Durairaj, P. Li, T. Liljeström, N. Wester, J. Etula, I. Leppänen, Y. Ge, K. S. Kontturi, T. Tammelin, T. Laurila and J. Koskinen, *ACS Appl. Nano Mater.*, 2021, **4**, 5842–5853.
44 F. V. Ferreira, L. P. Souza, T. M. M. Martins, J. H. Lopes, B. D. Mattos, M. Mariano, I. F. Pinheiro, T. M. Valverde, S. Livi, J. A. Camilli, A. M. Goes, R. F. Gouveia, L. M. F. Lona and O. J. Rojas, *Nanoscale*, 2019, **11**, 19842–19849.
45 M. Nagalakshmaiah, M. Rajinipriya, S. Afrin, M. A. Ansari, M. Asad and Z. Karim, in *Bio-based Polymers and Nanocomposites*, ed. M. L. Sanyang and M. Jawaid, Springer International Publishing, Cham, 2019, pp. 49–65.
46 S. Swingler, A. Gupta, H. Gibson, M. Kowalczuk, W. Heaselgrave and I. Radecka, *Polymers*, 2021, **13**, 412.
47 S. Yu, J. Sun, Y. Shi, Q. Wang, J. Wu and J. Liu, *Environ. Sci. Ecotechnol.*, 2021, **5**, 100077.
48 M. N. Norizan, S. S. Shazleen, A. H. Alias, F. A. Sabaruddin, M. R. M. Asyraf, E. S. Zainudin, N. Abdullah, M. S. Samsudin, S. H. Kamarudin and M. N. F. Norrrahim, *Nanomaterials*, 2022, **12**, 3483.
49 T. V. Patil, D. K. Patel, S. D. Dutta, K. Ganguly, T. S. Santra and K.-T. Lim, *Bioactive Mater.*, 2022, **9**, 566–589.
50 W. Yan, J. Liu, X. Zheng, J. Zhang and K. Tang, *e-Polymers*, 2023, **23**, 20230010.
51 D. K. Patel, S. D. Dutta, J. Hexiu, K. Ganguly and K.-T. Lim, *Int. J. Biol. Macromol.*, 2020, **162**, 1429–1441.
52 X. He, Q. Xiao, C. Lu, Y. Wang, X. Zhang, J. Zhao, W. Zhang, X. Zhang and Y. Deng, *Biomacromolecules*, 2014, **15**, 618–627.
53 J. Thunberg, T. Kalogeropoulos, V. Kuzmenko, D. Hägg, S. Johannesson, G. Westman and P. Gatenholm, *Cellulose*, 2015, **22**, 1459–1467.
54 K. Liu and J. M. Catchmark, *Carbohydr. Polym.*, 2019, **219**, 12–20.
55 A. Ghilan, R. Nicu, D. E. Ciolacu and F. Ciolacu, *Materials*, 2023, **16**, 4447.
56 M. Moniri, A. Boroumand Moghaddam, S. Azizi, R. Abdul Rahim, A. Bin Ariff, W. Zuhainis Saad, M. Navaderi and R. Mohamad, *Nanomaterials*, 2017, **7**, 257.
57 P. Tayeb and A. H. Tayeb, *Carbohydr. Polym.*, 2019, **224**, 115149.

58 S. Brethauer, R. L. Shahab and M. H. Studer, *Appl. Microbiol. Biotechnol.*, 2020, **104**, 5201–5212.
59 A. Dal Fovo, J. Striova, D. Quintero Balbas, S. Mattana, N. Tacconi, R. Cicchi and R. Fontana, *RSC Adv.*, 2022, **12**, 26744–26752.
60 J. Shojaeiarani, D. S. Bajwa and S. Chanda, *Composites, Part C*, 2021, **5**, 100164.
61 S. L. Leong, S. I. X. Tiong, S. P. Siva, F. Ahamed, C.-H. Chan, C. L. Lee, I. M. L. Chew and Y. K. Ho, *J. Environ. Chem. Eng.*, 2022, **10**, 108145.
62 P. V. Krasteva, J. Bernal-Bayard, L. Travier, F. A. Martin, P.-A. Kaminski, G. Karimova, R. Fronzes and J.-M. Ghigo, *Nat. Commun.*, 2017, **8**, 2065.
63 W. D. Jang, T. Y. Kim, H. U. Kim, W. Y. Shim, J. Y. Ryu, J. H. Park and S. Y. Lee, *Biotechnol. Bioeng.*, 2019, **116**, 3372–3381.
64 L. J. Gibson, *J. R. Soc., Interface*, 2012, **9**, 2749–2766.
65 L. Solhi, V. Guccini, K. Heise, I. Solala, E. Niinivaara, W. Xu, K. Mihhels, M. Kröger, Z. Meng, J. Wohlert, H. Tao, E. D. Cranston and E. Kontturi, *Chem. Rev.*, 2023, **123**, 1925–2015.
66 Y. Qi, Y. Guo, A. A. Liza, G. Yang, M. H. Sipponen, J. Guo and H. Li, *Cellulose*, 2023, **30**, 4115–4147.
67 R. Tarrahi, A. Khataee, A. Karimi and Y. Yoon, *Chemosphere*, 2022, **288**, 132529.
68 C. T. Brett, *International Review of Cytology*, Elsevier, 2000, vol. 199, pp. 161–199.
69 T. I. Baskin, *Protoplasma*, 2001, **215**, 150–171.
70 S. Iwamoto, W. Kai, A. Isogai and T. Iwata, *Biomacromolecules*, 2009, **10**, 2571–2576.
71 Y. Nishiyama, *J. Wood Sci.*, 2009, **55**, 241–249.
72 Y. Nishiyama, P. Langan and H. Chanzy, *J. Am. Chem. Soc.*, 2002, **124**, 9074–9082.
73 J. L. Fredricks, A. M. Jimenez, P. Grandgeorge, R. Meidl, E. Law, J. Fan and E. Roumeli, *J. Polym. Sci.*, 2023, **61**, 2585–2632.
74 S. Amine, A. Montembault, M. Fumagalli, A. Osorio-Madrazo and L. David, *Polymers*, 2021, **13**, 2023.
75 P. Samyn and A. Osorio-Madrazo, in *Handbook of Nanofibers*, ed. A. Barhoum, M. Bechelany and A. S. H. Makhlouf, Springer International Publishing, Cham, 2019, pp. 287–321.
76 F. H. Isikgor and C. R. Becer, *Polym. Chem.*, 2015, **6**, 4497–4559.
77 L. I. Mikhalovska, V. M. Gun'ko, A. A. Rugal, O. I. Oranska, Y. I. Gornikov, C. Morvan, N. Follain, C. Domas, E. M. Pakhlov and S. V. Mikhalovsky, *RSC Adv.*, 2012, **2**, 2032.
78 N. Zhang, S. Li, L. Xiong, Y. Hong and Y. Chen, *Modelling Simul. Mater. Sci. Eng*, 2015, **23**, 085010.
79 U. P. Agarwal, *Molecules*, 2019, **24**, 1659.
80 P. Langan, N. Sukumar, Y. Nishiyama and H. Chanzy, *Cellulose*, 2005, **12**, 551–562.
81 Y. Zhang, W. Deng, M. Wu, M. Rahmaninia, C. Xu and B. Li, *Nanomaterials*, 2023, **13**, 1489.
82 A. Dufresne, J.-Y. Cavaill and M. R. Vignon, *J. Appl. Polym. Sci.*, 1997, **64**, 1185–1194.
83 D. Abol-Fotouh, M. A. Hassan, H. Shokry, A. Roig, M. S. Azab and A. E.-H. B. Kashyout, *Sci. Rep.*, 2020, **10**, 3491.
84 H. P. S. Abdul Khalil, A. S. Adnan, E. B. Yahya, N. G. Olaiya, S. Safrida, Md. S. Hossain, V. Balakrishnan, D. A. Gopakumar, C. K. Abdullah, A. A. Oyekanmi and D. Pasquini, *Polymers*, 2020, **12**, 1759.
85 M. Zhao, L. Robertsén, L. Wågberg and T. Pettersson, *Cellulose*, 2022, **29**, 2617–2632.
86 M. Jakob, A. R. Mahendran, W. Gindl-Altmutter, P. Bliem, J. Konnerth, U. Müller and S. Veigel, *Prog. Mater. Sci.*, 2022, **125**, 100916.
87 D. Trache, A. F. Tarchoun, M. Derradji, T. S. Hamidon, N. Masruchin, N. Brosse and M. H. Hussin, *Front. Chem.*, 2020, **8**, 392.
88 J. George and S. N. Sabapathi, *Nanotechnol., Sci. Appl.*, 2015, **2015**(8), 45–54.
89 P. Mali and A. P. Sherje, *Carbohydr. Polym.*, 2022, **275**, 118668.
90 O. M. Vanderfleet, M. S. Reid, J. Bras, L. Heux, J. Godoy-Vargas, M. K. R. Panga and E. D. Cranston, *Cellulose*, 2019, **26**, 507–528.
91 P. G. Gan, S. T. Sam, M. F. B. Abdullah and M. F. Omar, *J. Appl. Polym. Sci.*, 2020, **137**, 48544.
92 R. Nasseri, C. P. Deutschman, L. Han, M. A. Pope and K. C. Tam, *Mater. Today Adv.*, 2020, **5**, 100055.
93 P. Liu, X. Guo, F. Nan, Y. Duan and J. Zhang, *ACS Appl. Mater. Interfaces*, 2017, **9**, 3085–3092.
94 F. D'Acierno, W. Y. Hamad, C. A. Michal and M. J. MacLachlan, *Biomacromolecules*, 2020, **21**, 3374–3386.
95 J. Mao, A. Osorio-Madrazo and M.-P. Laborie, *Cellulose*, 2013, **20**, 1829–1840.
96 H.-M. Ng, L. T. Sin, T.-T. Tee, S.-T. Bee, D. Hui, C.-Y. Low and A. R. Rahmat, *Composites, Part B*, 2015, **75**, 176–200.
97 S. Soleimani, A. Heydari and M. Fattahi, *Starch Stärke*, 2022, **74**, 2200159.
98 T. Yang, X. Li, N. Xu, Y. Guo, G. Liu and J. Zhao, *Bioresour. Bioprocess.*, 2023, **10**, 42.
99 C. M. Pacheco, C. Bustos A and G. Reyes, *J. Dispersion Sci. Technol.*, 2020, **41**, 1731–1741.
100 X. Hu, M. Song, S. Li, Y. Chu, W. Zhang and Z. Deng, *Chemosphere*, 2023, **343**, 140212.
101 Y. Zhou, T. Saito, L. Bergström and A. Isogai, *Biomacromolecules*, 2018, **19**, 633–639.
102 Y. Xu, Y. Xu, W. Deng, H. Chen and J. Xiong, *Int. J. Biol. Macromol.*, 2023, **246**, 125604.
103 L. Douard, J. Bras, T. Encinas and M. N. Belgacem, *Carbohydr. Polym.*, 2021, **252**, 117136.
104 S. Zhu, H. Sun, T. Mu, Q. Li and A. Richel, *Food Chem.*, 2023, **403**, 134496.
105 Z. Pang, P. Wang and C. Dong, *Cellulose*, 2018, **25**, 7053–7064.
106 D. Z. Haddis, M. Chae, J. Asomaning and D. C. Bressler, *Carbohydr. Polym.*, 2024, **323**, 121460.
107 N. Carter, I. Grant, M. Dewey, M. Bourque and D. J. Neivandt, *Front. Nanotechnol.*, 2021, **3**, 729743.
108 P. Xi, F. Quan, Y. Sun and Y. Jiang, *Composites, Part B*, 2022, **242**, 110078.
109 M. Mohammadalipour, S. Karbasi, T. Behzad, Z. Mohammadalipour and M. Zamani, *Int. J. Biol. Macromol.*, 2022, **220**, 1402–1414.

110 S. Widiarto, E. Pramono, Suharso, A. Rochliadi and I. M. Arcana, *Fibers*, 2019, **7**, 44.
111 C. Carneiro Pessan, J. Silva Bernardes, S. H. P. Bettini and E. R. Leite, *Carbohydr. Polym.*, 2023, **304**, 120505.
112 C. Yao, F. Li, T. Chen and Y. Tang, *Ind. Crops Prod.*, 2023, **206**, 117575.
113 P. Nehra and R. P. Chauhan, *Iran. Polym. J.*, 2022, **31**, 771–778.
114 X. Liu, Y. Jiang, C. Qin, S. Yang, X. Song, S. Wang and K. Li, *Cellulose*, 2018, **25**, 7065–7078.
115 B. S. Santucci, J. Bras, M. N. Belgacem, A. A. D. S. Curvelo and M. T. B. Pimenta, *Ind. Crops Prod.*, 2016, **91**, 238–248.
116 Y. Chen, Y. He, D. Fan, Y. Han, G. Li and S. Wang, *J. Nanomater.*, 2017, **2017**, 1–12.
117 M. Gama, P. Gatenholm and D. Klemm, *Bacterial Nano-Cellulose: A Sophisticated Multifunctional Material*, CRC Press, Boca Raton, 1st edn, 2016.
118 C. Sharma and N. K. Bhardwaj, *Mater. Sci. Eng., C*, 2019, **104**, 109963.
119 P. Lv, Y. Yao, D. Li, H. Zhou, M. A. Naeem, Q. Feng, J. Huang, Y. Cai and Q. Wei, *Carbohydr. Polym.*, 2017, **172**, 93–101.
120 D. Lahiri, M. Nag, B. Dutta, A. Dey, T. Sarkar, S. Pati, H. A. Edinur, Z. Abdul Kari, N. H. Mohd Noor and R. R. Ray, *IJMS*, 2021, **22**, 12984.
121 C. Zhong, *Front. Bioeng. Biotechnol.*, 2020, **8**, 605374.
122 K. Qiu and A. N. Netravali, *Polym. Rev.*, 2014, **54**, 598–626.
123 D. Klemm, B. Heublein, H. Fink and A. Bohn, *Angew. Chem., Int. Ed.*, 2005, **44**, 3358–3393.
124 D. Klemm, D. Schumann, F. Kramer, N. Heßler, M. Hornung, H.-P. Schmauder and S. Marsch, in *Polysaccharides II*, ed. D. Klemm, Springer Berlin Heidelberg, Berlin, Heidelberg, 2006, vol. 205, pp. 49–96.
125 D. Klemm, D. Schumann, F. Kramer, N. Heßler, D. Koth and B. Sultanova, *Macromol. Symp.*, 2009, **280**, 60–71.
126 M. Ioelovich, *Fabrication and Self-Assembly of Nanobiomaterials*, Elsevier, 2016, pp. 243–288.
127 H. Luo, G. Xiong, D. Hu, K. Ren, F. Yao, Y. Zhu, C. Gao and Y. Wan, *Mater. Chem. Phys.*, 2013, **143**, 373–379.
128 N. Halib, I. Ahmad, M. Grassi and G. Grassi, *Int. J. Pharm.*, 2019, **566**, 631–640.
129 G. F. Picheth, C. L. Pirich, M. R. Sierakowski, M. A. Woehl, C. N. Sakakibara, C. F. De Souza, A. A. Martin, R. Da Silva and R. A. De Freitas, *Int. J. Biol. Macromol.*, 2017, **104**, 97–106.
130 A. Retegi, N. Gabilondo, C. Peña, R. Zuluaga, C. Castro, P. Gañan, K. De La Caba and I. Mondragon, *Cellulose*, 2010, **17**, 661–669.
131 H. Suryanto, M. Muhajir, T. A. Sutrisno, Mudjiono, N. Zakia and U. Yanuhar, *IOP Conf. Ser.: Mater. Sci. Eng.*, 2019, **515**, 012053.
132 A. G. N. Sofiah, J. Pasupuleti, M. Samykano, K. Kadirgama, S. P. Koh, S. K. Tiong, A. K. Pandey, C. T. Yaw and S. K. Natarajan, *Polymers*, 2023, **15**, 3044.
133 D. Aki, S. Ulag, S. Unal, M. Sengor, N. Ekren, C.-C. Lin, H. Yılmazer, C. B. Ustundag, D. M. Kalaskar and O. Gunduz, *Mater. Des.*, 2020, **196**, 109094.
134 M. Vielreicher, D. Kralisch, S. Völkl, F. Sternal, A. Arkudas and O. Friedrich, *Sci. Rep.*, 2018, **8**, 9401.
135 M. M. Abeer, M. C. I. Mohd Amin and C. Martin, *J. Pharm. Pharmacol.*, 2014, **66**, 1047–1061.
136 S. M. Choi and E. J. Shin, *Nanomaterials*, 2020, **10**, 406.
137 Y. Shi, H. Jiao, J. Sun, X. Lu, S. Yu, L. Cheng, Q. Wang, H. Liu, S. Biranje, J. Wang and J. Liu, *Carbohydr. Polym.*, 2022, **285**, 119208.
138 C. Yadav, J.-M. Lee, P. Mohanty, X. Li and W.-D. Jang, *Nanoscale*, 2023, **15**, 15108–15145.
139 H. Seddiqi, E. Oliaei, H. Honarkar, J. Jin, L. C. Geonzon, R. G. Bacabac and J. Klein-Nulend, *Cellulose*, 2021, **28**, 1893–1931.
140 M. Akter, M. Bhattacharjee, A. K. Dhar, F. B. A. Rahman, S. Haque, T. U. Rashid and S. M. F. Kabir, *Gels*, 2021, **7**, 30.
141 L. Cellante, R. Costa, I. Monaco, G. Cenacchi and E. Locatelli, *New J. Chem.*, 2018, **42**, 5237–5242.
142 R. Alimohammadzadeh, A. A. Rafi, L. Goclik, C.-W. Tai and A. Cordova, *Carbohydr. Polym. Technol. Appl.*, 2022, **3**, 100205.
143 Y. Wang, X. Wang, Y. Xie and K. Zhang, *Cellulose*, 2018, **25**, 3703–3731.
144 T. Heinze, O. A. El Seoud and A. Koschella, *Cellulose Derivatives*, Springer International Publishing, Cham, 2018, pp. 429–477.
145 J. You, X. Zhang, Q. Mi, J. Zhang, J. Wu and J. Zhang, *Cellulose*, 2022, **29**, 9583–9596.
146 C. Vinatier, D. Magne, P. Weiss, C. Trojani, N. Rochet, G. F. Carle, C. Vignes-Colombeix, C. Chadjichristos, P. Galera, G. Daculsi and J. Guicheux, *Biomaterials*, 2005, **26**, 6643–6651.
147 K. Jin, Y. Tang, X. Zhu and Y. Zhou, *Int. J. Biol. Macromol.*, 2020, **162**, 1109–1117.
148 M. Hu, J. Yang and J. Xu, *Drug Delivery*, 2021, **28**, 607–619.
149 I. Rocha, N. Ferraz, A. Mihranyan, M. Strømme and J. Lindh, *Cellulose*, 2018, **25**, 1899–1910.
150 S. S. Bhutada, M. Sriram and D. S. Katti, *Carbohydr. Polym.*, 2021, **268**, 118256.
151 K. Min and G. Tae, *Biomater. Res.*, 2023, **27**, 28.
152 J. H. Jordan, M. W. Easson and B. D. Condon, *Nanomaterials*, 2019, **9**, 1232.
153 Y. S. Abdullaevich, Y. K. Ergashovich, S. A. Abdukhalilovich and G. I. Shavkat O'G'Li, *Polym. Eng. Sci.*, 2022, **62**, 677–686.
154 G. Juncu, A. Stoica-Guzun, M. Stroescu, G. Isopencu and S. I. Jinga, *Int. J. Pharm.*, 2016, **510**, 485–492.
155 G. Mosconi, M. L. Formica, S. D. Palma and R. Rojas, *New J. Chem.*, 2024, **48**, 406–415.
156 R. K. Singh and A. K. Singh, *Waste Biomass Valor*, 2013, **4**, 129–137.
157 M. K. Patoary, S. R. Islam, A. Farooq, M. A. Rashid, S. Sarker, Md. Y. Hossain, M. A. N. Rakib, M. Al-Amin and L. Liu, *Ind. Crops Prod.*, 2023, **201**, 116965.
158 L. Zha, Y. Zheng, J. Che and Y. Xiao, *New J. Chem.*, 2021, **45**, 22354–22360.
159 S. Wu, Y. Gong, S. Liu, Y. Pei and X. Luo, *Carbohydr. Polym.*, 2021, **254**, 117421.

160 G. M. A. Khan, M. A. Haque, M. Terano and M. S. Alam, *J. Appl. Polym. Sci.*, 2014, **131**, 40139.
161 M. H. Rahaman, M. A. Haque, M. A. Rahman, M. M. Rana, M. M. Parvez and S. M. N. Alam, *Reactions*, 2022, **3**, 213–223.
162 M. Spaic, D. P. Small, J. R. Cook and W. Wan, *Cellulose*, 2014, **21**, 1529–1540.
163 J. C. Courtenay, J. G. Filgueiras, E. R. deAzevedo, Y. Jin, K. J. Edler, R. I. Sharma and J. L. Scott, *J. Mater. Chem. B*, 2019, **7**, 53–64.
164 C. Warwar Damouny, P. Martin, G. Vasilyev, R. Vilensky, R. Fadul, I. Redenski, S. Srouji and E. Zussman, *Biomacromolecules*, 2022, **23**, 3222–3234.
165 J. Pajorova, A. Skogberg, D. Hadraba, A. Broz, M. Travnickova, M. Zikmundova, M. Honkanen, M. Hannula, P. Lahtinen, M. Tomkova, L. Bacakova and P. Kallio, *Biomacromolecules*, 2020, **21**, 4857–4870.
166 N. Forsman, A. Lozhechnikova, A. Khakalo, L.-S. Johansson, J. Vartiainen and M. Österberg, *Carbohydr. Polym.*, 2017, **173**, 392–402.
167 Q. Chen, R. P. Garcia, J. Munoz, U. Pérez De Larraya, N. Garmendia, Q. Yao and A. R. Boccaccini, *ACS Appl. Mater. Interfaces*, 2015, **7**, 24715–24725.
168 A. Yamaguchi, H. Nakayama, Y. Morita, H. Sakamoto, T. Kitamura, M. Hashimoto and S. Suye, *ACS Omega*, 2020, **5**, 18826–18830.
169 S. Lombardo and W. Thielemans, *Cellulose*, 2019, **26**, 249–279.
170 K. Mazeau and L. Charlier, *Cellulose*, 2012, **19**, 337–349.
171 J. R. G. Navarro, J. Rostami, A. Ahlinder, J. B. Mietner, D. Bernin, B. Saake and U. Edlund, *Biomacromolecules*, 2020, **21**, 1952–1961.
172 Z. Zhang, G. Sèbe, Y. Hou, J. Wang, J. Huang and G. Zhou, *J Appl. Polym. Sci.*, 2021, **138**, 51458.
173 X. Lan, Z. Ma, A. R. A. Szojka, M. Kunze, A. Mulet-Sierra, M. J. Vyhlidal, Y. Boluk and A. B. Adesida, *Front. Bioeng. Biotechnol.*, 2021, **9**, 766399.
174 R. Sharma, K. H. Putera, M. M. Banaszak Holl, G. Garnier and V. S. Haritos, *Int. J. Biol. Macromol.*, 2024, **254**, 127972.
175 M. Mujtaba, A. Negi, A. W. T. King, M. Zare and J. Kuncova-Kallio, *Curr. Opin. Biomed. Eng.*, 2023, **28**, 100475.
176 H. E. Emam and T. I. Shaheen, *Carbohydr. Polym.*, 2022, **278**, 118925.
177 W. Fang, T. Song, L. Wang, T. Han, Z. Xiang and O. J. Rojas, *Carbohydr. Polym.*, 2023, **308**, 120663.
178 Y. Xie, Y. Pan and P. Cai, *Ind. Crops Prod.*, 2022, **176**, 114381.
179 B. P. Frank, D. P. Durkin, E. R. Caudill, L. Zhu, D. H. White, M. L. Curry, J. A. Pedersen and D. H. Fairbrother, *ACS Appl. Nano Mater.*, 2018, **1**, 7025–7038.
180 J. Jo, H. Kim, S.-Y. Jeong, C. Park, H. S. Hwang and B. Koo, *Nanomaterials*, 2021, **11**, 1542.
181 C. Boyer, G. Réthoré, P. Weiss, C. d'Arros, J. Lesoeur, C. Vinatier, B. Halgand, O. Geffroy, M. Fusellier, G. Vaillant, P. Roy, O. Gauthier and J. Guicheux, *Front. Bioeng. Biotechnol.*, 2020, **8**, 23.
182 B. Mahendiran, S. Muthusamy, G. Janani, B. B. Mandal, S. Rajendran and G. S. Krishnakumar, *ACS Biomater. Sci. Eng.*, 2022, **8**, 2000–2015.
183 J. Luo, N. Semenikhin, H. Chang, R. J. Moon and S. Kumar, *Carbohydr. Polym.*, 2018, **181**, 247–255.
184 L. Fan, X. Zhou, P. Wu, W. Xie, H. Zheng, W. Tan, S. Liu and Q. Li, *Int. J. Biol. Macromol.*, 2014, **66**, 245–253.
185 A. Randhawa, S. D. Dutta, K. Ganguly, T. V. Patil, D. K. Patel and K.-T. Lim, *Applied Sciences*, 2022, **12**, 7090.
186 B. Thomas, M. C. Raj, K. B. Athira, M. H. Rubiyah, J. Joy, A. Moores, G. L. Drisko and C. Sanchez, *Chem. Rev.*, 2018, **118**, 11575–11625.
187 S. Thiangtham, J. Runt and H. Manuspiya, *Carbohydr. Polym.*, 2019, **208**, 314–322.
188 W. Li, Y. Xue, M. He, J. Yan, L. A. Lucia, J. Chen, J. Yu and G. Yang, *Nanomaterials*, 2021, **11**, 2778.
189 A. S. Kazachenko, N. Yu Vasilieva, Y. D. Berezhnaya, O. Yu Fetisova, V. S. Borovkova, Y. N. Malyar, I. G. Sudakova, V. V. Sychev, N. Issaoui, M. A. Lutoshkin and A. A. Karacharov, *Polymers*, 2023, **15**, 1116.
190 Z. Qin, L. Ji, X. Yin, L. Zhu, Q. Lin and J. Qin, *Carbohydr. Polym.*, 2014, **101**, 947–953.
191 A. Adewuyi, C. A. Otuechere, O. L. Adebayo, C. Anazodo and F. V. Pereira, *Chem.-Biol. Interact.*, 2018, **284**, 56–68.
192 G. Portocarrero Huang, R. Menezes, R. Vincent, W. Hammond, L. Rizio, G. Collins and T. L. Arinzeh, *Tissue Eng., Part A*, 2017, **23**, 1011–1021.
193 A. Dixit, A. Mahajan, R. Saxena, S. Chakraborty and D. S. Katti, *Biomater. Sci.*, 2024, **12**, 2067–2085.
194 A. Ashames, F. Pervaiz, M. Al-Tabakha, K. Khalid, N. Hassan, H. Shoukat, M. Buabeid and G. Murtaza, *J. Saudi Chem. Soc.*, 2022, **26**, 101541.
195 T. Su, Q.-X. Wu, Y. Chen, J. Zhao, X.-D. Cheng and J. Chen, *Int. J. Pharm.*, 2019, **555**, 291–302.
196 H. Kono, E. Tsukamoto and K. Tajima, *ACS Omega*, 2021, **6**, 34107–34114.
197 W. Klunklin, K. Jantanasakulwong, Y. Phimolsiripol, N. Leksawasdi, P. Seesuriyachan, T. Chaiyaso, C. Insomphun, S. Phongthai, P. Jantrawut, S. R. Sommano, W. Punyodom, A. Reungsang, T. M. P. Ngo and P. Rachtanapun, *Polymers*, 2020, **13**, 81.
198 R. Ramakrishnan, J. T. Kim, S. Roy and A. Jayakumar, *Int. J. Biol. Macromol.*, 2024, **259**, 129194.
199 N. Ninan, M. Muthiah, I.-K. Park, A. Elain, S. Thomas and Y. Grohens, *Carbohydr. Polym.*, 2013, **98**, 877–885.
200 J. Liuyun, L. Yubao and X. Chengdong, *J. Biomed. Sci.*, 2009, **16**, 65.
201 G. Janarthanan, H. N. Tran, E. Cha, C. Lee, D. Das and I. Noh, *Mater. Sci. Eng., C*, 2020, **113**, 111008.
202 J. Namkaew, P. Laowpanitchakorn, N. Sawaddee, S. Jirajessada, S. Honsawek and S. Yodmuang, *Molecules*, 2021, **26**, 578.
203 S. Parvaneh, M. Pourmadadi, M. Abdouss, S. A. Pourmousavi, F. Yazdian, A. Rahdar and A. M. Díez-Pascual, *Int. J. Biol. Macromol.*, 2023, **241**, 124566.
204 S. Javanbakht and A. Shaabani, *Int. J. Biol. Macromol.*, 2019, **133**, 21–29.
205 J. Wei, S. Jia, L. Zhang, Y. Zhou, Y. Lv, X. Zhang and Z. Shao, *J. Appl. Polym. Sci.*, 2021, **138**, 50092.

206 A. Rees, L. C. Powell, G. Chinga-Carrasco, D. T. Gethin, K. Syverud, K. E. Hill and D. W. Thomas, *BioMed Res. Int.*, 2015, **2015**, 1–7.
207 P. Khadivar, S. Khajeniazi and A. Karimi, *J. Mater. Res. Technol.*, 2022, **19**, 3966–3979.
208 I. Ali, A. Rizwan, T. T. Vu, S.-H. Jo, C.-W. Oh, Y. H. Kim, S.-H. Park and K. T. Lim, *Int. J. Biol. Macromol.*, 2024, **260**, 129549.
209 Y. Zheng, L. Wang, X. Bai, Y. Xiao and J. Che, *Colloids Surf., A*, 2022, **635**, 127958.
210 D. A. Osorio, B. E. J. Lee, J. M. Kwiecien, X. Wang, I. Shahid, A. L. Hurley, E. D. Cranston and K. Grandfield, *Acta Biomater.*, 2019, **87**, 152–165.
211 Q. Liu, Q. Li, M. Hatakeyama and T. Kitaoka, *Int. J. Biol. Macromol.*, 2023, **253**, 126842.
212 Q. Wang, Ö. Karadas, J. M. Rosenholm, C. Xu, T. Näreoja and X. Wang, *Adv Funct Mater.*, 2024, 2400431.
213 T. Gullinkala and I. Escobar, *J. Membr. Sci.*, 2010, **360**, 155–164.
214 Q. Wang, X. Chen, S. Zeng, P. Chen, Y. Xu, W. Nie, R. Xia and Y. Zhou, *Int. J. Biol. Macromol.*, 2023, **240**, 124515.
215 W. He, Z. Zhang, Y. Zheng, S. Qiao, Y. Xie, Y. Sun, K. Qiao, Z. Feng, X. Wang and J. Wang, *J Biomed. Mater. Res*, 2020, **108**, 1086–1098.
216 S. Andra, S. K. Balu, J. Jeevanandam, M. Muthalagu and M. K. Danquah, *Cellulose*, 2021, **28**, 5895–5910.
217 P. Willberg-Keyriläinen, P. Pitkänen, J. Hulkko, M. Asikainen and H. Setälä, *Heliyon*, 2019, **5**, e01349.
218 B. J. Boese and R. R. Breaker, *Nucleic Acids Res.*, 2007, **35**, 6378–6388.
219 M. Horue, M. L. Cacicedo, M. A. Fernandez, B. Rodenak-Kladniew, R. M. Torres Sánchez and G. R. Castro, *Mater. Sci. Eng., C*, 2020, **116**, 111152.
220 H. Kim, S. Han, K. Choi, J. Lee, S.-H. Lee, Y.-W. Won and K. S. Lim, *Biotechnol. Bioproc. E*, 2023, **28**, 83–90.
221 G. Xu, R. Nigmatullin, T. T. Koev, Y. Z. Khimyak, I. P. Bond and S. J. Eichhorn, *ACS Appl. Mater. Interfaces*, 2022, **14**, 12722–12733.
222 M. Yusefi, K. Shameli, M. S. Lee-Kiun, S.-Y. Teow, H. Moeini, R. R. Ali, P. Kia, C. J. Jie and N. H. Abdullah, *Int. J. Biol. Macromol.*, 2023, **233**, 123388.
223 L. A. Goetz, B. Jalvo, R. Rosal and A. P. Mathew, *J. Membr. Sci.*, 2016, **510**, 238–248.
224 F. Hoeng, J. Bras, E. Gicquel, G. Krosnicki and A. Denneulin, *RSC Adv.*, 2017, **7**, 15372–15381.
225 M.-H. Song, T. P. T. Pham and Y.-S. Yun, *Sci. Rep.*, 2020, **10**, 13905.
226 A. Kumar, K. Dixit and N. Sinha, *Ceramics International*, 2023, **49**, 17639–17649.
227 X. Zhang, C. Wang, M. Liao, L. Dai, Y. Tang, H. Zhang, P. Coates, F. Sefat, L. Zheng, J. Song, Z. Zheng, D. Zhao, M. Yang, W. Zhang and P. Ji, *Carbohydr. Polym.*, 2019, **213**, 27–38.
228 F. L. Hatton, E. Malmström and A. Carlmark, *Eur. Polym. J.*, 2015, **65**, 325–339.
229 I. D. A. A. Fernandes, G. M. Maciel, I. S. Ribeiro, A. C. Pedro, D. G. Bortolini, V. R. Ribeiro, L. Barros and C. W. I. Haminiuk, *Int. J. Biol. Macromol.*, 2023, **240**, 124349.
230 I. Spiridon, N. Anghel, M. V. Dinu, S. Vlad, A. Bele, B. I. Ciubotaru, L. Verestiuc and D. Pamfil, *Polymers*, 2020, **12**, 1191.
231 M. E. Mahmoud, R. M. El-Sharkawy and G. A. A. Ibrahim, *J. Mol. Liq.*, 2022, **368**, 120676.
232 A. Gennari, R. Simon, E. V. Benvenutti, S. Nicolodi, G. Renard, J. M. Chies, G. Volpato and C. F. Volken De Souza, *Int. J. Biol. Macromol.*, 2024, **256**, 128418.
233 N. B. Haro-Mares, J. C. Meza-Contreras, F. A. López-Dellamary, A. Richaud, F. Méndez, B. G. Curiel-Olague, G. Buntkowsky and R. Manríquez-González, *Surf. Interfaces*, 2022, **35**, 102412.
234 Y. Chen, X. Zhang and X. Luo, *Colloids Surf., B*, 2023, **223**, 113184.
235 N. O. Gomes, E. Carrilho, S. A. S. Machado and L. F. Sgobbi, *Electrochim. Acta*, 2020, **349**, 136341.
236 K. Neubauerova, M. C. C. G. Carneiro, L. R. Rodrigues, F. T. C. Moreira and M. G. F. Sales, *Sens. Bio-Sens. Res.*, 2020, **29**, 100368.
237 L. Ning, Y. Jia, X. Zhao, R. Tang, F. Wang and C. You, *Int. J. Biol. Macromol.*, 2022, **222**, 1500–1510.
238 Y. Y. Khine, R. Batchelor, R. Raveendran and M. H. Stenzel, *Macromol. Rapid Commun.*, 2020, **41**, 1900499.
239 L. Ji, F. Zhang, L. Zhu and J. Jiang, *Int. J. Biol. Macromol.*, 2021, **170**, 459–468.
240 Z. Cui, J. Lin, C. Zhan, J. Wu, S. Shen, J. Si and Q. Wang, *J. Biomater. Sci., Polym. Ed.*, 2020, **31**, 561–577.
241 Y. Yin, X. Tian, X. Jiang and P. Zhu, *Ind. Crops Prod.*, 2022, **188**, 115575.
242 F. Lin, X. Lu, Z. Wang, Q. Lu, G. Lin, B. Huang and B. Lu, *Cellulose*, 2019, **26**, 1825–1839.
243 R. Blažic, K. Marušić and E. Vidović, *Gels*, 2023, **9**, 94.
244 Y. Zhong, J. Wang, Z. Yuan, Y. Wang, Z. Xi, L. Li, Z. Liu and X. Guo, *Colloids Surf., B*, 2019, **179**, 462–469.
245 E. Toshikj, A. Tarbuk, K. Grgić, B. Mangovska and I. Jordanov, *Cellulose*, 2019, **26**, 777–794.
246 J. Wang, X. Han, W. Wu, X. Wang, L. Ding, Y. Wang, S. Li, J. Hu, W. Yang, C. Zhang and S. Jiang, *Int. J. Biol. Macromol.*, 2023, **231**, 123343.
247 T. Nypelö, B. Berke, S. Spirk and J. A. Sirviö, *Carbohydr. Polym.*, 2021, **252**, 117105.
248 U.-J. Kim, S. Kuga, M. Wada, T. Okano and T. Kondo, *Biomacromolecules*, 2000, **1**, 488–492.
249 I. Nikolits, S. Radwan, F. Liebner, W. Dietrich, D. Egger, F. Chariyev-Prinz and C. Kasper, *ACS Appl. Bio Mater.*, 2023, **6**, 543–551.
250 T. Saito, S. Kimura, Y. Nishiyama and A. Isogai, *Biomacromolecules*, 2007, **8**, 2485–2491.
251 A. Isogai and L. Bergström, *Curr. Opin. Green Sustainable Chem.*, 2018, **12**, 15–21.
252 A. Isogai, T. Saito and H. Fukuzumi, *Nanoscale*, 2011, **3**, 71–85.
253 P. Sharma, V. K. Pal, H. Kaur and S. Roy, *Biomacromolecules*, 2022, **23**, 2496–2511.
254 H. Yin, P. Song, X. Chen, Q. Huang and H. Huang, *Int. J. Biol. Macromol.*, 2022, **221**, 1606–1617.

255 C.-N. Wu, S.-C. Fuh, S.-P. Lin, Y.-Y. Lin, H.-Y. Chen, J.-M. Liu and K.-C. Cheng, *Biomacromolecules*, 2018, **19**, 544–554.
256 D. Shao, Q. Gao, Y. Sheng, S. Li and Y. Kong, *Int. J. Biol. Macromol.*, 2022, **202**, 37–45.
257 F. Xie, P. De Wever, P. Fardim and G. Van Den Mooter, *Molecules*, 2021, **26**, 1030.
258 A. T. Thodikayil, A. Yadav, P. Hariprasad and S. Saha, *Int. J. Biol. Macromol.*, 2024, **254**, 127604.
259 R. E. Abouzeid, R. Khiari, D. Beneventi and A. Dufresne, *Biomacromolecules*, 2018, **19**, 4442–4452.
260 M. A. Mariño, K. Oyarce, C. Tobar, R. S. Del Río, M. G. Paredes, P. Pavez, M. Sarabia, A. Amoroso, J. L. Concha, J. Norambuena-Contreras, G. C. Barjas and J. Castaño, *Cellulose*, 2024, **31**, 363–379.
261 D. Srivastava, J. Ahopelto and A. J. Karttunen, *Molecules*, 2022, **27**, 6240.
262 M. Wohlert, T. Benselfelt, L. Wågberg, I. Furó, L. A. Berglund and J. Wohlert, *Cellulose*, 2022, **29**, 1–23.
263 R. K. Mishra, S. K. Ha, K. Verma and S. K. Tiwari, *J. Sci.: Adv. Mater. Dev.*, 2018, **3**, 263–288.
264 A. L. Barnette, C. Lee, L. C. Bradley, E. P. Schreiner, Y. B. Park, H. Shin, D. J. Cosgrove, S. Park and S. H. Kim, *Carbohydr. Polym.*, 2012, **89**, 802–809.
265 P. C. S. Faria-Tischer, C. A. Tischer, L. Heux, S. Le Denmat, C. Picart, M.-R. Sierakowski and J.-L. Putaux, *Mater. Sci. Eng., C*, 2015, **51**, 167–173.
266 Z. Ling, S. Chen, X. Zhang, K. Takabe and F. Xu, *Sci. Rep.*, 2017, **7**, 10230.
267 Q. Wu, J. Xu, S. Zhu, Y. Kuang, B. Wang and W. Gao, *Carbohydr. Polym.*, 2020, **249**, 116827.
268 P. Zugenmaier, *Prog. Polym. Sci.*, 2001, **26**, 1341–1417.
269 D. Srivastava, M. S. Kuklin, J. Ahopelto and A. J. Karttunen, *Carbohydr. Polym.*, 2020, **243**, 116440.
270 P. Chen, Y. Ogawa, Y. Nishiyama, A. E. Ismail and K. Mazeau, *Cellulose*, 2018, **25**, 4345–4355.
271 S. A. Kedzior, J. O. Zoppe, R. M. Berry and E. D. Cranston, *Curr. Opin. Solid State Mater. Sci.*, 2019, **23**, 74–91.
272 Y. Yue, J. Han, G. Han, Q. Zhang, A. D. French and Q. Wu, *Carbohydr. Polym.*, 2015, **133**, 438–447.
273 H. Wang, S. Li, T. Wu, X. Wang, X. Cheng and D. Li, *Polymers*, 2019, **11**, 153.
274 M. Wada, T. Okano and J. Sugiyama, *J. Wood Sci.*, 2001, **47**, 124–128.
275 X. Wang, C. H. Chang, J. Jiang, Q. Liu, Y. Liao, J. Lu, L. Li, X. Liu, J. Kim, A. Ahmed, A. E. Nel and T. Xia, *Small*, 2019, **15**, 1901642.
276 G. Kandhola, A. Djioleu, K. Rajan, N. Labbé, J. Sakon, D. J. Carrier and J.-W. Kim, *Bioresour. Bioprocess.*, 2020, **7**, 19.
277 K. J. Nagarajan, N. R. Ramanujam, M. R. Sanjay, S. Siengchin, B. Surya Rajan, K. Sathick Basha, P. Madhu and G. R. Raghav, *Polym. Compos.*, 2021, **42**, 1588–1630.
278 R. K. Mishra, A. Sabu and S. K. Tiwari, *J. Saudi Chem. Soc.*, 2018, **22**, 949–978.
279 B. Anwar, B. Bundjali, Y. Sunarya and I. M. Arcana, *Fibers Polym.*, 2021, **22**, 1228–1236.
280 S. Manan, M. W. Ullah, M. Ul-Islam, Z. Shi, M. Gauthier and G. Yang, *Prog. Mater. Sci.*, 2022, **129**, 100972.
281 J. M. Dugan, J. E. Gough and S. J. Eichhorn, *Nanomedicine*, 2013, **8**, 287–298.
282 K. Daicho, K. Kobayashi, S. Fujisawa and T. Saito, *Biomacromolecules*, 2020, **21**, 939–945.
283 M. Ioelovich, *Polymers*, 2021, **13**, 4313.
284 P. Phanthong, P. Reubroycharoen, X. Hao, G. Xu, A. Abudula and G. Guan, *Carbon Resour. Convers.*, 2018, **1**, 32–43.
285 F. Fortess, *Text. Res. J.*, 1949, **19**, 23–35.
286 T. Kuga, N. Sunagawa and K. Igarashi, *Cellulose*, 2022, **29**, 2999–3015.
287 J. R. Olson, C. J. Jourdain and R. J. Rousseau, *Can. J. For. Res.*, 1985, **15**, 393–396.
288 M. Y. Khalid, A. Al Rashid, Z. U. Arif, W. Ahmed and H. Arshad, *J. Mater. Res. Technol.*, 2021, **14**, 2601–2623.
289 Y. Feng, H. Cölfen and R. Xiong, *J. Mater. Chem. B*, 2023, **11**, 5321–5349.
290 F. V. Ferreira, A. G. Souza, R. Ajdary, L. P. De Souza, J. H. Lopes, D. S. Correa, G. Siqueira, H. S. Barud, D. D. S. Rosa, L. H. C. Mattoso and O. J. Rojas, *Bioactive Mater.*, 2023, **29**, 151–176.
291 L. Geng, Y. Shi, W. Fang, K. Jiang, P. Fan and Y. Zhang, *Mater. Today Commun.*, 2023, **35**, 106414.
292 G. Guhados, W. Wan and J. L. Hutter, *Langmuir*, 2005, **21**, 6642–6646.
293 A. Šturcová, G. R. Davies and S. J. Eichhorn, *Biomacromolecules*, 2005, **6**, 1055–1061.
294 B. Joseph, V. K. Sagarika, C. Sabu, N. Kalarikkal and S. Thomas, *J. Bioresour. Bioprod.*, 2020, **5**, 223–237.
295 R. R. Lahiji, X. Xu, R. Reifenberger, A. Raman, A. Rudie and R. J. Moon, *Langmuir*, 2010, **26**, 4480–4488.
296 R. Rusli and S. J. Eichhorn, *Appl. Phys. Lett.*, 2008, **93**, 033111.
297 N. Lin and A. Dufresne, *Eur. Polym. J.*, 2014, **59**, 302–325.
298 A. Sugawara, T.-A. Asoh, Y. Takashima, A. Harada and H. Uyama, *Polym. Degrad. Stab.*, 2020, **177**, 109157.
299 A. A. B. Omran, A. A. B. A. Mohammed, S. M. Sapuan, R. A. Ilyas, M. R. M. Asyraf, S. S. Rahimian Koloor and M. Petrů, *Polymers*, 2021, **13**, 231.
300 R. J. Moon, A. Martini, J. Nairn, J. Simonsen and J. Youngblood, *Chem. Soc. Rev.*, 2011, **40**, 3941.
301 P. Panchal, E. Ogunsona and T. Mekonnen, *Processes*, 2018, **7**, 10.
302 B. L. Pelegrini, F. Ré, M. M. De Oliveira, T. Fernandes, J. H. De Oliveira, A. G. Oliveira Junior, E. M. Girotto, C. V. Nakamura, A. R. Sampaio, A. Valim and M. M. De Souza Lima, *Macro Mater. Eng.*, 2019, **304**, 1900092.
303 R. T. Olsson, M. A. S. Azizi Samir, G. Salazar-Alvarez, L. Belova, V. Ström, L. A. Berglund, O. Ikkala, J. Nogués and U. W. Gedde, *Nat. Nanotechnol.*, 2010, **5**, 584–588.
304 P. Raj, A. Mayahi, P. Lahtinen, S. Varanasi, G. Garnier, D. Martin and W. Batchelor, *Cellulose*, 2016, **23**, 3051–3064.
305 P. Gatenholm and D. Klemm, *MRS Bull.*, 2010, **35**, 208–213.
306 X. Wu, R. J. Moon and A. Martini, *Cellulose*, 2014, **21**, 2233–2245.

307 T. Saito, R. Kuramae, J. Wohlert, L. A. Berglund and A. Isogai, *Biomacromolecules*, 2013, **14**, 248–253.
308 T. Pal, S. Pramanik, K. D. Verma, S. Z. Naqvi, P. K. Manna and K. K. Kar, *Handbook of Fly Ash*, Elsevier, 2022, pp. 243–270.
309 D. Marković, B. Ćetenović, A. Vuković, V. Jokanović and T. Marković, *Nanobiomaterials in Dentistry*, Elsevier, 2016, pp. 269–307.
310 A. J. Kerin, M. R. Wisnom and M. A. Adams, *Proc. Inst. Mech. Eng. H*, 1998, **212**, 273–280.
311 Z. L. Li, Q. Lu, J. R. Honiball, S. H. Wan, K. W. Yeung and K. M. Cheung, *J. Biomed. Mater. Res.*, 2023, **111**, 1888–1902.
312 A. Guo, Z. Sun, N. Sathitsuksanoh and H. Feng, *Nanomaterials*, 2020, **10**, 2476.
313 M. A. Aziz, M. Zubair and M. Saleem, *Case Studies Construction Mater.*, 2021, **15**, e00761.
314 D. Barnat-Hunek, M. Grzegorczyk-Frańczak, M. Szymańska-Chargot and G. Łagód, *Polymers*, 2019, **11**, 2088.
315 A. L. Buyanov, I. V. Gofman and N. N. Saprykina, *J. Mech. Behav. Biomed. Mater.*, 2019, **100**, 103385.
316 E. B. Heggset, B. L. Strand, K. W. Sundby, S. Simon, G. Chinga-Carrasco and K. Syverud, *Cellulose*, 2019, **26**, 581–595.
317 M. Kim, S. Kim, N. Han, S. Lee and H. Kim, *Carbohydr. Polym.*, 2023, **300**, 120218.
318 Z. Yu, J. Zhan, H. Wang, H. Zheng, J. Xie and X. Wang, *J. Phys.: Conf. Ser.*, 2020, **1653**, 012059.
319 M. Sobanwa, T. J. Foster and N. J. Watson, *Food Hydrocolloids*, 2020, **101**, 105460.
320 D. Liu, H. Zhang, X. Dong, L. Sang and M. Qi, *Front. Bioeng. Biotechnol.*, 2022, **10**, 959409.
321 Y. Jiang, J. Zhou, Z. Yang, D. Liu, X. Xv, G. Zhao, H. Shi and Q. Zhang, *J. Mater. Sci.*, 2018, **53**, 11883–11900.
322 M. A. Hubbe, P. Tayeb, M. Joyce, P. Tyagi, M. Kehoe, K. Dimic-Misic and L. Pal, *BioRes*, 2017, **12**, 9556–9661.
323 M. M. Hassan, N. Tucker and M. J. Le Guen, *Carbohydr. Polym.*, 2020, **230**, 115675.
324 T. Tadros, in *Encyclopedia of Colloid and Interface Science*, ed. T. Tadros, Springer Berlin Heidelberg, Berlin, Heidelberg, 2013, pp. 1020–1042.
325 S.-A. Jin and R. J. Spontak, *Adv. Ind. Eng. Polym. Res.*, 2023, **6**, 356–381.
326 V. Hynninen, J. Patrakka and Nonappa, *Materials*, 2021, **14**, 5137.
327 M. E. Lamm, K. Li, J. Qian, L. Wang, N. Lavoine, R. Newman, D. J. Gardner, T. Li, L. Hu, A. J. Ragauskas, H. Tekinalp, V. Kunc and S. Ozcan, *Adv. Mater.*, 2021, **33**, 2005538.
328 K. Markstedt, A. Mantas, I. Tournier, H. Martínez Ávila, D. Hägg and P. Gatenholm, *Biomacromolecules*, 2015, **16**, 1489–1496.
329 Y. Ai, Z. Lin, W. Zhao, M. Cui, W. Qi, R. Huang and R. Su, *J. Mater. Chem. B*, 2023, **11**, 7004–7023.
330 X. Dong, X. Guo, Q. Liu, Y. Zhao, H. Qi and W. Zhai, *Adv. Funct. Mater.*, 2022, **32**, 2203610.
331 N. E. Zander, H. Dong, J. Steele and J. T. Grant, *ACS Appl. Mater. Interfaces*, 2014, **6**, 18502–18510.
332 S. Ma, M. Zhang, B. Yang, S. Song, J. Nie and P. Lu, *BioRes*, 2018, **13**, 5894–5908.
333 F. V. Borbolla-Jiménez, S. I. Peña-Corona, S. J. Farah, M. T. Jiménez-Valdés, E. Pineda-Pérez, A. Romero-Montero, M. L. Del Prado-Audelo, S. A. Bernal-Chávez, J. J. Magaña and G. Leyva-Gómez, *Pharmaceutics*, 2023, **15**, 1914.
334 J. C. Muñoz-García, K. R. Corbin, H. Hussain, V. Gabrielli, T. Koev, D. Iuga, A. N. Round, D. Mikkelsen, P. A. Gunning, F. J. Warren and Y. Z. Khimyak, *Biomacromolecules*, 2019, **20**, 4180–4190.
335 J. Li, C. Wu, P. K. Chu and M. Gelinsky, *Mater. Sci. Eng., R*, 2020, **140**, 100543.
336 J. Liu, Y. Shi, L. Cheng, J. Sun, S. Yu, X. Lu, S. Biranje, W. Xu, X. Zhang, J. Song, Q. Wang, W. Han and Z. Zhang, *Cellulose*, 2021, **28**, 5643–5656.
337 S. Ilkar Erdagi, F. Asabuwa Ngwabebhoh and U. Yildiz, *Int. J. Biol. Macromol.*, 2020, **149**, 651–663.
338 P. Maturavongsadit, L. K. Narayanan, P. Chansoria, R. Shirwaiker and S. R. Benhabbour, *ACS Appl. Bio Mater.*, 2021, **4**, 2342–2353.
339 L. Berglund, P. Squinca, Y. Baş, E. Zattarin, D. Aili, J. Rakar, J. Junker, A. Starkenberg, M. Diamanti, P. Sivlér, M. Skog and K. Oksman, *Biomacromolecules*, 2023, **24**, 2264–2277.
340 C. Chang, J. Peng, L. Zhang and D.-W. Pang, *J. Mater. Chem.*, 2009, **19**, 7771.
341 A. M. L. Piloto, D. S. M. Ribeiro, S. S. M. Rodrigues, J. L. M. Santos, P. Sampaio and M. G. F. Sales, *Microchim. Acta*, 2022, **189**, 134.
342 H. Luo, J. Dong, F. Yao, Z. Yang, W. Li, J. Wang, X. Xu, J. Hu and Y. Wan, *Nano-Micro Lett.*, 2018, **10**, 42.
343 L. Li, Z. Lin, X. Yang, Z. Wan and S. Cui, *Sci. Bull.*, 2009, **54**, 1622–1625.
344 H. Najaf Zadeh, T. Huber, V. Nock, C. Fee and D. Clucas, *Bioengineering*, 2020, **7**, 58.
345 E. Campodoni, M. Montanari, S. M. Dozio, E. B. Heggset, S. Panseri, M. Montesi, A. Tampieri, K. Syverud and M. Sandri, *Nanomaterials*, 2020, **10**, 1219.
346 L. Orgéas, S. Gupta, F. Martoïa and P. J. J. Dumont, *Mater. Des.*, 2022, **223**, 111201.
347 J. Joy, J. Pereira, R. Aid-Launais, G. Pavon-Djavid, A. R. Ray, D. Letourneur, A. Meddahi-Pellé and B. Gupta, *Int. J. Biol. Macromol.*, 2018, **107**, 1922–1935.
348 H. Samadian, S. Zamiri, A. Ehterami, S. Farzamfar, A. Vaez, H. Khastar, M. Alam, A. Ai, H. Derakhshankhah, Z. Allahyari, A. Goodarzi and M. Salehi, *Sci. Rep.*, 2020, **10**, 8312.
349 M. Bordoni, E. Karabulut, V. Kuzmenko, V. Fantini, O. Pansarasa, C. Cereda and P. Gatenholm, *Cells*, 2020, **9**, 682.
350 L. Diaz-Gomez, I. Gonzalez-Prada, R. Millan, A. Da Silva-Candal, A. Bugallo-Casal, F. Campos, A. Concheiro and C. Alvarez-Lorenzo, *Carbohydr. Polym.*, 2022, **278**, 118924.
351 J. Batta-Mpouma, G. Kandhola, J. Sakon and J.-W. Kim, *Biomacromolecules*, 2022, **23**, 4085–4096.
352 A. Sannino, S. Pappadà, M. Madaghiele, A. Maffezzoli, L. Ambrosio and L. Nicolais, *Polymer*, 2005, **46**, 11206–11212.

353 R. Vel, A. Bhatt, A. Priyanka, A. Gauthaman, V. Anilkumar, A. S. Safeena and S. Ranjith, *Mater. Today Commun.*, 2022, **33**, 104335.
354 R. Xing, L. Ning, L. Li, L. He, H. Lin, C. You and F. Wang, *J. Drug Delivery Sci. Technol.*, 2023, **86**, 104654.
355 V. Mohanta, G. Madras and S. Patil, *ACS Appl. Mater. Interfaces*, 2014, **6**, 20093–20101.
356 X. Huang, Y. Wang, Y. Wang and L. Yang, *Molecules*, 2023, **28**, 1301.
357 C. Wang, J. Bai, P. Tian, R. Xie, Z. Duan, Q. Lv and Y. Tao, *Front. Bioeng. Biotechnol.*, 2021, **9**, 732513.
358 P. Pooyan, R. Tannenbaum and H. Garmestani, *J. Mech. Behav. Biomed. Mater.*, 2012, **7**, 50–59.
359 P. Pooyan, I. T. Kim, K. I. Jacob, R. Tannenbaum and H. Garmestani, *Polymer*, 2013, **54**, 2105–2114.
360 E. Ten, J. Turtle, D. Bahr, L. Jiang and M. Wolcott, *Polymer*, 2010, **51**, 2652–2660.
361 P. Zou, J. Yao, Y.-N. Cui, T. Zhao, J. Che, M. Yang, Z. Li and C. Gao, *Gels*, 2022, **8**, 364.
362 J. Han, T. Lei and Q. Wu, *Cellulose*, 2013, **20**, 2947–2958.
363 K. Hou, Y. Li, Y. Liu, R. Zhang, B. S. Hsiao and M. Zhu, *Polymer*, 2017, **123**, 55–64.
364 J. Hu, Y. Wu, Q. Yang, Q. Zhou, L. Hui, Z. Liu, F. Xu and D. Ding, *Carbohydr. Polym.*, 2022, **275**, 118697.
365 S. Mandin, S. Moreau, M. Talantikite, B. Novalès, J.-E. Maigret, B. Cathala and C. Moreau, *Gels*, 2021, **7**, 5.
366 Y. Zhou, S. Fu, Y. Pu, S. Pan, M. V. Levit and A. J. Ragauskas, *RSC Adv.*, 2013, **3**, 19272.
367 R. Dash, Y. Li and A. J. Ragauskas, *Carbohydr. Polym.*, 2012, **88**, 789–792.
368 S. Rahmani, Z. Khoubi-Arani, S. Mohammadzadeh-Komuleh and M. Maroufkhani, in *Handbook of Nanocelluloses*, ed. A. Barhoum, Springer International Publishing, Cham, 2022, pp. 263–296.
369 J. Adhikari, S. Dasgupta, P. Das, D. A. Gouripriya, A. Barui, P. Basak, M. Ghosh and P. Saha, *Int. J. Biol. Macromol.*, 2024, **261**, 129661.
370 M. F. Abdullah, A. Andriyana, F. Muhamad and B. C. Ang, *J. Polym. Res.*, 2023, **30**, 257.
371 N. S. Lameirinhas, M. C. Teixeira, J. P. F. Carvalho, B. F. A. Valente, R. J. B. Pinto, H. Oliveira, J. L. Luís, L. Pires, J. M. Oliveira, C. Vilela and C. S. R. Freire, *Int. J. Biol. Macromol.*, 2023, **229**, 849–860.
372 K. Yan, X. Zhang, Y. Liu, J. Cheng, C. Zhai, K. Shen, W. Liang and W. Fan, *Mater. Des.*, 2023, **225**, 111531.
373 S. D. Dutta, J. Hexiu, D. K. Patel, K. Ganguly and K.-T. Lim, *Int. J. Biol. Macromol.*, 2021, **167**, 644–658.
374 X. Wang, Q. Wang and C. Xu, *Bioengineering*, 2020, **7**, 40.
375 M. P. Sekar, H. Budharaju, S. Sethuraman and D. Sundaramurthi, *SLAS Technol.*, 2023, **28**, 183–198.
376 H. Baniasadi, R. T. Polez, E. Kimiaei, Z. Madani, O. J. Rojas, M. Österberg and J. Seppälä, *Int. J. Biol. Macromol.*, 2021, **192**, 1098–1107.
377 S. Shin, S. Park, M. Park, E. Jeong, K. Na, H. J. Youn and J. Hyun, *BioResources*, 2017, **12**, 2941–2954.
378 N. Ashammakhi, S. Ahadian, C. Xu, H. Montazerian, H. Ko, R. Nasiri, N. Barros and A. Khademhosseini, *Mater. Today Bio*, 2019, **1**, 100008.
379 H. Baniasadi, R. Ajdary, J. Trifol, O. J. Rojas and J. Seppälä, *Carbohydr. Polym.*, 2021, **266**, 118114.
380 R. Prathapan, B. A. Glatz, A. K. Ghosh, S. Michel, A. Fery, G. Garnier and R. F. Tabor, *Langmuir*, 2019, **35**, 7155–7160.
381 B. He, S. Yang, Z. Qin, B. Wen and C. Zhang, *Sci. Rep.*, 2017, **7**, 11841.
382 A. I. Cernencu, A. Lungu, I.-C. Stancu, A. Serafim, E. Heggset, K. Syverud and H. Iovu, *Carbohydr. Polym.*, 2019, **220**, 12–21.
383 D. Cafiso, A. A. Septevani, C. Noè, T. Schiller, C. F. Pirri, I. Roppolo and A. Chiappone, *Sustainable Mater. Technol.*, 2022, **32**, e00444.
384 A. Sadeghianmaryan, S. Naghieh, H. Alizadeh Sardroud, Z. Yazdanpanah, Y. Afzal Soltani, J. Sernaglia and X. Chen, *Int. J. Biol. Macromol.*, 2020, **164**, 3179–3192.
385 X. Li, B. Liu, B. Pei, J. Chen, D. Zhou, J. Peng, X. Zhang, W. Jia and T. Xu, *Chem. Rev.*, 2020, **120**, 10793–10833.
386 Z. Xie, M. Gao, A. O. Lobo and T. J. Webster, *Polymers*, 2020, **12**, 1717.
387 Y.-L. Tsai, P. Theato, C.-F. Huang and S. Hsu, *Appl. Mater. Today*, 2020, **20**, 100778.
388 S. C. Pandanaboina, A. B. RanguMagar, K. D. Sharma, B. P. Chhetri, C. M. Parnell, J. Y. Xie, M. Srivatsan and A. Ghosh, *JFB*, 2021, **12**, 64.
389 R. R. Palem, B. J. Kim, I. Baek, H. Choi, M. Suneetha, G. Shimoga and S.-H. Lee, *Carbohydr. Polym.*, 2024, **334**, 122020.
390 H. Xie, G. Shi, R. Wang, X. Jiang, Q. Chen, A. Yu and A. Lu, *Carbohydr. Polym.*, 2024, **334**, 122014.
391 M. Nouri-Felekori, N. Nezafati, M. Moraveji, S. Hesaraki and T. Ramezani, *Int. J. Biol. Macromol.*, 2021, **183**, 2030–2043.
392 S. Palantöken, K. Bethke, V. Zivanovic, G. Kalinka, J. Kneipp and K. Rademann, *J. Appl. Polym. Sci.*, 2020, **137**, 48380.
393 A. N. Frone, D. M. Panaitescu, C. A. Nicolae, A. R. Gabor, R. Trusca, A. Casarica, P. O. Stanescu, D. D. Baciu and A. Salageanu, *Mater. Sci. Eng., C*, 2020, **110**, 110740.
394 S. Dutta, P. Samanta and D. Dhara, *Int. J. Biol. Macromol.*, 2016, **87**, 92–100.
395 N. Chen, H. Wang, C. Ling, W. Vermerris, B. Wang and Z. Tong, *Carbohydr. Polym.*, 2019, **225**, 115207.
396 X. Jiang, F. Zeng, X. Yang, C. Jian, L. Zhang, A. Yu and A. Lu, *Acta Biomater.*, 2022, **141**, 102–113.
397 I. Ali, M. Gulfam, S.-H. Jo, J.-W. Seo, A. Rizwan, S.-H. Park and K. T. Lim, *Int. J. Biol. Macromol.*, 2022, **219**, 109–120.
398 R. Ajdary, G. Reyes, J. Kuula, E. Raussi-Lehto, T. S. Mikkola, E. Kankuri and O. J. Rojas, *ACS Polym. Au*, 2022, **2**, 97–107.
399 J. Tie, H. Chai, Z. Mao, L. Zhang, Y. Zhong, X. Sui and H. Xu, *Carbohydr. Polym.*, 2021, **273**, 118600.
400 C. Huang, Q. Ye, J. Dong, L. Li, M. Wang, Y. Zhang, Y. Zhang, X. Wang, P. Wang and Q. Jiang, *Smart Mater. Med.*, 2023, **4**, 1–14.

401 M. Suneetha, H. Kim and S. S. Han, *Int. J. Biol. Macromol.*, 2024, **256**, 128364.
402 X. Xun, Y. Li, M. Ni, Y. Xu, J. Li, D. Zhang, G. Chen, H. Ao, H. Luo, Y. Wan and T. Yu, *Composites, Part B*, 2024, **275**, 111277.
403 M. Hojabri, T. Tayebi, M. Kasravi, A. Aghdaee, A. Ahmadi, R. Mazloomnejad, R. Tarasi, A. Shaabani, S. Bahrami and H. Niknejad, *Int. J. Biol. Macromol.*, 2023, **240**, 124492.
404 K.-T. Le, C.-T. Nguyen, T.-D. Lac, L.-G. T. Nguyen, T. L. Tran and H. Tran-Van, *J. Drug Delivery Sci. Technol.*, 2023, **82**, 104318.
405 M. P. Arrieta, E. Fortunati, N. Burgos, M. A. Peltzer, J. López and L. Peponi, *Multifunctional Polymeric Nanocomposites Based on Cellulosic Reinforcements*, Elsevier, 2016, pp. 205–252.
406 S. Kalia, A. Dufresne, B. M. Cherian, B. S. Kaith, L. Avérous, J. Njuguna and E. Nassiopoulos, *Int. J. Polym. Sci.*, 2011, **2011**, 1–35.
407 A. A. Singh, M. E. Genovese, G. Mancini, L. Marini and A. Athanassiou, *ACS Sustainable Chem. Eng.*, 2020, **8**, 4128–4136.
408 S. Sundararajan, A. B. Samui and P. S. Kulkarni, *Sol. Energy*, 2017, **144**, 32–39.
409 L. Del Valle, A. Díaz and J. Puiggalí, *Gels*, 2017, **3**, 27.
410 S.-Q. Chen, Q. Liao, O. W. Meldrum, L. Guo, K. Wang, S. Zhang, Y. Liu, X. Chen, J. Zhu and L. Li, *Carbohydr. Polym.*, 2023, **321**, 121268.
411 P. Maturavongsadit, G. Paravyan, R. Shrivastava and S. R. Benhabbour, *Materialia*, 2020, **12**, 100681.
412 F. Coelho, M. Cavicchioli, S. S. Specian, R. M. Scarel-Caminaga, L. D. A. Penteado, A. I. D. Medeiros, S. J. D. L. Ribeiro and T. S. D. O. Capote, *PLoS One*, 2019, **14**, e0221286.
413 L. Li, L. Wang, X. Luan, Y. Pang, K. Zhang, Y. Cheng, Z. Ji and J. Pang, *Carbohydr. Polym.*, 2023, **320**, 121235.
414 H. P. Felgueiras, M. A. Teixeira, T. D. Tavares, N. C. Homem, A. Zille and M. T. P. Amorim, *J. Appl. Polym. Sci.*, 2020, **137**, 48626.
415 H. Dong, J. F. Snyder, D. T. Tran and J. L. Leadore, *Carbohydr. Polym.*, 2013, **95**, 760–767.
416 C. Palo-Nieto, A. Blasi-Romero, C. Sandström, D. Balgoma, M. Hedeland, M. Strømme and N. Ferraz, *Mater. Adv.*, 2023, **4**, 1555–1565.
417 E. A. Bakr, M. Gaber, D. R. Saad and N. Salahuddin, *Int. J. Biol. Macromol.*, 2023, **230**, 123315.
418 J.-H. Seo, S. Y. Lee, C. Hwang, M. Yang, J. Lee, S.-H. Lee and H.-J. Cho, *Int. J. Biol. Macromol.*, 2020, **162**, 798–809.
419 N. S. V. Capanema, I. C. Carvalho, A. A. P. Mansur, S. M. Carvalho, A. P. Lage and H. S. Mansur, *ACS Appl. Nano Mater.*, 2019, **2**, 7393–7408.
420 E. Tamahkar, *Chem. Pap.*, 2021, **75**, 3979–3987.
421 T. M. S. U. Gunathilake, Y. C. Ching, H. Uyama, N. D. Hai and C. H. Chuah, *Cellulose*, 2022, **29**, 1821–1840.
422 H. Roy, K. Hasan Parvej, M. Mozammal Hosen, Md Shahinoor Islam and S. H. Firoz, *Arabian J. Chem.*, 2024, **17**, 105763.
423 B. Niknafs, M. Meskaraf-asadabadi, K. Hamdi and E. Ghanbari, *Int. J. Biol. Macromol.*, 2024, **266**, 131167.
424 E. Ghanbari, M. Khazaei, A. Mehdipour, A. Khoshfeterat and B. Niknafs, *Cell J.*, 2023, **25**, 483–495.
425 X. Yang, J. Huang, C. Chen, L. Zhou, H. Ren and D. Sun, *ACS Appl. Mater. Interfaces*, 2023, **15**, 10506–10519.
426 F. Yu, H. Shi, K. Wang, H. Li and L. Peng, *Int. J. Biol. Macromol.*, 2022, **222**, 1238–1249.
427 S. Li, D. Wang, H. Xiao, H. Zhang, S. Cao, L. Chen, Y. Ni and L. Huang, *Carbohydr. Polym.*, 2021, **255**, 117352.
428 A. Díez-Pascual and A. Rahdar, *Nanomaterials*, 2022, **12**, 949.
429 G. Liu, Z. Ding, Q. Yuan, H. Xie and Z. Gu, *Front. Chem.*, 2018, **6**, 439.
430 W. Yuan, G.-M. Weng, J. Lipton, C. M. Li, P. R. Van Tassel and A. D. Taylor, *Adv. Colloid Interface Sci.*, 2020, **282**, 102200.
431 A. Díez-Pascual and P. Shuttleworth, *Materials*, 2014, **7**, 7472–7512.
432 W. Li, X. Li, W. Li, T. Wang, X. Li, S. Pan and H. Deng, *Eur. Polym. J.*, 2012, **48**, 1846–1853.
433 S. Kariminia, M. Shamsipur and K. Mansouri, *J. Mater. Chem. B*, 2024, **12**, 176–186.
434 M. Khamrai, S. L. Banerjee, S. Paul, A. K. Ghosh, P. Sarkar and P. P. Kundu, *ACS Appl. Bio Mater.*, 2021, **4**, 428–440.
435 F. Zhang, N. Zhang, H.-X. Meng, H.-X. Liu, Y.-Q. Lu, C.-M. Liu, Z.-M. Zhang, K.-Y. Qu and N.-P. Huang, *ACS Biomater. Sci. Eng.*, 2019, **5**, 3022–3031.
436 S. Choy, D. V. Lam, S.-M. Lee and D. S. Hwang, *ACS Appl. Mater. Interfaces*, 2019, **11**, 38440–38447.
437 H.-W. Kang, S. J. Lee, I. K. Ko, C. Kengla, J. J. Yoo and A. Atala, *Nat. Biotechnol.*, 2016, **34**, 312–319.
438 P. Bhattacharjee and M. Ahearne, *Pharmaceutics*, 2021, **13**, 319.
439 A. Sommer, P. Dederko-Kantowicz, H. Staroszczyk, S. Sommer and M. Michalec, *IJMS*, 2021, **22**, 3346.
440 D. Fu, Y. Xie, L. Zhou, L. Zhang, T. Zheng and J. Shen, *Carbohydr. Polym.*, 2024, **325**, 121572.
441 M. Uva, M. Tambasco, G. Grassi, I. Corsi, G. Protano and A. Atrei, *J. Environ. Chem. Eng.*, 2017, **5**, 3632–3639.
442 R. Cruz-Medina, D. A. Ayala-Hernández, A. Vega-Rios, E. I. López-Martínez, M. E. Mendoza-Duarte, A. Estrada-Monje and E. A. Zaragoza-Contreras, *Polymers*, 2021, **13**, 2342.
443 L. Wang, W. Zhao, Y. Zhao, W. Li, G. Wang and Q. Zhang, *Theranostics*, 2023, **13**, 673–684.
444 D. Zhao, J. Huang, Y. Zhong, K. Li, L. Zhang and J. Cai, *Adv Funct Materials*, 2016, **26**, 6279–6287.
445 M. Xeroudaki, M. Rafat, P. Moustardas, A. Mukwaya, S. Tabe, M. Bellisario, B. Peebo and N. Lagali, *Acta Biomater.*, 2023, **172**, 234–248.
446 S. R. S. Veloso, A. G. Azevedo, P. F. Teixeira and C. B. P. Fernandes, *Gels*, 2023, **9**, 574.
447 F. Doustdar, A. Olad and M. Ghorbani, *Int. J. Biol. Macromol.*, 2022, **208**, 912–924.
448 Z. Rao, Y. Dong, J. Liu, X. Zheng, Y. Pei and K. Tang, *Int. J. Biol. Macromol.*, 2022, **222**, 3155–3167.
449 P. C. Nath, S. Debnath, M. Sharma, K. Sridhar, P. K. Nayak and B. S. Inbaraj, *Foods*, 2023, **12**, 350.

450 A. K. Singh, P. Itkor and Y. S. Lee, *Gels*, 2023, **9**, 433.
451 H. Nasution, H. Harahap, N. F. Dalimunthe, M. H. S. Ginting, M. Jaafar, O. O. H. Tan, H. K. Aruan and A. L. Herfananda, *Gels*, 2022, **8**, 568.
452 A. A. D. N. Pomari, T. L. D. A. Montanheiro, C. P. De Siqueira, R. S. Silva, D. B. Tada and A. P. Lemes, *J. Compos. Sci.*, 2019, **3**, 84.
453 F. J. Burpo, J. L. Palmer, A. N. Mitropoulos, E. A. Nagelli, L. A. Morris, M. Y. Ryu and J. K. Wickiser, *JoVE*, 2019, 59176.
454 Y. Jia, M. Huo, H. Huang, W. Fu, Y. Wang, J. Zhang and S. Jia, *Proc. Inst. Mech. Eng., Part N*, 2015, **229**, 41–48.
455 M. Hajiabbas, I. Alemzadeh, M. Vossoughi and A. Shamloo, *Chem. Eng. Commun.*, 2021, **208**, 976–992.
456 D.-J. Lim, *IJMS*, 2022, **23**, 5444.
457 J. Tang, Y. Li, Y. Song, X. Wu, G. Yu and K. C. Tam, *Carbohydr. Polym.*, 2020, **244**, 116512.
458 A. Azarniya, E. Tamjid, N. Eslahi and A. Simchi, *Int. J. Biol. Macromol.*, 2019, **134**, 280–289.
459 F. Xu, C. Dawson, M. Lamb, E. Mueller, E. Stefanek, M. Akbari and T. Hoare, *Front. Bioeng. Biotechnol.*, 2022, **10**, 849831.
460 Y. Zeng, C. Huang, D. Duan, A. Lou, Y. Guo, T. Xiao, J. Wei, S. Liu, Z. Wang, Q. Yang, L. Zhou, Z. Wu and L. Wang, *Acta Biomater.*, 2022, **153**, 108–123.
461 G. G. De Lima, B. D. Ferreira, M. Matos, B. L. Pereira, M. J. D. Nugent, F. A. Hansel and W. L. E. Magalhães, *Carbohydr. Polym.*, 2020, **245**, 116612.
462 M. Bustamante-Torres, D. Romero-Fierro, B. Arcentales-Vera, K. Palomino, H. Magaña and E. Bucio, *Gels*, 2021, **7**, 182.
463 H. Kang, R. Liu and Y. Huang, *Macromol. Chem. Phys.*, 2016, **217**, 1322–1334.
464 X. Zhang, X. Ma, T. Hou, K. Guo, J. Yin, Z. Wang, L. Shu, M. He and J. Yao, *Angew. Chem.*, 2019, **131**, 7444–7448.
465 C. Wu, J. Li, Y. Zhang, X. Li, S. Wang and D. Li, *ChemSusChem*, 2023, **16**, e202300518.
466 M. Ghasemi, M. Tsianou and P. Alexandridis, *Bioresour. Technol.*, 2017, **228**, 330–338.
467 B. Lindman, B. Medronho, L. Alves, C. Costa, H. Edlund and M. Norgren, *Phys. Chem. Chem. Phys.*, 2017, **19**, 23704–23718.
468 D. E. Ciolacu and D. M. Suflet, *Biomass as Renewable Raw Material to Obtain Bioproducts of High-Tech Value*, Elsevier, 2018, pp. 401–439.
469 C. Xie, G. Liu, L. Wang, Q. Yang, F. Liao, X. Yang, B. Xiao and L. Duan, *Pharmaceutics*, 2024, **16**, 430.
470 Z. Xie, B.-L. Hu, R.-W. Li and Q. Zhang, *ACS Omega*, 2021, **6**, 9319–9333.
471 T. Kopač, A. Ručigaj and M. Krajnc, *Int. J. Biol. Macromol.*, 2020, **159**, 557–569.
472 Y. Dong, S. Zhao, W. Lu, N. Chen, D. Zhu and Y. Li, *RSC Adv.*, 2021, **11**, 10794–10803.
473 O. Haske-Cornelius, S. Bischof, B. Beer, M. Jimenez Bartolome, E. Olatunde Olakanmi, M. Mokoba, G. M. Guebitz and G. S. Nyanhongo, *Eur. Polym. J.*, 2019, **120**, 109201.
474 S. Zhao, Z. Chen, Y. Dong, W. Lu and D. Zhu, *Gels*, 2022, **8**, 146.
475 X. Zhang, W. Wang, Y. Wang, Y. Wang, X. Wang, G. Gao, G. Chen and A. Liu, *Food Hydrocolloids*, 2018, **84**, 1–8.
476 W. Song, J. Ko, Y. H. Choi and N. S. Hwang, *APL Bioengineering*, 2021, **5**, 021502.
477 X. Xue, Y. Hu, S. Wang, X. Chen, Y. Jiang and J. Su, *Bioactive Mater.*, 2022, **12**, 327–339.
478 R. Naranjo-Alcazar, S. Bendix, T. Groth and G. Gallego Ferrer, *Gels*, 2023, **9**, 230.
479 L. Trachsel, C. Johnbosco, T. Lang, E. M. Benetti and M. Zenobi-Wong, *Biomacromolecules*, 2019, **20**, 4502–4511.
480 L. Zhang, C. Wan, J. Su, C. Zhang, S. Wei, W. Tian, X. Liu, W. Cheng, X. Li, X. Li, X. Guo, K.-T. Yong and Y. Wu, *Mater. Des.*, 2022, **215**, 110464.
481 L. Li, J. Guo, C. Kang and H. Song, *Polymers*, 2023, **15**, 1765.
482 K. J. De France, K. J. W. Chan, E. D. Cranston and T. Hoare, *Biomacromolecules*, 2016, **17**, 649–660.
483 T. Zhang, T. Zuo, D. Hu and C. Chang, *ACS Appl. Mater. Interfaces*, 2017, **9**, 24230–24237.
484 H. Xu, Y. Liu, Y. Xie, E. Zhu, Z. Shi, Q. Yang and C. Xiong, *Cellulose*, 2019, **26**, 8645–8654.
485 S. Mantha, S. Pillai, P. Khayambashi, A. Upadhyay, Y. Zhang, O. Tao, H. M. Pham and S. D. Tran, *Materials*, 2019, **12**, 3323.
486 P. Bertsch, M. Diba, D. J. Mooney and S. C. G. Leeuwenburgh, *Chem. Rev.*, 2023, **123**, 834–873.
487 S. A. Eming, P. Martin and M. Tomic-Canic, *Sci. Transl. Med.*, 2014, **6**, DOI: 10.1126/scitranslmed.3009337.
488 E. Y. X. Loh, N. Mohamad, M. B. Fauzi, M. H. Ng, S. F. Ng and M. C. I. Mohd Amin, *Sci. Rep.*, 2018, **8**, 2875.
489 N. T. Laçin, *Int. J. Biol. Macromol.*, 2014, **67**, 22–27.
490 M. Pandey, N. Mohamad, W.-L. Low, C. Martin and M. C. I. Mohd Amin, *Drug Delivery Transl. Res.*, 2017, **7**, 89–99.
491 S. Cometa, C. Licini, M. A. Bonifacio, P. Mastrorilli, M. Mattioli-Belmonte and E. De Giglio, *Carbohydr. Polym.*, 2022, **283**, 119145.
492 K. Zhang, D. Wu, L. Chang, W. Duan, Y. Wang, W. Li and J. Qin, *Int. J. Biol. Macromol.*, 2023, **230**, 123294.
493 F. Cheng, X. Yi, J. Dai, Z. Fan, J. He, Y. Huang and H. Li, *Cell Rep. Phys. Sci.*, 2023, **4**, 101619.
494 R. Khan, M. U. Aslam Khan, G. M. Stojanović, A. Javed, S. Haider and S. I. Abd Razak, *ACS Omega*, 2024, **9**, 6527–6536.
495 W. Song, T. Xu, L. Qian, S. Zhang, C. Wang, Y. Zhao, Z. He, V. Nica and Z. Miao, *Int. J. Biol. Macromol.*, 2023, **244**, 125353.
496 F. Wahid, X.-J. Zhao, X.-Q. Zhao, X.-F. Ma, N. Xue, X.-Z. Liu, F.-P. Wang, S.-R. Jia and C. Zhong, *ACS Appl. Mater. Interfaces*, 2021, **13**, 32716–32728.
497 N. S. V. Capanema, A. A. P. Mansur, I. C. Carvalho, S. M. Carvalho and H. S. Mansur, *Gels*, 2023, **9**, 166.
498 Z. Zhang, S. Lin, Y. Yan, X. You and H. Ye, *J. Biomater. Sci., Polym. Ed.*, 2021, **32**, 2402–2422.
499 M. Ghorbani, L. Roshangar and J. Soleimani Rad, *Eur. Polym. J.*, 2020, **130**, 109697.

500 X. Yu, X. Li, L. Kan, P. Pan, X. Wang, W. Liu and J. Zhang, *Int. J. Biol. Macromol.*, 2023, **238**, 124113.
501 L. Gu, T. Li, X. Song, X. Yang, S. Li, L. Chen, P. Liu, X. Gong, C. Chen and L. Sun, *Regener. Biomater.*, 2020, **7**, 195–202.
502 S. Chayanun, A. A. Soufivand, J. Faber, S. Budday, B. Lohwongwatana and A. R. Boccaccini, *Adv. Eng. Mater.*, 2024, **26**, 2300641.
503 J. Sinna, R. Jeencham, P. Mueangkhot, S. Sophon, P. Noralak, R. Raksapakdee, P. Numpaisal and Y. Ruksakulpiwat, *Polymers*, 2023, **15**, 4230.
504 P. Basu, N. Saha and P. Saha, *Int. J. Polym. Mater. Polym. Biomater.*, 2019, **68**, 134–144.
505 M. G. Raucci, M. A. Alvarez-Perez, C. Demitri, D. Giugliano, V. De Benedictis, A. Sannino and L. Ambrosio, *J. Biomed. Mater. Res.*, 2015, **103**, 2045–2056.
506 D. Burger, M. Beaumont, T. Rosenau and Y. Tamada, *Molecules*, 2020, **25**, 5097.
507 S. Saber-Samandari, S. Saber-Samandari, S. Kiyazar, J. Aghazadeh and A. Sadeghi, *Int. J. Biol. Macromol.*, 2016, **86**, 434–442.
508 S. Cui, S. Zhang and S. Coseri, *Carbohydr. Polym.*, 2023, **300**, 120243.
509 G. Priya, B. Madhan, U. Narendrakumar, R. V. Suresh Kumar and I. Manjubala, *ACS Omega*, 2021, **6**, 1246–1253.
510 H. Tohidi, N. Maleki-Jirsaraei, A. Simchi, F. Mohandes, Z. Emami, L. Fassina, F. Naro, B. Conti and F. Barbagallo, *Materials*, 2022, **15**, 5122.
511 E. Entcheva, H. Bien, L. Yin, C.-Y. Chung, M. Farrell and Y. Kostov, *Biomaterials*, 2004, **25**, 5753–5762.
512 S. Sedighim, Y. Chen, C. Xu, R. Mohindra, H. Liu, D. K. Agrawal and F. G. Thankam, *Biotechnol. Bioeng.*, 2023, **120**, 819–835.
513 C. Sun, Y. Xie, H. Zhu, X. Zheng, R. Hou, Z. Shi, J. Li and Q. Yang, *Biomacromolecules*, 2023, **24**, 5989–5997.
514 E. Ahmadi, P. Harirchi, P. Zahedi, B. Bakhshandeh, S. Zolfagharian and A. Khatibi, *Fibers Polym.*, 2023, **24**, 2293–2303.
515 Z. Shi, H. Gao, J. Feng, B. Ding, X. Cao, S. Kuga, Y. Wang, L. Zhang and J. Cai, *Angew. Chem., Int. Ed.*, 2014, **53**, 5380–5384.
516 K.-C. Cheng, C.-F. Huang, Y. Wei and S. Hsu, *NPG Asia Mater.*, 2019, **11**, 25.
517 L. Deng, Y. Huang, S. Chen, Z. Han, Z. Han, M. Jin, X. Qu, B. Wang, H. Wang and S. Gu, *Carbohydr. Polym.*, 2023, **308**, 120647.
518 H. Lu, X. Li, M. Zhang, C. Xu, W. Li and L. Wan, *Front. Bioeng. Biotechnol.*, 2022, **10**, 876936.
519 M. Tian, J. Shuai, B. A. Bishop, W. Zhang, J. Chen and X. Wang, *Chem. Eng. J.*, 2023, **476**, 146751.
520 T. Sultana, M. Hossain, S. Rahaman, Y. S. Kim, J.-G. Gwon and B.-T. Lee, *Carbohydr. Polym.*, 2021, **272**, 118482.
521 A. A. Shefa, T. Sultana, M. K. Park, S. Y. Lee, J.-G. Gwon and B.-T. Lee, *Mater. Des.*, 2020, **186**, 108313.
522 W. Hu, Z. Chen, X. Chen, K. Feng, T. Hu, B. Huang, J. Tang, G. Wang, S. Liu, G. Yang and Z. Wang, *Carbohydr. Polym.*, 2023, **319**, 121193.
523 G. Yang, Z. Zhang, K. Liu, X. Ji, P. Fatehi and J. Chen, *J. Nanobiotechnol.*, 2022, **20**, 312.
524 H. Mohaghegh, Z. Assadi, A. Derakhshan and E. Masaeli, *J. Pharm. Sci.*, 2023, **113**, 754–763.
525 H. Wu, G. R. Williams, J. Wu, J. Wu, S. Niu, H. Li, H. Wang and L. Zhu, *Carbohydr. Polym.*, 2018, **180**, 304–313.
526 Y. Li, X. Xun, Y. Xu, A. Zhan, E. Gao, F. Yu, Y. Wang, H. Luo and C. Yang, *Carbohydr. Polym.*, 2022, **276**, 118790.
527 Y.-C. Chen, H.-J. Liao, Y.-M. Hsu, Y.-S. Shen and C.-H. Chang, *Polymers*, 2022, **14**, 1474.
528 G. Osterhoff, E. F. Morgan, S. J. Shefelbine, L. Karim, L. M. McNamara and P. Augat, *Injury*, 2016, **47**, S11–S20.
529 X. Wang, S. Tang, S. Chai, P. Wang, J. Qin, W. Pei, H. Bian, Q. Jiang and C. Huang, *Carbohydr. Polym.*, 2021, **270**, 118342.
530 P. Wang and X. Wang, *Eng. Regener.*, 2022, **3**, 440–452.
531 C. Ao, Y. Niu, X. Zhang, X. He, W. Zhang and C. Lu, *Int. J. Biol. Macromol.*, 2017, **97**, 568–573.
532 S. Odabas, *J. Bioact. Compat. Polym.*, 2016, **31**, 411–422.
533 P. Daugela, M. Pranskunas, G. Juodzbalys, J. Liesiene, O. Baniukaitiene, A. Afonso and P. Sousa Gomes, *J. Tissue Eng. Regener. Med.*, 2018, **12**, 1195–1208.
534 M. Matinfar, A. S. Mesgar and Z. Mohammadi, *Mater. Sci. Eng., C*, 2019, **100**, 341–353.
535 M. Vallet-Regi and A. J. Salinas, *Mater. Today Bio*, 2021, **11**, 100121.
536 S. Simorgh, N. Alasvand, M. Khodadadi, F. Ghobadi, M. Malekzadeh Kebria, P. Brouki Milan, S. Kargozar, F. Baino, A. Mobasheri and M. Mozafari, *Methods*, 2022, **208**, 75–91.
537 M. N. Rahaman, D. E. Day, B. Sonny Bal, Q. Fu, S. B. Jung, L. F. Bonewald and A. P. Tomsia, *Acta Biomater.*, 2011, **7**, 2355–2373.
538 L. Li, P. Lu, Y. Liu, J. Yang and S. Li, *Polymers*, 2023, **15**, 2226.
539 N. Ma, D. Y. Cheung and J. T. Butcher, *J. Biomed. Mater. Res.*, 2022, **110**, 76–91.
540 S. Y. Srinivasan, M. Cler, O. Zapata-Arteaga, B. Dörling, M. Campoy-Quiles, E. Martínez, E. Engel, S. Pérez-Amodio and A. Laromaine, *ACS Appl. Bio Mater.*, 2023, **6**, 2860–2874.
541 R. Hou, Y. Xie, R. Song, J. Bao, Z. Shi, C. Xiong and Q. Yang, *Cellulose*, 2024, **31**, 4247–4262.
542 V. Kuzmenko, E. Karabulut, E. Pernevik, P. Enoksson and P. Gatenholm, *Carbohydr. Polym.*, 2018, **189**, 22–30.
543 S. Gnavi, B. Fornasari, C. Tonda-Turo, R. Laurano, M. Zanetti, G. Ciardelli and S. Geuna, *IJMS*, 2015, **16**, 12925–12942.
544 H.-T. Chang, R. A. Heuer, A. M. Oleksijew, K. S. Coots, C. B. Roque, K. T. Nella, T. L. McGuire and A. J. Matsuoka, *Acta Biomater.*, 2020, **108**, 111–127.
545 R. J. Dilley and W. A. Morrison, *Int. J. Biochem. Cell Biol.*, 2014, **56**, 38–46.
546 L. M. Miller and A. Gal, *Pathologic Basis of Veterinary Disease*, Elsevier, 2017, pp. 561–616.e1.
547 Y. Lee, S. I. Ahn and Y. Kim, *Encyclopedia of Biomedical Engineering*, Elsevier, 2019, pp. 384–393.
548 P. Libby, J. E. Buring, L. Badimon, G. K. Hansson, J. Deanfield, M. S. Bittencourt, L. Tokgözoğlu and E. F. Lewis, *Nat. Rev. Dis. Primers*, 2019, **5**, 56.